U.PORTO
FEUP FACULDADE DE ENGENHARIA
UNIVERSIDADE DO PORTO

Integrated Masters in Mechanical Engineering

Development of Multifunctional Composites - Analysis and Correlation of Performance Properties

João Korrodi de Azevedo Gomes Sottomayor

Supervisors:
Prof. Dr. António Torres Marques
Dr. Eng. Nuno M. P. Rocha

Porto, July 2015

Abstract

LY556 epoxy thermoset has been investigated as a carbon nanotube-loaded matrix for unidirectional prepreg carbon fiber-reinforced composite (Torayca IMS60). First the effect of the nanofiller, from 0.25 to 1.5wt.%, in the epoxy was assessed. Dynamic mechanical analysis (DMA) were performed to assess the flexural storage modulus, the glass-transition temperature T_g and loss coefficient tan δ as function of the nanotube content and type of functionalization, namely, pristine, carboxylic and thermally oxidized nanotubes.

DMA tests showed modulus enhancement for all nanotube functionalizations (up to 18% increase), although at distinct nanotube contents. The action of two dispersion agents was also studied, although with modulus deterioration.

Throughout the thesis, scanning electron microscopy (SEM) and transmission electron microscopy (TEM) have been used to analyze the different nanocomposites tested and to evaluate the nanotube agglomeration and dispersion within the epoxy matrix down to the nano scale.

In addition, an experimental procedure was implemented to assess the effect on the nanotube orientation of an physical alignment method applied during the curing process and dynamic mechanical tests revealed a substantial 14% increase in modulus. SEM imaging confirmed the existence of an alignment.

Finally, four analytical property prediction models were tested, revealing that the simple rule-of-mixtures cannot not be accurately correlated with the experimental data. On the other hand, two other models that have in consideration characteristics of nanotubes, presented better prediction capabilities.

Sumário

A utilização de resina *epoxy* LY556 carregada com nanotubos de carbono foi investigada no sentido de a utilizar como matriz para pré impregnados unidirecionais de fibra de carbono (Torayca IMS60). Primeiro, o efeito da adição de nanotubos na matriz, entre 0.25 e 1.5wt.%, foi estudado. Testes de *Dynamic Mechanical Analysis* (DMA) foram efetuados por forma a obter o módulo de armazenamento à flexão, a temperatura de transição vítrea T_g e o coeficiente de perdas tan δ, como função do conteúdo de nanotubos e tipo de funcionalização, nomeadamente, não tratados, *carboxylic* e oxidados termicamente.

Os testes de DMA revelaram um aumento do módulo (até 18%) para todos as funcionalizações, embora para conteúdos distintos. O efeito da adição de dois agentes dispersantes foi também estudado, embora com deterioração do módulo.

Ao longo da dissertação, imagens obtidas por microscopia eletrónica (SEM e TEM) foram utilizadas para analisar, à escala nanométrica, os diferentes nano compósitos testados e para avaliar os aglomerados e a dispersão dos nanotubos na matiz.

Seguidamente foi estudado um processo físico experimental de alinhamento dos nanotubos de carbono na matriz, durante o processo de cura. Testes DMA revelaram um aumento substancial de 14% no módulo. Imagens SEM confirmaram o alinhamento.

Finalmente, quatro métodos analíticos de previsão de propriedades foram implementados. Correlacionando com os valores experimentais, a duas regras das misturas implementadas exibiram previsões groseiras, enquanto que os outros dois métodos, que têm em consideração a natureza dos nanotubos, apresentaram melhores capacidades de previsão.

Acknowledgments

The author acknowledges partial funding from EC-FP7 project EUCARBON (GA284500) and project NORTE-07-024 FEDER-000033 - Composite Materials, Structures and Processes, within the Portuguese National Strategic Reference Framework (QREN), through the European Regional Development Fund (ERDF).

Firstly, I wish to express my gratitude to Prof. Dr. António Torres Marques and Dr. Eng. Nuno M. P. Rocha, supervisors of this thesis, for all the support and availability during the development of this thesis, even at the most occupied times.

To my INEGI lab group, Susana Silva, Marta Martins, Joana Prudêncio, Ana Moreira and Marina Torres, I thank for all the support and for all the valuable feedbacks and discussions.

To all my friends, in particular to Carolina Furtado, Pedro Cavaleiro and Rodrigo Furtado, a special thanks for the friendship and support throughout all this years.

To my girlfriend, Cristina Aguiar Pinto, that was always supportive and pushing me forward.

Lastly, a very special thanks to my parents, Francisco and Teresa, to my brother, Francisco, and to all my family for all the support and always being there for me.

Background

This thesis is included within the scope of EUCARBON project, coordinated by INEGI, and is focused on the evaluation of how carbon fiber reinforced composites are affected by the inclusion of carbon nanotubes in the polymeric matrix, from the resin, prepreg and cured composites levels.

The EUCARBON project aims to overcome the present recognized needs of European made space qualified carbon fiber and pre-impregnated materials. These materials are building blocks for technological innovation in space research. Presently, aerospace qualified carbon fiber is either produced outside Europe or produced in Europe under foreign countries supervision by only one source. This issue weakens European competitiveness in space, mainly related to the increased delivery lead times and costs. Therefore, the possibility for Europe to have free, unrestricted access to these materials requires their development in European facilities under European supervision. The following developments will result from the project:

- High and ultrahigh modulus carbon fibers to be produced in Europe by a European manufacturer;

- Space qualified pre-impregnated materials involving the developed carbon fibers and epoxy resins doped with carbon nanotubes. These novel materials will address one of the main issues linked to use of carbon fiber composites in space applications: their low thermal and electrical conductivity.

The main objective of this master's thesis is to study the effect on mechanical and thermal properties of adding carbon nanotubes to epoxy resin, with the target of developing novel carbon fiber reinforced composites.

The above technologies will be demonstrated with the conception, production and testing of demonstrator parts for use as satellites and launchers components. EUCARBON will also provide raw-materials for other strategic sectors of industry in Europe, such as aircraft, automotive and others.

Contents

List of Tables

List of Figures

Chapter 1

Introduction

1.1 Motivation

With a launch cost from 3000 to more than 10000 euros per Kg [1], weight reduction is the primary reason for using fiber-reinforced composites in space vehicles. In addition, the unique combination of mechanical properties and thermal stability is leading to an increasing number of applications for carbon fiber-reinforced epoxies in artificial satellites.

In the last couple of decades, material scientists and engineers have focused a huge research activity on carbon nanotube based nanocomposites. This attention is justified by the extraordinary mechanical and functional properties shown by this carbon nanofillers. This form of carbon nanostructure, in paper, represents an ideal candidate as an advanced filler material not only in a neat hosting system, but also in advanced matrices in traditional fiber reinforced composites, which can lead to the potential development of a new generation of multifunctional composite materials with exceptional mechanical, thermal and electrical properties.

Several studies have sought to verify the reinforcement effect of carbon nanotubes on the mechanical properties of polymer matrices [2–5]. Generally, these studies found that the elastic modules of the carbon nanotube polymer composites improved by adding only few weight percentages of this nanofiller. Although conflicting results about improvement in strength or fracture toughness have been reported, a common tendency is for the enhancements on Young's modulus.

The main objective of this master's thesis is to study the effect on mechanical and thermal properties of adding multi-walled carbon nanotubes, with specific functionalizations, into epoxy thermoset resin, with the target of using it as a matrix in carbon fiber reinforced composites.

1.2 Thesis Overview

- Chapter 2 begins with the study of carbon nanotubes, from the atomic structure to the synthesis processes, followed by a brief presentation of the epoxy resin. Then, carbon nanotube reinforced polymer composites are exploited, and the reasons why this composites do not fully use the exceptional properties of the carbon nanotubes are presented and thoroughly explained in the following subsections.

- In chapter 3, LY556 epoxy thermoset was investigated as a carbon nanotube-loaded matrix for fiber-reinforced composite. First the effect of the nanofiller in the epoxy was assessed. In this work, dynamic mechanical analysis were performed to assess the flexural storage and loss modulus, the glass-transition temperature T_g and loss coefficient tan δ as a function of the nanotube content and type of functionalization. In addition, the action of two dispersion agents in the loaded epoxy and the application of a physical alignment method during cure of the nanotube loaded prepreg were also explored.

- Chapter 4 presents several approaches, form the simple rule-of-mixtures to more complex multiscale models, developed to predict mechanical properties of nanocomposites. Afterwards, some of the models are applied and their prediction capabilities are tested.

- In chapter 5, concluding remarks of the work and study performed are drawn and some ideas of future work are presented.

Chapter 2

State-of-Art

2.1 Carbon Nanotubes

Carbon nanotubes (CNTs) are graphene sheets wrapped into a hollow cylinder, made of sp^2 covalent bonded carbon atoms - stronger than the sp^3 bonds found in diamond - organized in a hexagonal mesh [6, 7]. The first Transmission Electron Microscopy (TEM) evidence for the tubular nature of some nano-sized carbon filaments is believed to have appeared in 1952 in the Journal of Physical Chemistry of Russia [8], but was only in 1991, with Iijima et al.'s paper in Nature magazine [9], that it had an international projection and boosted the development [10].

CNTs exist in two different basic forms: Single-Walled Carbon Nanotubes (SWCNTs), which are the fundamental cylindrical structures (fig.2.1a), and Multi-Walled Carbon Nanotubes (MWCNTs), which can have two or more coaxially van der Waals bonded SWCNTs, separated by a fraction of a nanometer (0.34 nm) (fig.2.1b).

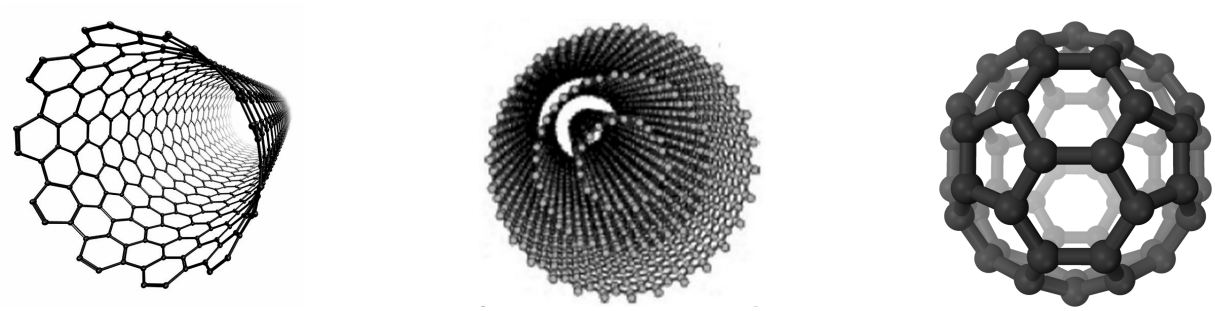

(a) (b) (c)

Figure 2.1: (a) Schematic representation of a Single-Walled Carbon Nanotube [11], (b) a Multi-Walled Carbon Nanotube [12] and (c) a Fullerene C_{60} [13].

Carbon nanotubes are only a few nanometers in diameter and can be tens of microns long. Usually, on each extremity they are closed with half of a fullerene molecule (fig.2.1c and 2.2), which consist of a spherical structure made of carbon atoms displaced in hexagons and pentagons.

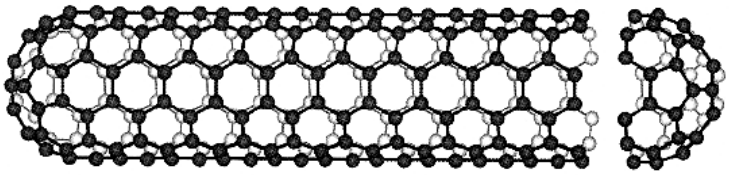

Figure 2.2: Single-walled carbon nanotube with the end closed with a C_{60} Fullerene [14].

Carbon nanotubes possess extraordinary mechanical, thermal and electric properties. Stiffness was first determined by observing the amplitude of thermal vibrations in transmission electron microscopy (TEM) and the average value was reported to be 1.8 TPa for multi-walled and 1.25 TPa for the single-walled ones [15, 16]. Experimental results of tensile tests operated inside a scanning electron microscope (SEM), showed that the strength of the outer shell of the MWCNT was between 11 and 63 GPa at fracture strains up to 12% and the elastic modulus ranged from 270 to 950 GPa [15].

The density of carbon nanotubes depends on the diameter and on the number of walls. Laurent et al. [17] developed an equation to determine the density of the carbon nanotube as a function of its diameter and number of walls.

$$d_{MW} = \frac{4000}{1315}\left(\frac{n}{d_{out}} - \frac{0.34\sum_{i=0}^{n-1} i}{d_{out}^2}\right) \tag{2.1}$$

where d_{MW} is the multi-walled carbon nanotube density, n is the number of walls and d_{out}, is the outer diameter, in nm, of the nanotube. The equation is graphically represented in the figure 2.3.

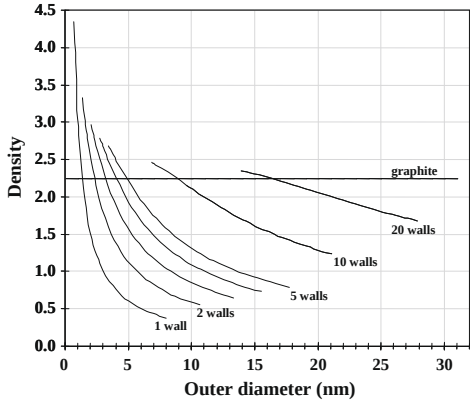

Figure 2.3: Density of carbon nanotube against diameter, for various values of number of walls [17].

2.1.1 Chirality

Single-walled carbon nanotubes can be fully described, with the exception of their length, by a single vector $\vec{C}$, called chiral vector. Two atoms in a planar graphene sheet are chosen and one is used as origin. The $\vec{C}$ is pointed from the first atom toward the second one (fig. 2.4a) and is defined by the following equation:

$$\vec{C} = n\vec{a_1} + m\vec{a_2} \tag{2.2}$$

where n and m are integers, and $\vec{a_1}$ and $\vec{a_1}$ are unit cell vectors of the two-dimensional lattice formed by the graphene sheets. The direction of the nanotube axis is perpendicular to this chiral vector.

The chiral angle θ is defined as the angle between chiral vector $\vec{C}$ and the "zigzag" axis.

$$\theta = \tan^{-1}\left(\frac{m\sqrt{3}}{m+2n}\right) \tag{2.3}$$

Three types of CNTs are revealed with these values:

1. when $n = m$ ($\theta = 0^0$), the nanotube is called "armchair" type;
2. when $m = 0$ ($\theta = 30^0$), it is called the "zigzag" type;
3. when $n \neq m$, so θ is between 0^0 and 30^0, it is a "chiral" tube.

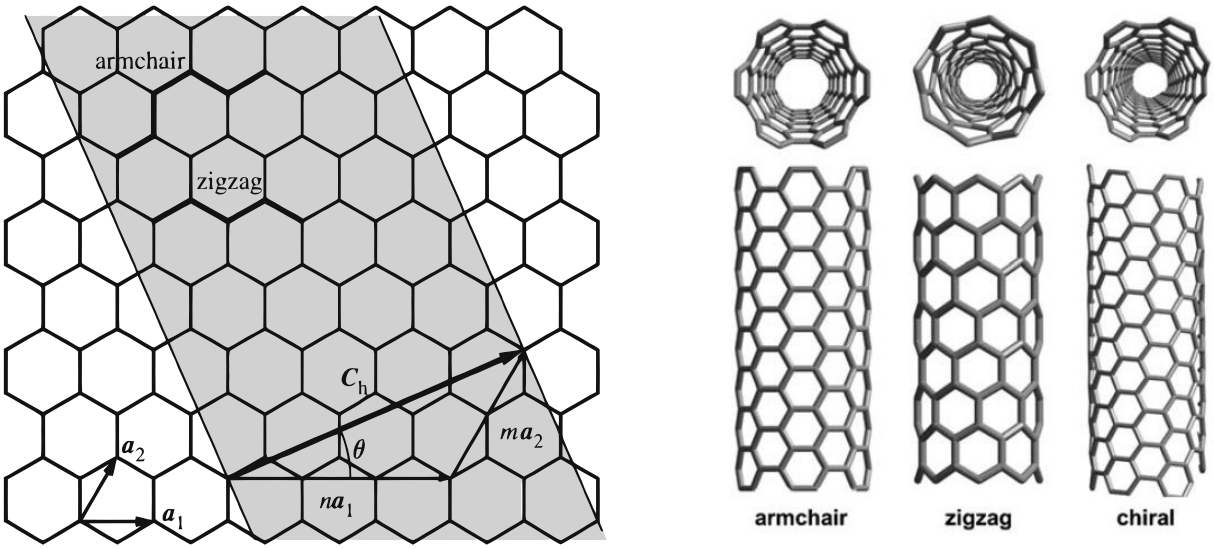

(a) (b)

Figure 2.4: (a) and (b): when $n = m$ ($\theta = 0^0$) the nanotube is called "armchair" type; when $m = 0$ ($\theta = 30^0$) it is called the "zigzag" type; when $n \neq m$ (θ between 0^0 and 30^0) it is a "chiral" tube [18, 7].

The values of (n, m) determine the "chirality" of the nanotube and it affects the mechanical, electronic and optical properties. Nanotubes with $|n - m| = 3q$ are metallic and those with $|n - m| = 3q \pm 1$ are semiconducting, with q as an integer).

For multi-walled, there are only a few possible (n, m) sequences that have a plausible intershell spacing (d) between two successive tubes, in the range from 0.344 nm to 0.36 nm. These values suggest a possible dependence of intershell distance on the tube size and some authors gives an empirical relationship to fit TEM experimental data:

$$d = 0.334 + 0.1e^{-r} \tag{2.4}$$

where r is the radius of the tube. As a consequence of the tube diameter increase, the intershell distance decreases to 0.344 nm [19].

The analysis in this dissertation will be mainly focused in the MWCNTs, which theoretically exhibit a relatively high elastic modulus and are moderately priced, therefore, have a high potential of being used in reinforcing composites on a commercial scale.

2.1.2 Synthesis of Carbon Nanotubes

There are many techniques used to produce SWCNTs or MWCNTs. Methods such as electric arc discharge, laser vaporization and chemical vapor deposition techniques are well established to produce a wide variety of CNTs and currently widespread at an industrial scale, e.g. Arkema, Nanocyl and Future Carbon. These methods are described in following sections.

2.1.2.1 Electric Arc Discharge

The electric arc discharge method, initially used for the production of the C_{60} fullerene, already mentioned in section 2.1, is perhaps the most common and easiest way to produce carbon nanotubes (CNTs). This method consist in striking an electric arc between graphite electrodes in an inert gas atmosphere, typically argon or helium, at controlled pressure, to generate the high temperatures, around 3000^oC, needed to vaporize carbon atoms into a plasma (fig.2.5) [20, 6]. A disadvantage is the production of graphitic impurities such as carbon soot with amorphous carbon and fullerens.

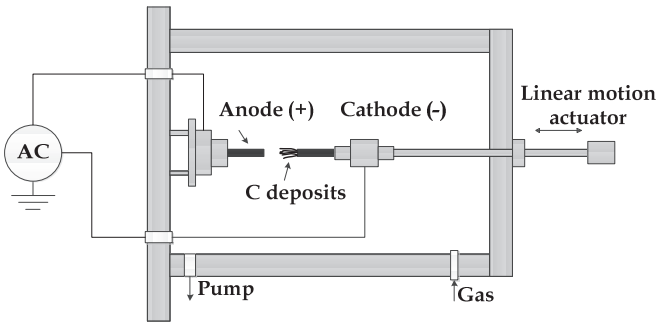

Figure 2.5: Schematic representation of the Electric Arc Discharge method [21].

2.1.2.2 Laser Vaporization

Laser vaporization, also known as laser ablation, uses an intense laser pulse to vaporize a carbon target. This carbon target, which also contains small amounts of transition metals, such as nickel and cobalt, playing the role of catalysts, is placed in a tube furnace at 1200^oC. As the target is ablated, inert gas passes through the chamber carrying the grown nanotubes on a cold finger for collection (fig.2.6). This method mainly produces bundles of Single-Walled carbon nanotubes in the form of ropes [6]. However, MWCNTs were found when a pure graphite target was used.

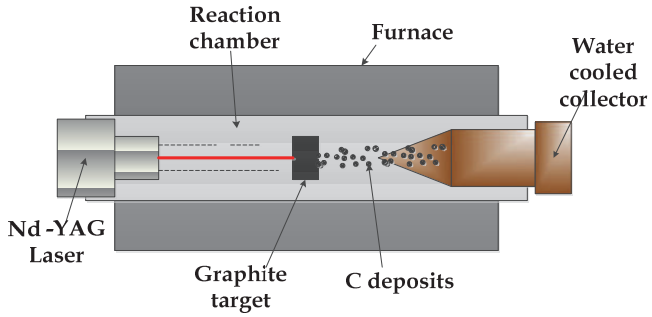

Figure 2.6: Schematic representation of the Laser Vaporization method [21].

2.1.2.3 Chemical Vapor Deposition

In chemical vapor deposition (CVD) a hydrocarbon vapor passes at atmospheric pressure through a tubular reactor in which a catalyst material is present. This catalyst, together with temperatures from 600 to 1200ºC, acts as a substrate and decompose the hydrocarbon, forming CNTs on its surface. The nanotubes are collected upon cooling the reactor to room temperature (fig.2.7).

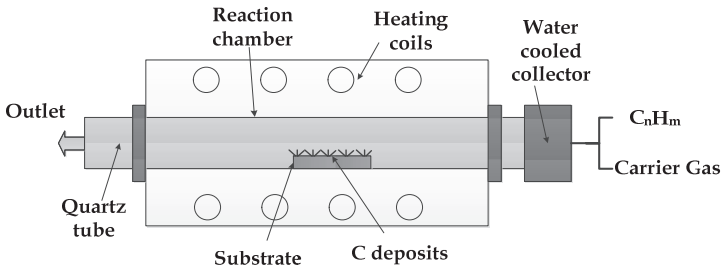

Figure 2.7: Schematic representation of the Chemical Vapor Deposition method [21].

Depending on the adhesion between the catalyst and the substrate, there are two different growth methods:

1. Tip Growth Method, where, during the growth, the catalyst particles remain in the extremity of the growing nanotubes

2. Base Growth Method, where the catalyst particles stay at the base of the nanotube

Comparing to the arc and laser methods, this technique is a simple, versatile and economic way to produce industrial quantities of cabon nanotubes at low temperatures and ambient pressure. In addition, there is more control over the structure and length of the nanotube and purity levels are higher. However, in crystallinity, arc and laser produced CNTs reveal superior levels [6, 22].

2.2 Epoxy Resin

Epoxy resins are generally formed from the crosslinking reaction of polyepoxides (monomer) and polyamines (hardener) to form a rigid network [23]. Chemically crosslinked systems (fig. 2.8) are typically known as thermosetting polymers because the crosslinking agent is heat activated.

Crosslinking proportionally increases the density of a polymer, and with this increase, molecular motion in the sample is hindered, causing a rise in the glass-transition temperature (T_g). The higher the T_g, the higher the cross-linked density and consequently the higher the modulus [24, 25], therefore, the T_g is strongly dependent on the curing process. Although an ordered molecular structure could conceptually exist, the overall molecular structure of a crosslinked epoxy is amorphous [26].

Figure 2.8: Crosslink schematic representation [27].

2.3 Carbon Nanotube Reinforced Polymer

Carbon nanotubes (CNTs) have gained significant interest to provide multifunctional character to carbon fiber reinforced composites. They offer strong potential as a nanoscale filler material because of their exceptional mechanical, thermal and electrical properties, already reviewed in chapter 2.1. The incorporation of this filler in a polymer matrix, such as epoxy resin, should result in a significant improvement in matrix properties. However, the obtained properties are inferior to the expectations. This can be explained by a number of reasons that are enumerated below and further explored in the following sections:

1. Some polymer matrices are more sensitive than others to the presence of the carbon nanotubes, therefore, a proper selection of the matrix is essential - section 2.3.1;

2. Van der Waals' attraction makes entangled agglomerates incapable of fully blending into the polymer with a good dispersion - section 2.3.2;

3. Poor interfacial interaction between CNTs and polymer matrix can lead to a insufficient load transfer - section 2.3.3;

4. Defects on the structure and geometry, such as bent and twisted CNTs - section 2.3.4;

5. Alignment of carbon nanotubes within the composites - section 2.3.5;

6. Level of purity of the carbon nanotubes used in the composites - section 2.3.6.

Although the CNT production cost is higher than conventional fillers, it should be balanced out by the low loading levels required, usually between 0.1 and 3%, and consequently, there is no significant weight addition. In addition, the processing equipment required for such nanocomposites is the same as that used for neat resins.

2.3.1 Proper Selection of the Polymer Matrix

Both thermosetting and thermoplastic polymers have been used as matrix materials in carbon nanotube/polymer composites. Depending on the polymer matrix and processing conditions, large variations in their measured properties are found. Therefore, the properties of carbon nanotube/polymer composites are highly polymer specific.

According to Lijie Ci et al. [28], the reinforcement role of carbon nanotubes gradually reduces while increasing the stiffness of matrix. By controlling the curing process, Lijie Ci and co-worker prepared carbon nanotube/epoxy nanocomposites with different matrix stiffness (fig.2.9). The reinforcement role was assessed in the different matrices according to the mechanical tests and SEM observations. In soft and ductile matrices, nanotubes show a significant reinforcement effect because of the possible accelerated curing process and the better interface adjoining. On the other hand, the interface interaction is poor in the stiff composite, due to complete cross-link of the polymer molecules surrounding the carbon nanotubes.

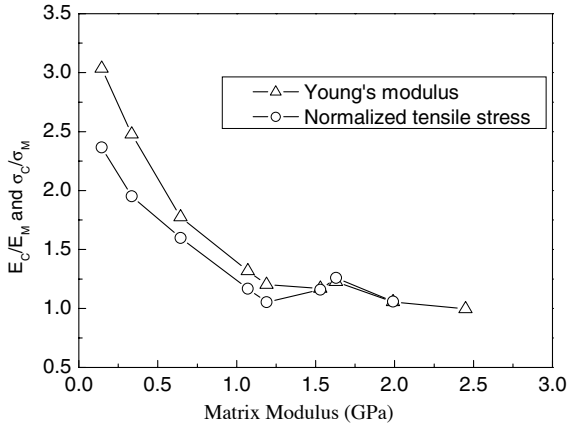

Figure 2.9: The evolution of the reinforcement of carbon nanotubes in epoxy composites with different matrix stiffness [28].

2.3.2 Dispersion

Carbon nanotubes, in all their forms, are difficult to disperse and dissolve in water and in organic medium and they are extremely resistant to wetting and, for a nanocomposite, a good dispersion of the nanofiller within the matrix is crucial. Since the extremely large surface area leads to strong tendency to form agglomerates, preventing re-aggregation of the nanofiller is a challenging task. A non uniform dispersion can lead to carbon nanotube agglomerates acting as defect sites and limiting the efficiency of CNT as reinforcement filler [29]. In order to evaluate the dispersion at nano scales, several methods can be used [30]:

- Microscopy, optical, transmission electron (TEM) or scanning electron (SEM), are commonly used to observe dispersion and can provide useful information about the aggregate size and microscale dispersion quality. SEM and TEM were used to assess dispersion qualitatively in cured samples. However, this method is qualitative and usually covers a small area of the sample, which may not be representative of the whole system.

- Rheological analysis of nanotube suspensions can provide insight into the microstructure and can be used to correlated with enhancement of properties. Rheological properties of the suspension are strongly influenced by the nanotube volume fraction and aspect ratio, polymer–CNT interactions and the state of nanotube dispersion and network formation.

- An effective quantitative method is ultraviolet–visible (UV–Vis) spectroscopy. Individual carbon nanotubes exhibit characteristic bands of absorption, whereas agglomerates are hardly absorptive in the wavelength region between 200 and 1200 nm. Furthermore, it is possible to correlate the amount of individual nanotubes in suspension with the intensity of the corresponding absorption spectrum. Therefore, UV–Vis spectroscopy can be used as a quantitative tool for nanoscale dispersion characterization in diluted uncured samples.

- Measuring the electrical conductivity, which is based on the fact that higher electrical conductivity is obtained in the case of better nanotube dispersion [31] is an indirect method to evaluate the dispersion.

- Other methods, such as Thermogravimetric Analysis (TGA) and Differential Ccanning Calorimetry (DSC) can be used as well. However, potential effects of additives can modify results. Due to the high viscosity of the resin used, the sedimentation technique is unfeasible.

The dispersion problem for carbon nanotubes (CNTs) is dimensionally different (fig.2.10) from other conventional fillers, such as spherical particles or short fibers, because CNTs are nanometer scale small diameter associated with high aspect ratios ($l/d > 1000$) and, consequently, extremely large surface area. In addition, the commercial CNT products are supplied in the form of heavily entangled aggregates, which results in inherent difficulties in dispersion and also in a high viscosity of the nanotube/polymer mixture [32, 7].

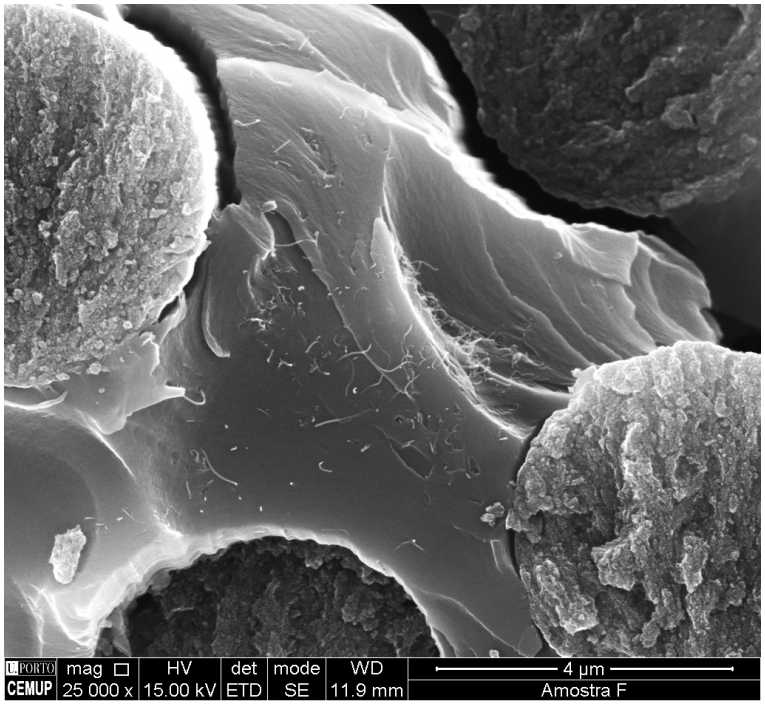

Figure 2.10: Scale difference between cabon nanotubes and carbon fibers

Table 2.1 compares the dimensions of common fillers, such as alumina Al_2O_3 particles, carbon fibers, graphite nanoplatelets (GNPs) and CNTs and the number of particles corresponding to a 1 mm^3 cube with a uniform filler volume fraction of 0.1% in volume.

Table 2.1: Dimension and corresponding number of particles in composites for different fillers [7].

Filler	Average Diameter d	Average Length l	Average Thickness t	N° of particles in $1mm^3$ and 0.1vol%	Surface area of each particles
Al_2O_3 particle	$100\mu m$	-	-	1.9	$S = \pi d^2$
Short Carbon Fibers	$5\mu m$	$200\mu m$	-	255	$S = \pi dl + \pi d^2/2$
GNP	-	$45\mu m$	7.5 nm	6.58×10^4	$S = 4l^2 + 2lt$
CNT	$12nm$	$20\mu m$	-	4.42×10^8	$S = \pi dl + \pi d^2/2$

The large quantity of particles and their size effect will lead to an exceptionally large surface area of nano-scale fillers in the composite. There is about 500 times difference in surface area between the Al_2O_3 and CNT particles. In figure 2.11, it is possible to compare the theoretical distribution of the different fillers. The inherent difficulty in the dispersion of CNTs into a polymer matrix is explained by this large surface area and particle agglomeration due to the electrostatic interaction and van der Waals force. The real distribution of the nano-scale fillers (C and D in Fig.2.11) should be more complex than the shown simulation. This agglomeration effect increases with increasing content of the nanotubes.

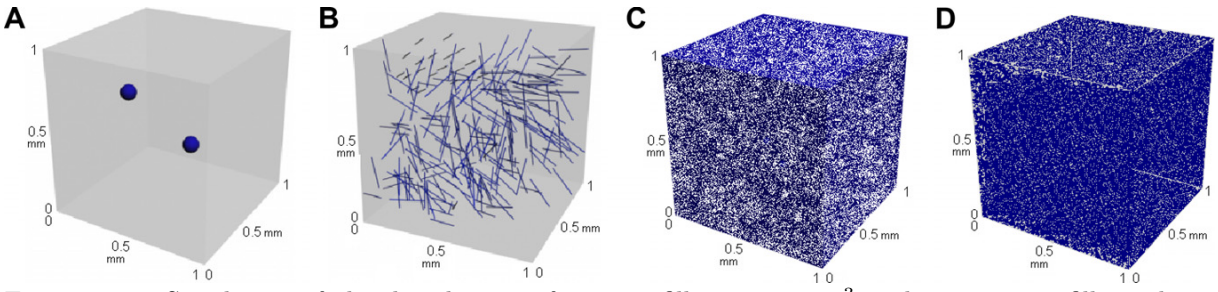

Figure 2.11: Simulation of the distribution of various fillers in 1 mm^3 with a constant filler volume fraction of 0.1% in volume. A: Al_2O_3 particle; B: Carbon Fiber; C: Graphite Nanopowder (GNP); D: Carbon nanotubes (CNT) [7].

Associated with this large surface, there is an increase in the viscosity of the uncured resin. This higher viscosity turns more difficult the processing of the resin and can preclude its use in industrial applications, such as the impregnation of carbon fibers 2.12b.

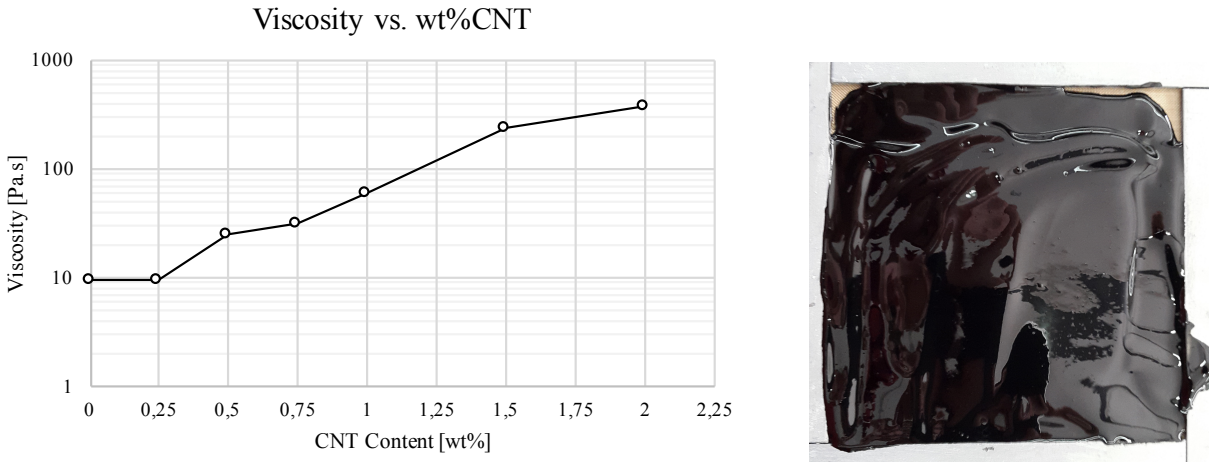

(a) (b)

Figure 2.12: (a) Viscosity as a function of the carbon nanotubes content, at a shear rate of $1s^{-1}$, and (b) visible high viscosity of a 0.75wt.% carbon nanotube filled epoxy.

Fig.2.13 shows scanning electron microscopy (SEM) image of CNT entanglements. It has been proven that these agglomerates result in diminished mechanical and electrical properties of composites as compared with theoretical predictions related to individual CNTs [33–35].

It is possible to achieve improved dispersion by applying various techniques, for example, employing physical treatment such as ultrasonication, ball milling, calendering, stirring, and extrusion [7], through functionalization of the nanotube [36] or even adding a dispersion agent [37].

The dispersion within the polymer matrix can be controlled as well through in-situ polymerization of nanotube/polymer monomer mixture, solution casting of suspension of carbon nanotubes in the dissolved polymers, melt mixing of carbon nanotubes/nanofibers with polymers, and the use of surfactants [32].

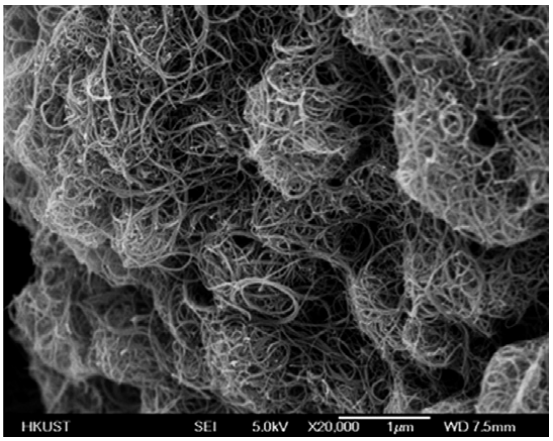

Figure 2.13: SEM image of entangled MWCNT agglomerates [7].

However, any treatment aimed at obtaining good dispersion, purification or chemical reactivity must be performed with care because certain implications and limitations associated with its use can exist. For example, ultrasonication use, with prolonged exposure, may induce structural damage to the nanotubes [3] as can extensive ball milling, decreasing the CNT length [38] and, consequently, lowering the aspect ratio, which can resulted in relatively less strong bond with the matrix [5].

Table 2.2: Comparison of various physical techniques for CNT dispersion in polymer composites [7]

Technique	Damage to CNTs	Suitable Polymer Matrix	Factors
Ultrasonication	Yes	Soluble polymer, low viscous polymer or oligomer, monomer	Power, mode of sonicator, sonication time
Calendering	No	Liquid polymer or oligomer, monomer	Rotation speed and gap
Ball Milling	Yes	Powder (polymer or monomer)	Milling time, rotation speed, size of balls and ball/CNT ratio
Shear Mixing	No	Soluble polymer, low viscous polymer or oligomer, monomer	Propeller's size and shape, mixing speed and time
Extrusion	No	Thermoplastics	Screw's temperature, configuration and rotation speed

2.3.2.1 Ultrasonication

Ultrasonication is a technique that uses ultrasound energy to agitate particles in a solution, and it is the most frequently used method for nanoparticle dispersion. Ultrasound waves promote the "peeling off" of individual nanoparticles located at the outer part of the nanoparticle bundles, or agglomerates, and thus results in the separation of individual nanoparticles from the bundles. This method is effective in dispersing CNTs in liquids with low viscosity, such as water, acetone or ethanol. However, most polymers have a higher viscosity and therefore need to be diluted using a solvent [7]. This technique was used to disperse the carbon nanotubes to enhance the Scanning Electron Microscope (SEM) visualization of the nanotubes without the resin.

2.3.2.2 Ball Milling

Ball milling is a type of grinding method that uses collision between very small rigid balls, as small as 100nm in diameter, concealed in a container to induce high pressure locally and grind the material into a fine powder (fig. 2.14). Different materials are used as balls including ceramic, flint pebbles and stainless steel. Ball milling of CNTs in the presence of chemicals not only enhances their dispersibility, but also introduces some functional groups onto the CNT surface [7].

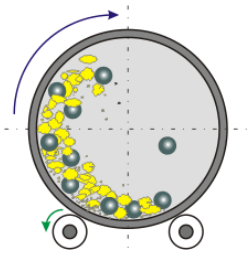

Figure 2.14: Schematic ball milling

2.3.2.3 Calendering

The calender is a machine tool that uses rollers to employ shear force and mix disperse or homogenize viscous materials. The general configuration of a calendering machine consists of three adjacent cylindrical rollers each of which runs at a different angular velocity (fig.2.15). The gaps between the rollers combined with the mismatch in angular velocity of the adjacent rollers, result in local high shear forces with a short residence time [4].

The first and third rollers, called the feeding and apron rollers (from the left to the right fig.2.15), rotate in the same direction while the center roller rotates in the opposite direction. In order to maximize dispersion, the processing cycle can be repeated several times. The narrow gaps can be mechanically or hydraulically adjusted and maintained (from 500 to about 5 μm), thus it is easy to get a controllable and narrow size distribution of particles in viscous materials.

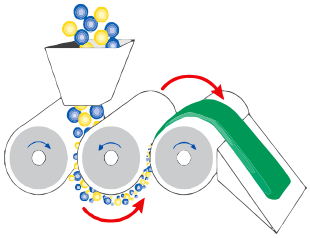

Figure 2.15: Schematic calendering process [7].

To disentangle and disperse CNT agglomerates into a polymer medium, a high shear stress is required. However, the dimensional disparities between the gaps and the typical diameter of the CNTs, suggests that this process only breaks the agglomerates into smaller ones with some desentangled individual CNTs [7].

2.3.2.4 Mechanical Stirring

Mechanical stirring (fig.2.16) is a commonly used technique to disperse nanoparticles. It consists in a propeller that rotates and creates shear stresses in the resin. The dispersion result can be controlled by the shape and size of the propeller, the duration and speed of stirring. Carbon nanotubes tend to re-agglomerate after the stirring, mainly because van der Waals attractive forces. During stirring, frictional contacts and elastic interlocking mechanisms that makes the desegregation more difficult [39]. Nevertheless, a relative fine dispersion can be achieved after intensive stirring of multi-walled nanotubes in epoxy resin [40].

Figure 2.16: Stirrer used in the mixing process.

2.3.2.5 Functionalization

Due to the aromatic nature of the bonds, the chemical stability of the carbon atoms is responsible for the inert interaction of the CNTs with the surrounding matrix. They can interact mainly through van der Waals (vdW) force, which is unable to provide an efficient load transfer between the CNTs and the matrix [7]. Therefore, methods to modify surface properties of the CNTs have potential. These methods can be divided into chemical functionalization and physical methods based on the interactions between the active molecules and carbon atoms on the CNTs.

Table 2.3: Comparison of various physical techniques for CNT dispersion in polymer composites [7].

Method	Type	Principle	Damage to CNTs	Easy to use	Interaction	CNT re-agglomeration
Chemical method	Side wall	Hybridization of C atoms from sp^2 to sp^3	Yes	No	Strong	Yes
	Defect	Defect transformation	Yes	Yes	Strong	Yes
Physical method	Polymer wrapping	vdW force, $\pi - \pi$ stacking	No	Yes	Variable	Yes
	Surfactant adsorption	Physical adsorption	No	Yes	Weak	Yes
	Endohedral	Capillary effect	No	No	Weak	Yes

Chemical functionalization can be used to tailor the interaction between the nanotubes and the polymer matrices, a solvent or even other nanotubes. It helps preventing the re-aggregation of the carbon nanotubes (CNTs) and leads to a better coupling with the polymeric matrix. The latter is very important for an efficient load transfer of the stresses to the nanotubes. Therefore, functionalization might improve solubility and processibility of the composite [36].

This functionalization is based on the covalent linkage of functional groups onto the carbon structure of CNTs. It can be performed at the sidewalls or at the end of the nanotubes. Direct covalent sidewall functionalization is associated with a change of hybridization from sp^2 to sp^3 and a simultaneous loss of π-conjugation system on graphene layer (fig.2.17a). This functionalization can be produced by reaction with some molecules of high chemical reactivity.

Defect functionalization is another method for covalent functionalization of CNTs and can be achieved by introducing some functional groups on defect sites of CNTs (fig.2.17b). This defect sites can be the open ends and/or holes in the sidewalls, pentagon or heptagon irregularities in the hexagon carbon nanotube framework. Using oxidizing agents, such as strong acids, can result in the formation of carboxylic (-COOH) or hydroxyl groups (-OH) on the surface of nanotubes. The chemically functionalized CNTs can produce strong interfacial bonds with many polymers, allowing CNT based nanocomposites to enhance mechanical and functional properties.

Carboxylic Acid functionalization procedure consists in grafting carboxylic acid functional groups onto the nanotubes surface. Carboxylic acid-functionalized multi-walled carbon nanotubes (MWCNT-COOH) are obtained by oxidation pristine MWCNTs via sonication in sulfuric-nitric acid [41].

Thermal oxidation process consist of a heat treatment ranging from 1500^oC to 2500^oC. Oxidation of carbon nanotubes removes impurities, such as amorphous carbon, and improves wetting by creating oxygen-terminated surfaces. Secondly, in the oxidation process, as the

temperature increases, removal of smaller diameter tubes can occur [42]. Finally, the thermal oxidation creates bonding sites on the tube walls by breaking the C–C bonds [43]. Composite materials may benefit by having tubes of a narrower range diameter distribution, free of amorphous carbon impurities and more bonding sites for better contact with the matrix [44].

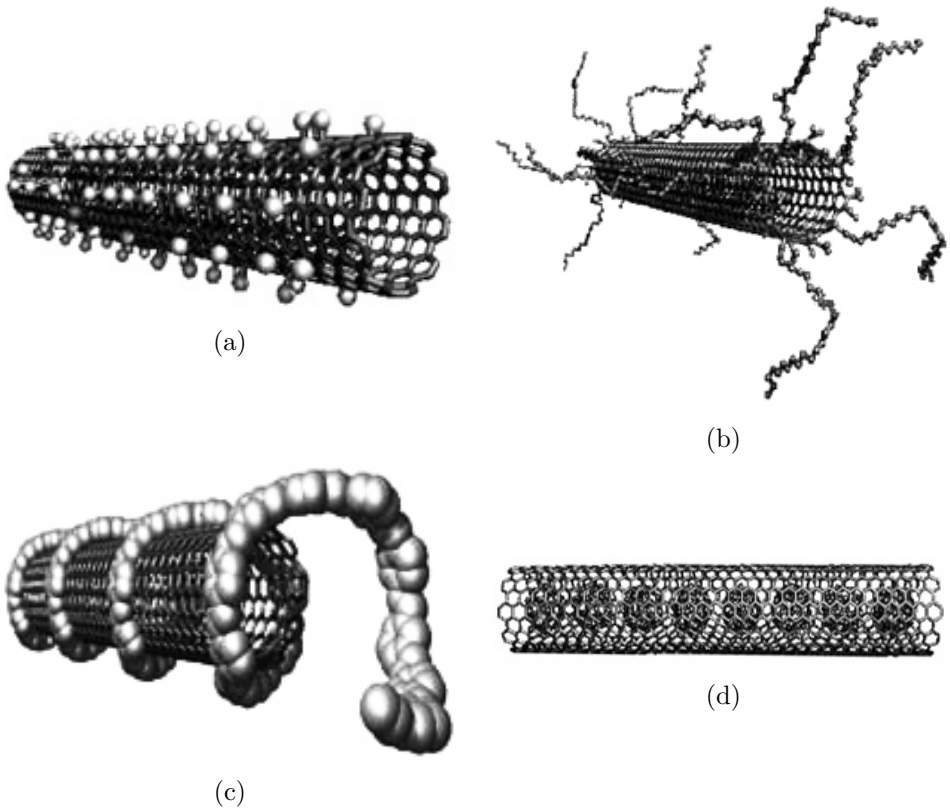

Figure 2.17: Chemical, or covalent, functionalization: (a) Sidewall and (b) Defect functionalization. Physical, or non-covalent, functionalization: (c) "Wrapping" and (d) Endohedral functionalization [36].

Physical functionalization is a non-covalent functionalization technique for tuning the interfacial properties of nanotubes. The suspension of CNTs in the presence of polymers or surfactants, such as poly(phenylene vinylene)[45] or polystyrene [46], forming a wrap of the polymer around the nanotubes (fig.2.17c), creating a supermolecular complexes of CNTs. The polymer wrapping is achieved through van der Waals interactions and $\pi - \pi$ stacking between CNTs and polymer chains containing aromatic rings [7]. All these previous mentioned functionalizations are exohedral, or in other words, applied to the exterior of the nanotube. A special case is the endohedral functionalization, i.e., the filling of the tubes interior with atoms or small molecules (fig.2.17d)[36].

A functionalized nanotube might have different mechanical or electrical properties from those of the neat nanotube, and thus it may be used for fine-tuning the chemistry and physics of CNTs. Although it can lead to significant improvement in CNT dispersion and stress transfer, it can also cause deterioration of intrinsic properties of the CNTs. For example, chemical functionalization often lead to tube fragmentation and the physical functionalization results in poor exfoliation. Therefore, dispersion and stabilization require compromises to be made [47, 6].

2.3.3 Load Transfer

The large surface area of the carbon nanotube filler means a large interface area present between the filler and matrix. In composites, a definition of this "'interface" is a surface formed by a common boundary of the reinforcement and the matrix that is in contact and maintains the bond for stress transfer. The load-bearing capability of a composite depends on that efficiency of stress transfer, which is largely controlled by the nature of the bonding at the interface region, in addition to the mechanical properties of the fiber and matrix [48]. In general, a strong interfacial bond corresponds to an effective transfer of the applied load to the reinforcement element, in this case the carbon nanotubes, theoretically resulting in improved mechanical properties [7].

In fibrous composites, the stress transfer between the matrix and fiber is transferred by shear stresses. At some critical value of the interfacial shear stress, either the matrix near the interface or the matrix–nanotube bond will rupture, resulting in debonding. This value for the shear stress is known as the InterFacial Shear Strength (IFSS) and reveals the maximum possible stress transferred to the nanotube, being an important parameter for any fiber-like reinforced composite [49].

It has been reported that the interfacial bonding between the carbon nanotubes and polymer resins is weak and the load transfer from the polymer to the nanotubes is not large enough for them to be broken under tensile loading. Instead, the CNTs tend to be pulled out [50, 28].

Commercially available nanotubes are usually 0.5–5 μm long. In the design of conventional composites, it is well known that the fiber length has a major influence on the stiffness and strength of the matrix. For effective load transfer, the fiber length has to exceed a critical value l_c (fig. 2.18) given by the following equation [51]:

$$l_c = \frac{\sigma_f^* d}{2\tau_c} \tag{2.5}$$

where σ_f^* is the tensile strength of the fiber, d is the fiber diameter and τ_c is the fiber–matrix bond strength or the shear yield strength of the matrix, whichever is smaller [52].

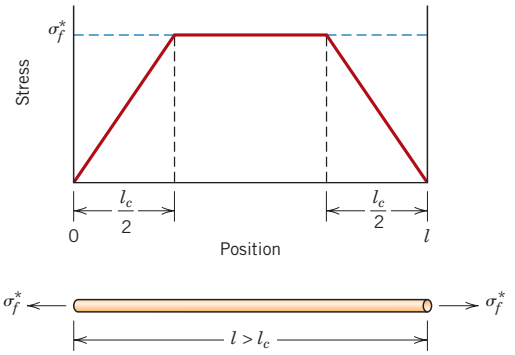

Figure 2.18: Stress–position profiles when fiber length l is greater than the critical length, for a fiber reinforced composite that is subjected to a tensile stress equal to the fiber tensile strength σ_f^* [52].

It has been found that the long-nanotube composite shows an increase in the stiffness relative to the polymer and behaves anisotropically under the different loading conditions. However, the short-nanotube composite shows no enhancement relative to the polymer, most probably because of its low aspect ratio [32].

2.3.4 Geometry Defects

It was observed that the number of defects, like structural defects, bends or twists (fig. 2.19a), affect the strength of the nanotubes [53]. Buckling of the CNTs happens presumably because of the shrinkage of the polymer matrix as the composite cools down, which originates compressive and/or bend stresses on the nanotubes [54, 55]. However, the creation of defects is not always a disadvantage, as can be analyzed in section 2.3.2.5.

Waviness of carbon nanotubes (fig.2.19b), as well as interfacial bonding conditions, play a critical role in determining the reinforcing efficiency in carbon nanotube reinforced composites. It is shown that the waviness can significantly reduce the stiffening effect of the nanotubes. The effective elastic constants of the composites are very sensitive to the waviness when debonding is small [56].

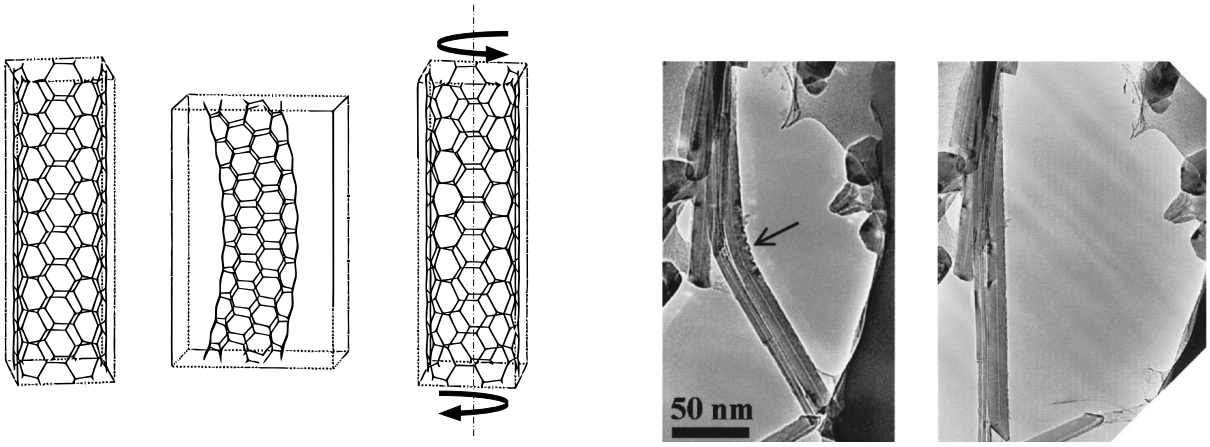

(a) (b)

Figure 2.19: (a) The left panel gives the ideal tube structure, the middle and right panels show the effects of uniform bend and twist on the structure [53]. (b) TEM image of a bent nanotube on the left and the restored shape on the right, showing the elastic nature of the deformation [55].

2.3.5 Alignment

The mechanical and electronic properties of carbon nanotubes are not only sensitive to their diameter and chirality (see section 2.1) but are also highly anisotropic. Thus, in order to maximize some properties, it is important to have a controllable alignment of the carbon nanotubes in the final composites [32]. Several techniques were developed to overcome this issue, and some of them, with applicability in thermosets, are described bellow:

- **Electrical field alignment** - The applied electric field induces a strong dipole moment in the axis parallel to the length of the nanotubes, they attempt to align perpendicular to the two parallel electrodes and along the electric field direction. However, the nanotubes are drawn by the strong Coulomb (electrostatic) forces at electrode edges and are largely deposited on the electrodes. Kumar et al. [57] reported a "few CNTs aligned vertically to the electrodes" when applied a DC electric field of 25 kV/cm between the electrodes (fig. 2.20).

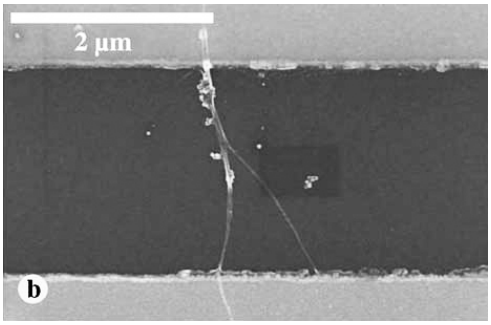

Figure 2.20: Aligned carbon naotubes between elecrodes [57].

Khan et al. [58] reported that nanotube alignment (fig.2.21) gave rise to improvements in mechanical properties (approximately 40% rise in modulus for 0.3 wt.%CNT) and electrical conductivity in the direction of orientation, compared to composites containing randomly-oriented CNTs.

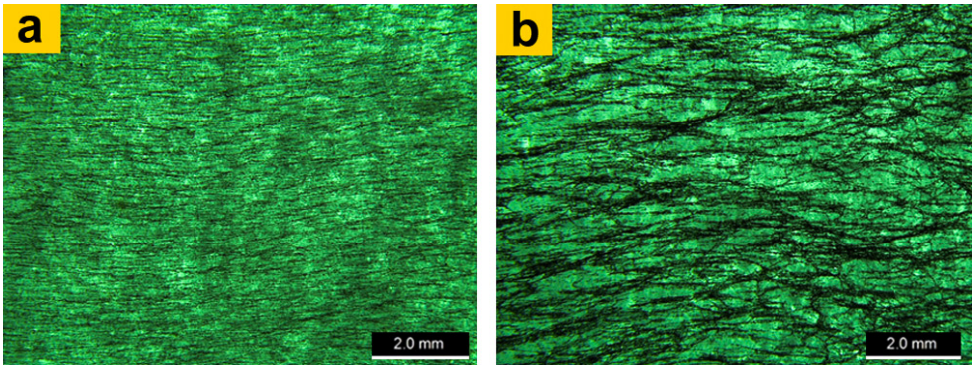

Figure 2.21: Optical micrographs of 0.3 wt.%CNT/epoxy showing MWCNT networks in composites cured after (a) 5 min and (b) 15 min of the application of the electric field [58].

- **Magnetic field alignment** - The nanotubes are aligned in a polymer matrix by polymerizing under a magnetic field. Magnetic susceptibility, electrical conductivity, and elastic modulus measurements showed clear anisotropy, indicating magnetic field induced alignment [59, 60]. Choi et al. [61] prepared aligned epoxy/CNT nanocomposites under a 25 T magnetic field. Their thermal and electrical properties along the magnetic field alignment direction are increased by 10 and 35%, compared with epoxy/MWCNT nanocomposites without the application of a magnetic field.

- **Magnetic field assisted alignment** - The movement of magnetic particles under an applied magnetic field provide drag force in the direction of field lines, imposing a direction to the nanotubes in the matrix (fig.2.22 and 2.23b). The magnetic particles can be removed by cutting the edge of the composite or with another magnet to recollect them [62]. In figure 2.23a it is possible to see the effect of the magnetic assisted induced alignment in the stress-strain curves.

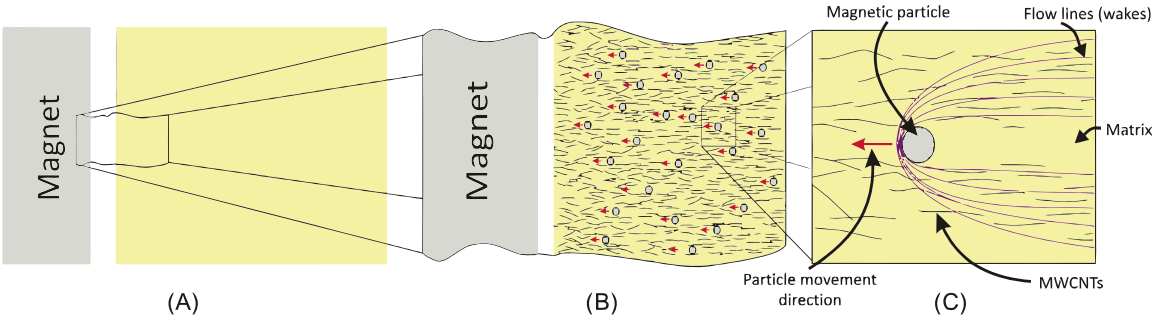

Figure 2.22: (A) Representative illustration of applying a magnetic field by a simple magnet, (B) uniform, unidirectional and non-turbulent movement of magnetical particles toward the magnet and (C) alignment of nanotubes along the flow lines by drag force caused from magnetical particles movement [62].

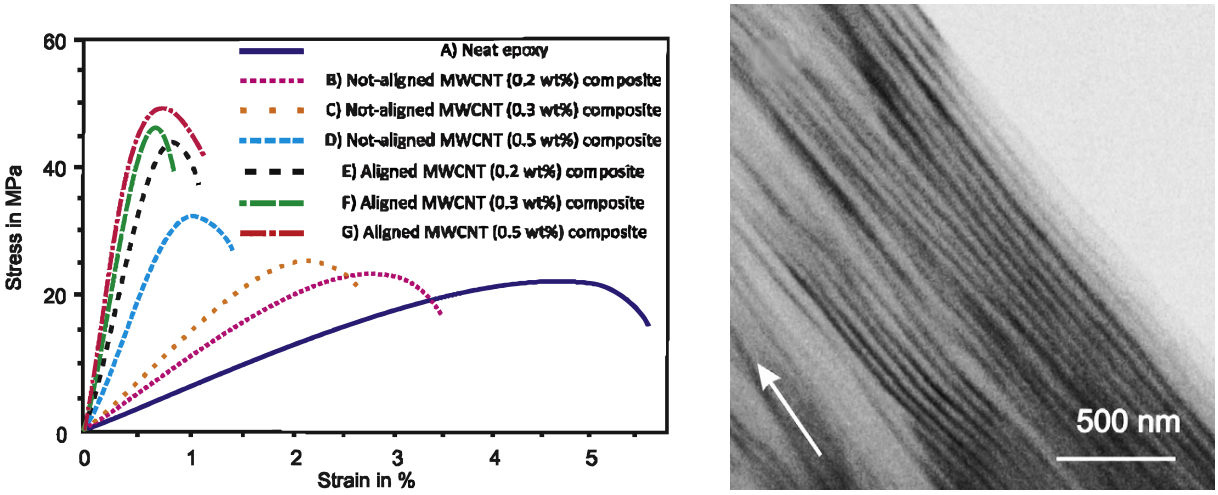

(a) (b)

Figure 2.23: (a) Stress vs. strain curves of MWCNT/epoxy composites [62] and (b) TEM images of aligned MWCNTs–epoxy composites [62].

2.3.6 Purity

Depending on the method used to produce carbon nanotubes, impurities such as carbon soot/ catalyst nanoparticles mixed with the nanotubes can exist, undermining the properties of the final composites [63]. Higher level of purity could be achieved using fabrication methods that produce less impurities (section 2.1) and by precisely controlling the manufacturing process [32, 64]. Heat treatments, such as the one present in the thermal oxidation functionalization process (section 2.3.2.5), can eliminate some carbon impurities, being possible to achieve higher values of purity [44].

2.4 Carbon Fiber Reinforced Plastic

Carbon fiber composites, particularly those with polymeric matrices, have become the dominant advanced composite materials for aerospace, automobile, high performance sporting goods, and other applications, due to their highest specific modulus and specific strength of all reinforcing fiber materials. Fibers are the load-carrying component while the matrix acts as a load transfer element, keeping them together, in the desired orientation and protected from the environment (fig.2.24) [65, 52].

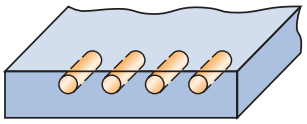

Figure 2.24: Schematic representation of a fibrous composite [52].

Carbon fibers refer to fibers which are composed by, at least, 92 wt.% carbon [65]. They can be chopped or continuous, with diameters ranging between 4 and 10 μm, and can be prepared from polymeric precursor materials such as polyacrylonitrile (PAN), cellulose (or rayon), pitch and polyvinylchloride. PAN based carbon fibers are the most common and have good strength and modulus properties, while pitch-based fibers have a higher modulus with a lower strength [66]. Carbon fiber can retain their properties at elevated temperatures, however high-temperature oxidation may be a problem. At room temperature, they are not affected by moisture or a wide variety of solvents, acids, and bases. In addition, carbon fibers are normally coated with a epoxy sizing that not only improves adhesion with the polymer matrix, but also protects [52].

"Prepreg", which is the industry's term for continuous-fiber reinforcement impregnated with a polymer resin, is probably the most widely used form of composite for structural applications. This material has to be stored at negative temperatures and is used in a partially cured state that is finished with heat and pressure (for example, with an autoclave).

Laminate (fig. 2.25), which is a consolidated stack of thin two-dimensional sheets, or layers, of fibers embedded in a matrix that have a preferred high-strength direction, is the most common form of continuous fiber-reinforced composite and it is used in structural applications. Mechanical properties of the laminate are controlled by the layer stacking sequence and the volume percentage and orientation of the fibers in each layer. This way, it is possible to optimize the mechanical properties to a specific load solicitation [52].

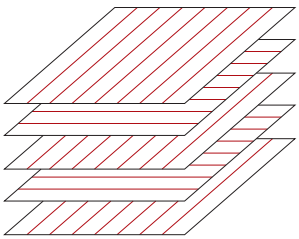

Figure 2.25: Schematic representation of a laiminate stack [52].

For each fiber–matrix combination, a critical fiber length l_c exists, which depends on diameter d and tensile strength σ_f^* of the fiber and on the bond strength between them and the matrix or the shear yield strength of the matrix, whichever is smaller, τ_c.

$$l_c = \frac{\sigma_f^* d}{2\tau_c} \tag{2.6}$$

For continuous and aligned fibers ($l > 15l_c$), mechanical properties are highly anisotropic. In the alignment direction, reinforcement and strength are maximum and perpendicular to the alignment, they are a minimum. Rule-of-mixtures expressions for the modulus in the longitudinal (eq.2.7) and transverse orientations (eq.2.8) are known to compute an accurate estimation.

$$E_c^L = V_f E_f + (1 - V_f) E_m \tag{2.7}$$

$$E_c^T = \frac{E_m E_f}{V_f E_m + (1 - V_f) E_f} \tag{2.8}$$

where E is the elastic modulus and V stands for the volume fraction, respectively, and subscripts c, f and m represent composite, fiber and matrix, respectively [52].

The introduction of carbon nanotubes in advanced matrices of traditional fiber reinforced composites may lead to the potential development of a new generation of multifunctional composite materials with exceptional mechanical, thermal and electrical properties. However this area is rather uncharted. It has been reported that the addition of carbon nanotubes into fibrous composites may enhance a number of properties. Thostenson et al. [67] reported that the presence of carbon nanotubes, synthesized on the surface of carbon fibers, improves the interfacial shear strength of the composites.

2.5 Thermogravimetric Analysis

Thermogravimetric analysis (TGA) is an experimental technique in which the mass of a sample is measured as a function of temperature or time. The sample is typically heated at a constant heating rate (dynamic measurement) or held at a constant temperature (isothermal measurement), depending on the type of information required about the sample. Additionally, the atmosphere used in the experiment plays an important role and can be reactive, oxidizing or inert. In this work, only dynamic mode with inert Nitrogen atmosphere was used, in order to obtain the effective fiber content for the composite samples.

Figure 2.26: TA Instruments SDT Q600 [27].

The equipment present in the laboratory is a SDT Q600 (TA Instruments, New Castle, US) (fig. 2.26), which is a simultaneous thermogravimetric (TGA) and differential scanning calorimeter (DSC) analyzer.

The results of a TGA measurement are typically displayed as a curve in which mass, or per cent mass, is plotted against temperature and/or time (fig. 2.27). Mass variation occurs when the samples looses material, and it can be caused, for example, by the following factors:

- Evaporation of volatile constituents; drying; desorption of gases, moisture and other volatile substances; loss of water of crystallisation;
- Oxidative decomposition of organic substances;
- Thermal decomposition with the formation of gaseous products. With organic compounds, this process is known as pyrolysis or carbonisation.

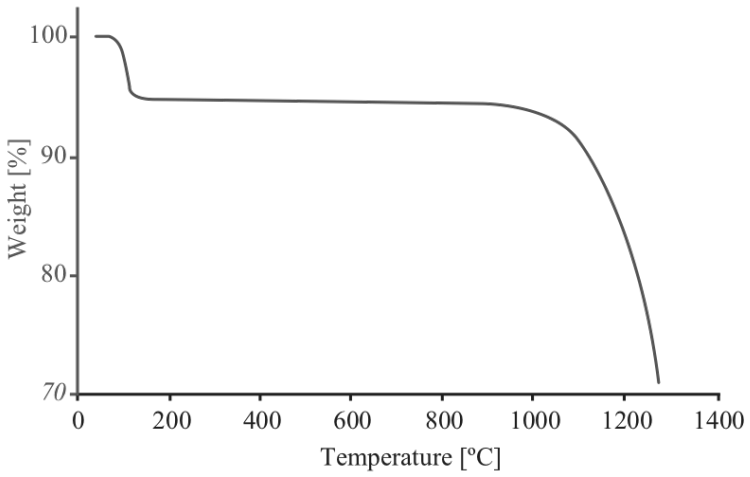

Figure 2.27: Example of TGA curve, for a soda ash sample [27].

2.6 Dynamic Mechanical Analysis

Dynamic Mechanical Analysis (DMA), or Dynamic Mechanical Thermal Analysis (DMTA), is a technique used to measure the mechanical properties of a wide range of materials, including polymers. Polymers behave both like an elastic solid and a viscous fluid, thus the term viscoelastic. DMA differs from other mechanical testing devices in two ways.

Figure 2.28: TA Instruments DMA Q800 [27]

1. In many applications, viscous component is critical and typical tensile test devices focus only on the elastic component. It is the viscous component that determines properties such as impact resistance.
2. DMA works primarily in the linear viscoelastic range and typical tensile test devices work primarily outside this range. Therefore, DMA is more sensitive to structure.

Viscoelastic properties are measured using either transient or dynamic oscillatory tests. Transient tests include creep and stress relaxation. In creep, a constant stress is applied to the sample while deformation is measured against time. After a certain time, the stress is removed and the recovery is measured (fig.2.29a). In stress relaxation, a constant deformation is applied to the sample while the decreasing of the stress against time is recorded (fig.2.29b). Both tests are used to assess the viscoelastic behavior of materials.

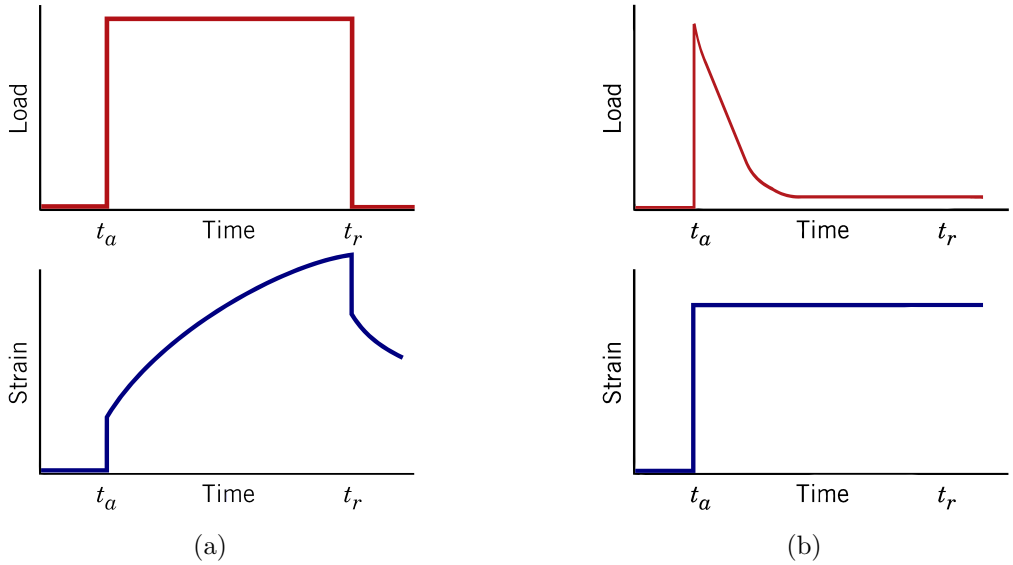

Figure 2.29: (a) Creep test - Constant stress is applied while deformation is measured against time. After a certain time, the stress is removed and the recovery is measured. (b) Stress relaxation test - Constant deformation is applied while the decreasing of the stress against time is recorded

The most common test is the dynamic oscillatory test, where a sinusoidal stress is applied to the material and a sinusoidal strain is measured (fig. 2.30b). Also measured is the phase difference, δ, between the two sine waves. The phase angle is expressed in radians or degrees and will be zero degrees for purely elastic materials and 90 degrees for purely viscous materials. Polymers will exhibit an intermediate phase difference.

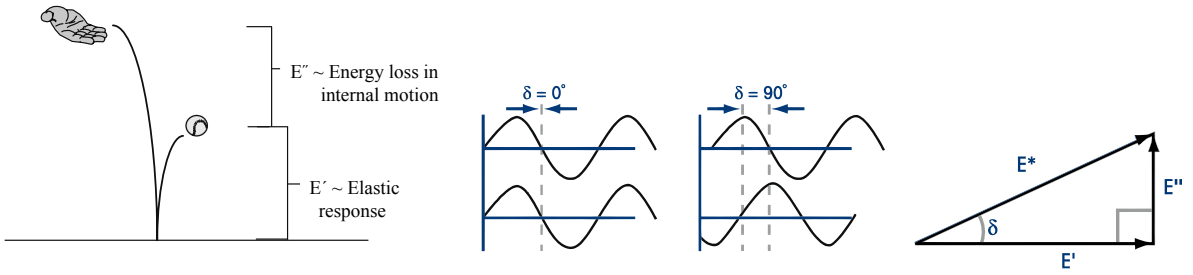

(a) (b) (c)

Figure 2.30: (a) Elastic response of a ball that is dropped. (b) $\delta = 0^o$ for purely elastic materials. $\delta = 90^o$ for purely viscous materials. Polymers exhibit an intermediate phase difference. (c) From the complex modulus E* and δ, the storage modulus E' and the loss modulus E'' can be computed.

Since the modulus is the quotient of stress and strain, the complex modulus E*, can be calculated. From E* and the measurement of δ, the storage modulus E' and loss modulus E'' can be computed (fig.2.30a and 2.30c). The real part E' of the modulus may be used for assessing the elastic properties, while the imaginary part E'' for the viscous properties.

According to ISO 6721-1[68], the storage modulus E' represents the stiffness of a viscoelastic material and is proportional to the elastic energy stored during a loading cycle. It is roughly the same as the elastic modulus for a single, low load and rapid stress solicitation with totally reversible deformation. The loss modulus E'' is defined as being proportional to the energy dissipated during a loading cycle. It represents, for example, energy lost as heat with molecular motions, and is a measure of vibrational energy that has been converted and that cannot be recovered.

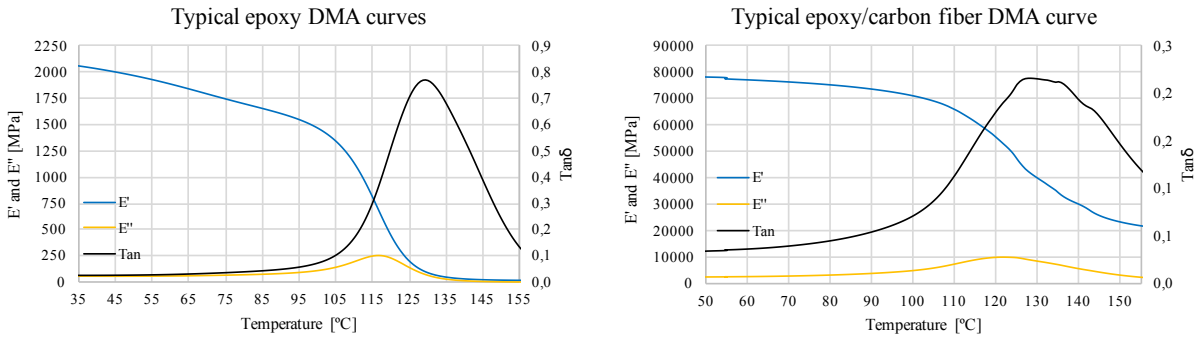

(a) (b)

Figure 2.31: Example of DMA curves for (a) neat epoxy resin and (b) carbon fiber reinforced epoxy.

The tangent of phase difference δ, also known as the loss factor, is the ratio of loss modulus to storage modulus, and is another common parameter that provides information on the relationship between the elastic and loss component. It is a measure of the energy lost and represents mechanical damping or internal friction in a viscoelastic system. High tan δ values are indicative of a material that has a higher plastic strain component, while a low value indicates a more elastic behavior. These parameters can be determined as a function of time, temperature (fig.2.31), frequency, or amplitude (stress or strain) depending on the objective [27, 68].

These variations in measurements with temperature are caused by changes in the free volume of a polymer, which can be defined as the space a molecule has for internal movement. As the space available for the polymer chains to move increases, progressively larger segments may move, giving rise to thermal transitions. Changes in free volume can be monitored as the volumetric change in the polymer, the absorption or release of heat associated with that change, the loss of stiffness, increased flow, or the change in relaxation time.

Although glass-transition temperature (T_g) can be determined by several methods, along this thesis, it will be considered as the temperature associated to the maximum tan δ value. T_g in a polymer corresponds to the expansion of the free volume, allowing greater chain mobility above this transition [69].

Chapter 3

Experimental Work

The experimental part of this work is composed of two different, yet interrelated, parts. Firstly, only two phase nanocomposites, i.e. epoxy reinforced with multi-walled carbon nanotubes, were produced and tested. Experiments involve three types of nanotubes from Future Carbon: untreated (M1), carboxylic acid-functionalized (M2) and thermally oxidized nanotubes (M3). This part is essential to understand the effect of the nanofiller in the polymer matrix. Finally, samples of carbon fiber pre-impregnated with the previous mentioned two phase nanocomposite were fabricated.

3.1 Epoxy Nanocomposite

The experimental work of this part consisted in producing several small-sized test specimens, with different sorts of carbon nanotubes (CNTs)- neat carbon nanotubes, carboxylic functionalized nanotubes and thermally oxidized functionalized nanotubes - with the objective of evaluating the action of this nanofiller on the mechanical and thermal properties of the epoxy/carbon nanotube composite.

It has been reported by several authors [70, 3] that, in general, contents above 1% are rather detrimental to mechanical properties of a polymer and that the critical wt.% threshold was estimated to be between 0.5 and 1 wt.% CNTs [71]. Therefore, content of carbon nanotubes was limited to 0.25, 0.5 and 0.75wt.%. An additional 1.5wt.% was made only for the untreated nanotubes. In addition, the effect of the presence of two dispersion agents - B and R - in the properties of the epoxy/nanotube composite was studied.

Epoxy thermoset resin are widely use as a matrix material, due to its excellent strength and chemical resistance, low shrinkage and processing versatility. However, their inherent brittleness, tendency to delaminate and low fracture toughness can limit their use. Araldite LY556 epoxy resin (Huntsman Corp., US) was used due to it's a space grade classification (appendix B). The technical sheet of the resin reveals, for the mixture system 1 (table 3.1) and for the cure path chosen (2h at 120^{o}C), an expected flexural modulus between 2800-3000 MPa and a glass-transition temperature between 122 - 126^{o}C.

Table 3.1: Infromation of the constituents used for the resin. For more detailed information, see Appendix B

Constituent	Density $[g/cm^3]$	Mix ratio [parts by weight]
Araldite®LY556	1.17	100
Aradur®1571	1.2	23
Accelerator 1573	1.08	3
Hardener XB 3471	1	14

In the following schematic diagram (fig.3.1) it is possible to see the various samples used:

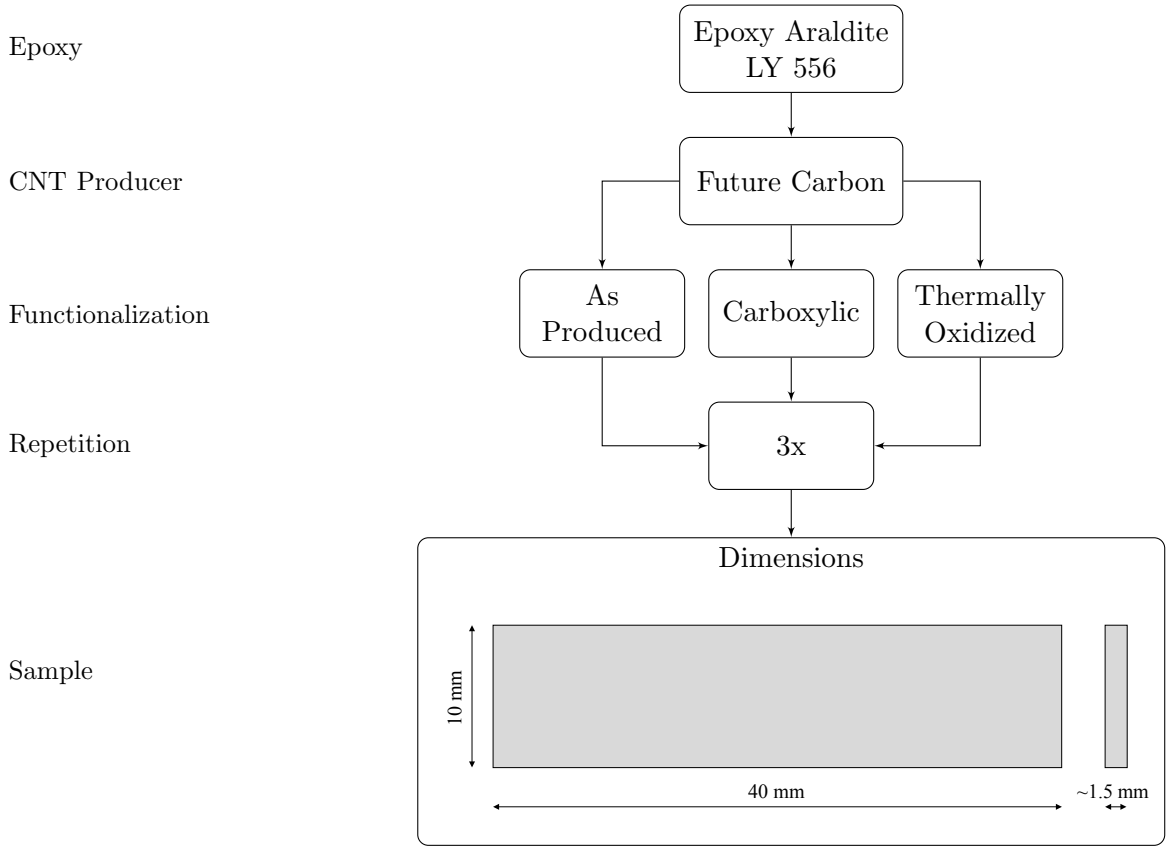

Figure 3.1: Schematic representation of the experimental epoxy nanocomposite samples used.

3.1.1 Porosity

Depending on the production and mixture processes, and on the viscosity of the material, more or less air can get trapped in the sample. Porosity has a negative influence on the modulus of the system, therefore, it is important to know the actual volume of porosity present on each sample. Ishai and Cohen [72, 73] proposed in 1967 a analytical model to predict the elastic modulus of porous epoxies with porosity volume of less than 30%.

$$\frac{E_p}{E_0} = 1 - V_p^{\frac{2}{3}} \tag{3.1}$$

where E_p and E_0 is the modulus of the porous and non-porous, respectively, and the V_p is volume fraction of porosity.

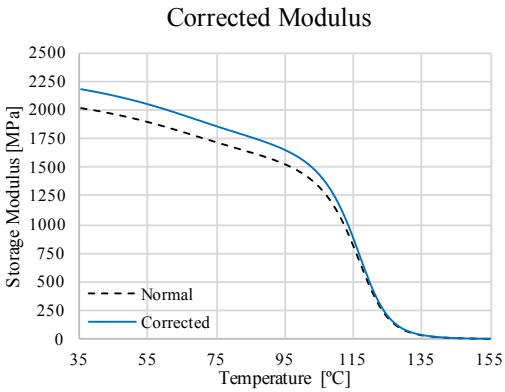

(a) (b)

Figure 3.2: (a) High contrast image of a discarded epoxy/carbon nanotube sample. Superficial porosities are filled with white epoxy powder, resulted from the sandpapering process. (b) Corrected modulus of a 0.5wt.% pristine carbon nanotube epoxy composite.

First, the Archimedes principle was used to determined the density of each epoxy sample, comparing the mass inside and outside distilled water. However, only interior porosity influences the mass inside the water, therefore, the superficial open pores are not included (fig.3.2a). Density variation can be explained by the existence of internal pores filled with air (fig.3.3b), and the presence of these pores reduces the mass value inside the water due to the impulsion force caused by the difference of densities between the water and air. In order to compute the pore volume content for each specimen, a reference density value had to be chosen, and the higher density between the neat epoxy specimens was selected (1.198). Consistently, this specimen revealed to be the least visually void affected. All storage modulus values presented were corrected (fig.3.2b) with the equation 3.1.

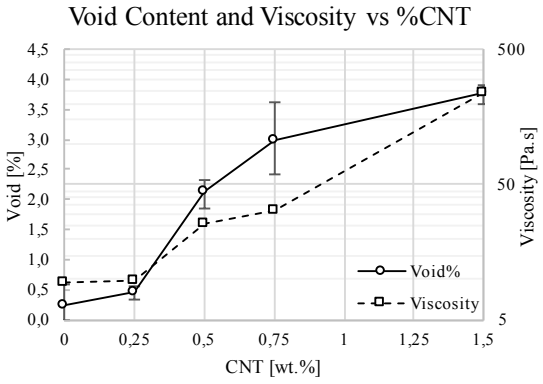

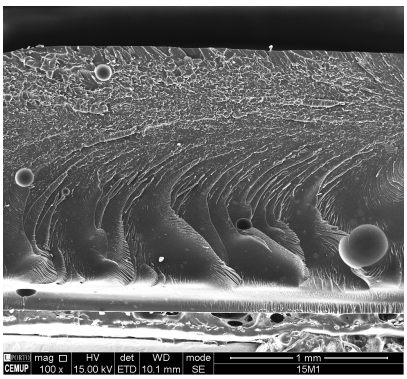

(a) (b)

Figure 3.3: (a) The presence of this voids of air is aggravated by the increasing content of pristine carbon nanotubes and (b) note the spheroidal voids visible in SEM image of the fracture surface of an epoxy sample with 1.5wt.% pristine nanotubes.

The presence of these voids of air is aggravated by the increasing content of carbon nanotubes (fig. 3.3a). All specimens passed a pre-oven "bubble crushing" stage, however, as seen in the section 2.3.2, the viscosity increases with the increasing carbon nanotube content, which proportionally turns the air removal process more difficult.

Since the multi-walled carbon nanotube contents added are rather small (<1.5 wt.%) and their density (see section 2.1) is only slightly superior to the epoxy resin (1.9 to 1.2), the nanotube influence in the epoxy nanocomposite density was neglected.

3.1.2 Experimental Procedure

Mechanical stirring was used to disperse the carbon nanotubes into the epoxy resin (fig.3.4a and 3.4b). With this method it is possible to control the rotation speed and the mixing duration. All solutions were mixed for 60 minutes with a mixing speed of 2000 rpm. The various samples were cured in an oven for 2 hours at 120^oC with a heating rate of 10^oC/min (fig.3.4c). Then, each "square" samples was cut into DMA sized 40×10×1.5mm test specimens with a rotating saw (fig.3.4d and 3.4e).

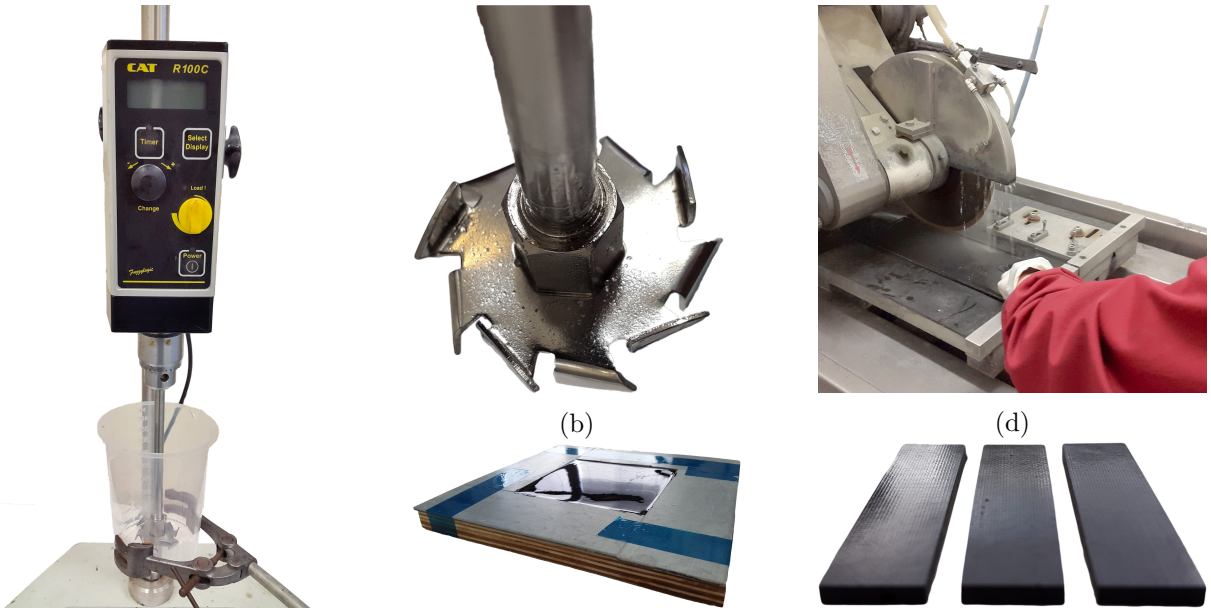

(a) (b) (c) (d) (e)

Figure 3.4: (a) Mechanical stir machine, (b) stirrer blade, (c) mold with nano loaded resin, (d) samples cutting process the samples at INEGI Porto and (e) three samples.

3.1.2.1 Dynamic Mechanical Tests

All tests were preformed with the single cantilever bending mode (fig.3.5), with constant strain of 1% and at a single frequency of 1Hz. The temperature ranged from ambient to 160^{o}C, with a temperature ramp of 5^{o}C/min. The glass-transition temperature (T_g) was determined as the peak in the tanδ. Since the storage modulus decreases to very low values from the T_g, which is around 130^{o}C, higher temperatures were not required. The temperature ramp and the frequency value were chosen taking into account several reports [74, 75, 63, 51]. This mode is useful to study the flexural behavior of the material over a wide range of temperatures and to find the T_g.

Figure 3.5: Single cantilever mode used in the DMA machine.

3.1.3 Results and Discussion

In all dynamic mechanical tests, the curves of tan δ and storage modulus against temperature were obtained. In the following section, these curves are exhibited for the various contents of carbon nanotubes and functionalizations tested. At the end of the section, an overview of the tests is done in order to analyze the behavior of the nanocomposite.

For an addition of **0.25wt.%** of carbon nanotubes, although the storage modulus E' decreases for the pristine (M1) and carboxylic (M2), it increases by more than 6% for the thermally oxidized (M3) (fig.3.6).

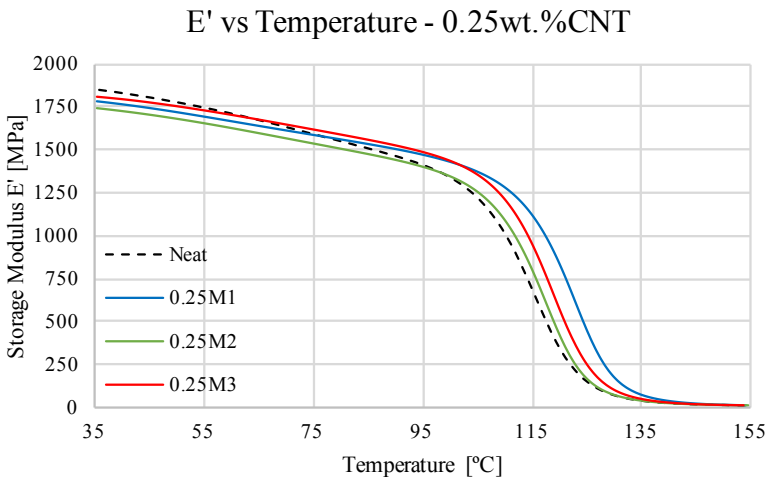

Figure 3.6: Storage modulus against temperature, for 0.25wt.% of each carbon nanotube functionalization.

The glass-transition temperature T_g suffered a considerable increase of 5^oC for a 0.25% addition of the pristine (M1) nanotubes. For the carboxylic (M2) and the thermally oxidized (M3), the T_g shifts are negligible. Loss coefficient maximum values do not reveal any considerable changes, comparing to the neat epoxy (fig.3.7).

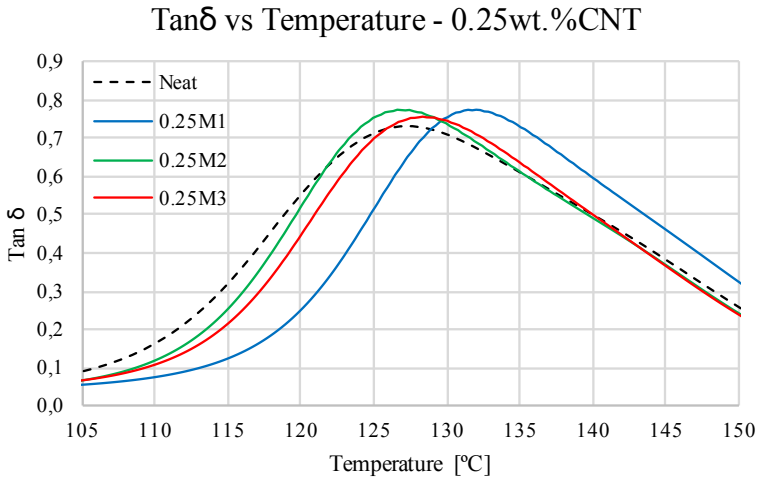

Figure 3.7: Loss coefficient tan δ against temperature, for 0.25wt.% of each carbon nanotube functionalization.

For an addition of **0.5wt.%** of carbon nanotubes, the storage modulus E' suffers a significant increase of more than 17% and 15% for the M1 and M3 functionalizations, respectively. On the other hand, M2 functionalization had nearly no effect on the modulus (fig.3.8).

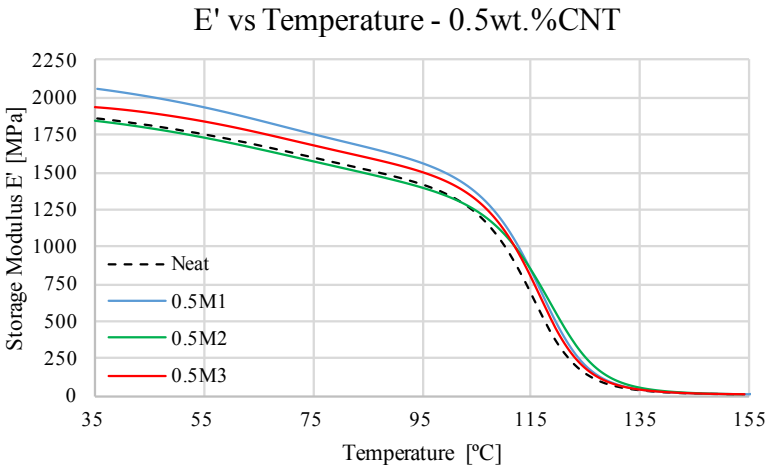

Figure 3.8: Storage modulus against temperature, for 0.5wt.% of each carbon nanotube functionalization.

The glass-transition temperature T_g suffered an increase of 3^oC for the addition of the pristine (M1) and carboxylic (M2) functionalized nanotubes. For the thermally oxidized (M3), the T_g shifts are negligible. Loss coefficient tan δ maximum values do not reveal any considerable changes (fig.3.9).

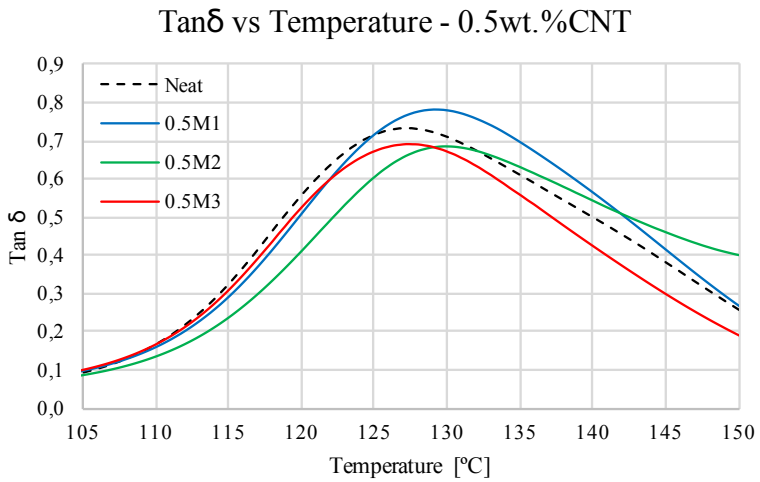

Figure 3.9: Loss coefficient tan δ against temperature, for 0.5wt.% of each carbon nanotube functionalization. It is possible to see the glass-transition temperature T_g shift.

For **0.75wt.%** nanotube content, the modulus suffered a significant increase of more than 18% for the carboxylic (M2). Comparing to 0.5%, pristine (M1) and thermally oxidized (M3) nanotubes reduced their increase in the modulus, with M1 actually canceling the effect and returning to the neat epoxy modulus, and M3 rising the modulus by only 5% (fig.3.10).

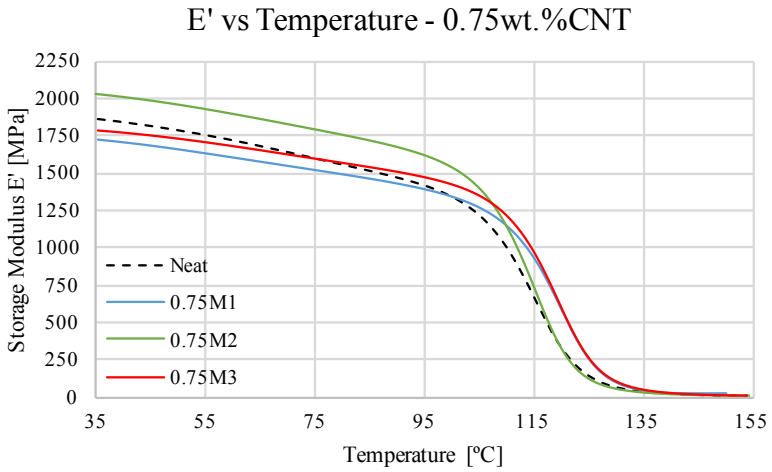

Figure 3.10: Storage modulus against temperature, for 0.75wt.% of each nanotube functionalization.

The glass-transition temperature T_g suffered a considerable increase of 8^oC for a 0.75wt.% addition of the pristine (M1) nanotubes. For the carboxylic (M2) and the thermally oxidized (M3), the T_g shifts are small, with a decrease of 2 degrees for the M2 and an increase of almost 2^oC for the M3. Loss coefficient tan δ maximum values reveal a significant increase of 21 and 13% for the M1 and M2, respectively (fig.3.11).

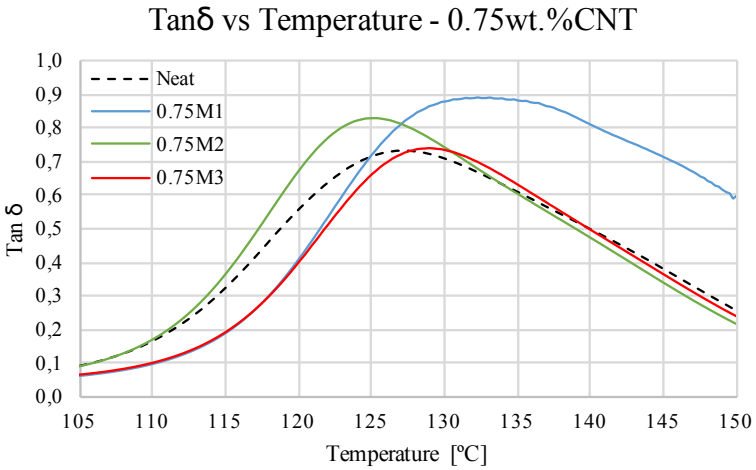

Figure 3.11: Loss coefficient tan δ against temperature, for 0.75wt.% of each carbon nanotube functionalization, showingthe glass-transition temperature T_g shifts for the various CNT functionalizations.

Song et al. [50] reported that the storage modulus of a resin increases with increasing nanotube loading, regardless of the dispersion (fig. 3.12), and explained it with the fact that "nanotubes form a percolated structure due to their high aspect ratio of about 1000 and high surface area". However, in our nanocomposite system, this behavior could not be assessed.

Analyzing the following figure 3.13, it is possible to conclude that 0.25% of pristine (M1) and carboxylic (M2) functionalized nanotubes, do not bring any stiffness enhancement, which induces the fact that, at this low content reinforcement, the nanotubes actually act as defect sites and do not play a reinforcement role. However, the thermally oxidized carbon nanotubes (M3) stand out with an increase in the modulus of more than 6%, which might reveal better bonding between the nanotubes and the matrix permitted by the functionalization, that allows a more efficient load transfer and better dispersion.

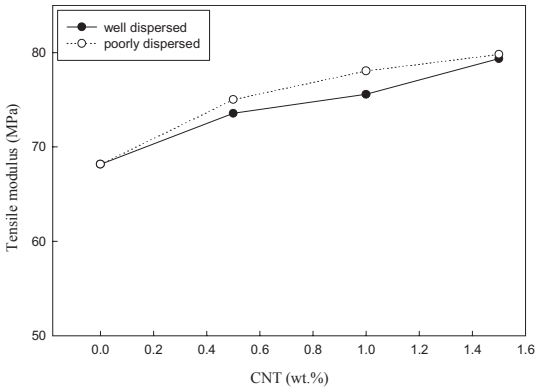

Figure 3.12: Tensile modulus of CNTs/epoxy composites with respect to CNTs loading [50].

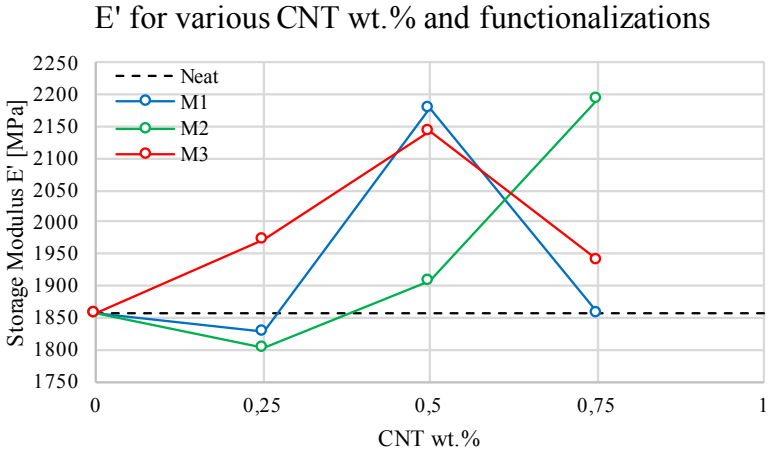

Figure 3.13: Storage modulus E' at 35°C, for the various contents and functionalizations. Interrupted line is the neat epoxy modulus.

When the nanotube contents are raised to 0.5%, M1 and M3 nanotubes stand out, acting as reinforcement and increasing considerably the modulus of the system by more than 17% and 15%, respectively. This can be explained by load transfer to the nanotubes, even if they are in bundles, increasing the modulus of the system. Carboxylic (M2) functionalized nanotubes only reveal a substantial increase (of 18%) for 0.75wt.% addition, while M1 and M3 reduce their influence at this content.

This behavior suggests that M1 and M3 functionalizations have their maximum effect on the storage modulus somewhere between 0.25 and 0.75%, and with contents above the latter, nanotubes tend to agglomerate and the amount of the nanotubes contacting each other increases, triggering an attenuation of the reinforcing efficiency. This can be explained by the reduction of the load transfer efficiency between the nanotubes and the surrounding matrix and a decrease of the effective aspect ratio of the nanotubes [35]. Another factor that could influence is the extremely high viscosity of the resins with M1 and M3, which might hamper the process of dispersion.

M2 nanotubes might have an even higher enhancement of modulus for contents over 0.75%,

which might be explained by the lower viscosity comparing to the other functionalization at the same loading. At this loading, although they show a tendency for a poorer dispersion, they can be dispersed more easily at higher amount of CNT. However, average values with a relatively large scatter can drive to divergent conclusions. As can be seen in figure 3.16, in some cases the scatter is too large to be possible to assess conclusions with total assurance. This scatter can also induce that the dispersion was not even and some samples had more nanotubes than others.

Abdalla et al. [76], as well as in other reports [77, 78], reported that with functionalization it is possible to achieve a better dispersion, which can be assessed by the higher viscosity in the rheological analysis, indicative of stronger interfacial interactions. Therefore, the higher viscosity systems such as M3 are considered the ones with better dispersion (fig. 3.14). In addition, the modified nanotubes (M3) reveal higher enhancement in modulus compared to the pristine (fig. 3.15). Although carboxylic carbon nanotubes are functionalized, they reveal lower viscosity and consistently lower modulus.

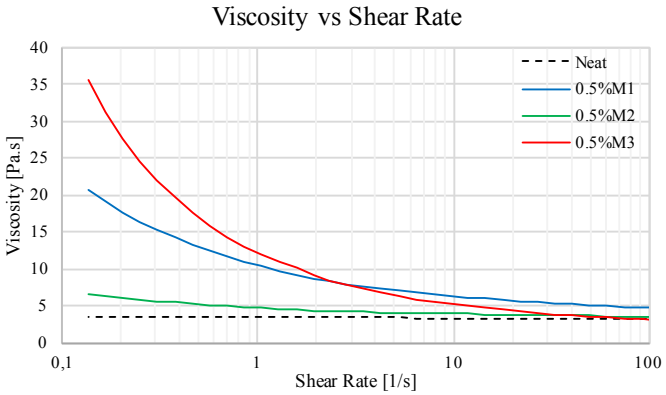

Figure 3.14: Viscosity against shear rate.

High viscosity at the low shear rates, as can be seen in figure 3.14 from our rheological analysis, can be attributed to the formation of a percolated structure by the carbon nanotubes [76]. This structure breaks down as the shear rate increases, resulting in similar viscosities at higher shear rates for all the systems.

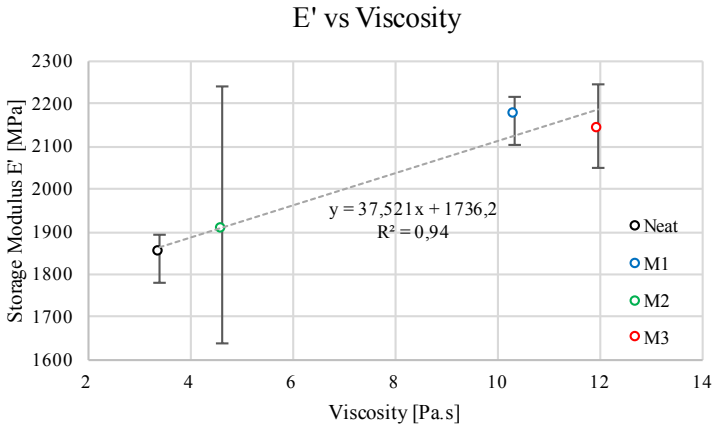

Figure 3.15: Storage modulus against viscosity.

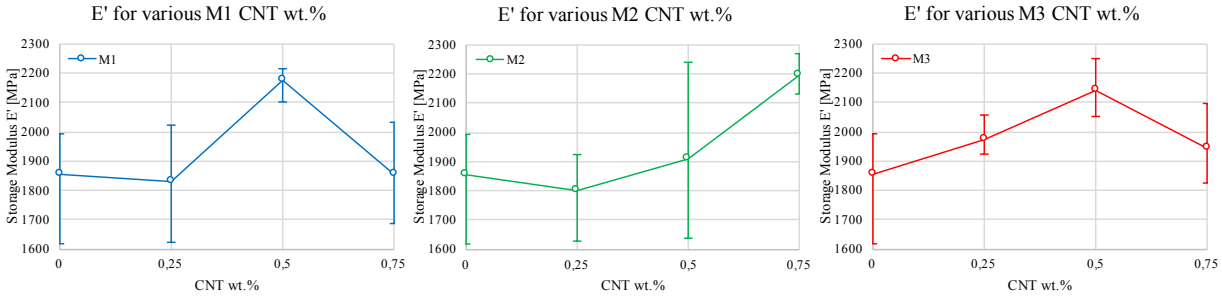

(a) (b) (c)

Figure 3.16: Storage modulus E', with the respective scatter, for the various contents and functionalizations: (a) M1 Pristine (b) M2 Carboxylic and (c) M3 Thermally Oxidized carbon nanotubes.

Glass-transition temperature is known to depend largely on the crosslinking density [26], with T_g rising with increasing crosslink density, and chain rigidity. Both parameters cannot be completely decoupled and the sensitivity of T_g to the crosslinks increases with increasing chain rigidity [79]. However, the cure process in all the epoxy samples was theoretically the same, i.e., 2 hours at 120^{o}C with ramps of 10^{o}C/min, therefore, the crosslink density should be constant. Therefore, the variation of the glass-transition temperature should be caused by the presence of carbon nanotubes, by restricted mobility from enhanced polymer nanotube interactions.. However, similarly to what happened for the modulus, there is not a linear behavior with the nanotube content increasing, as can be seen in figure 3.17.

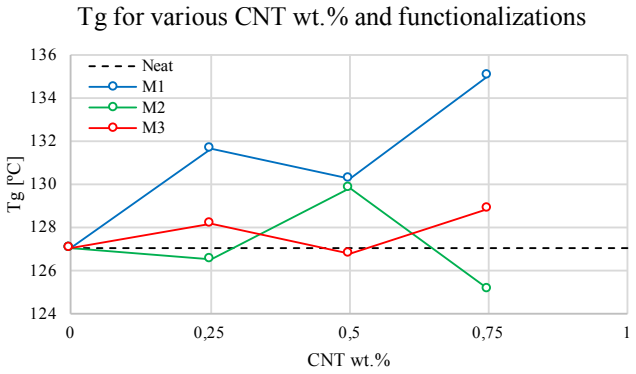

Figure 3.17: Glass-transition temperature (T_g) for the various contents and functionalizations.

Nevertheless, it is possible to conclude that M1 nanotubes have the highest impact, raising T_g by 8^{o}C for the 0.75wt.%. This effect may be related with a balance between the hindrance in the movement of the polymer chain segments that increase the composite rigidity, caused by introduction of the nanotubes as a reinforcement element, and the reduction on the crosslinking degree due to the replacement of the crosslinks sites with nanotubes. This latter is higher for the M3 due to the better dispersion (determined by the viscosity) that increases the surface area. This phenomena needs to be further exploited and related with both variables. This raise enhances the capacity of maintaining the modulus of the system with the increase in temperature.

An inverse relationship can be observed in figure 3.18 between the modulus and the T_g, and can be explained by the presence of carbon nanotubes, which act as defect sites that undermine the crosslink network, consequently decreasing the T_g, but, at the same time, reinforcing the structure and consequently increasing the modulus of the system. This behavior was also

registered for the thermally oxidized (M3) nanotubes (fig. 3.19a), but not for the Carboxylic (M2) (fig. 3.19b).

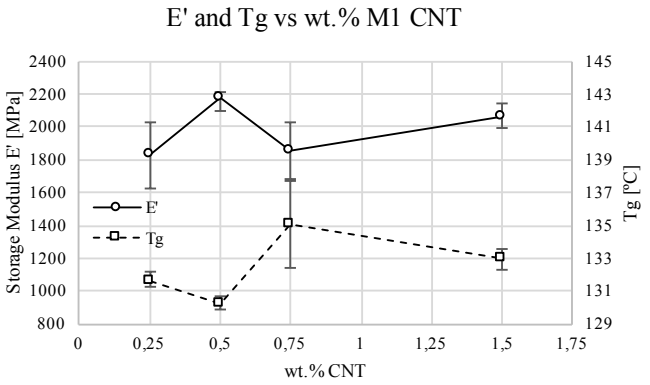

Figure 3.18: Glass-transition temperature (T_g) for the various contents of pristine M1 carbon nanotubes.

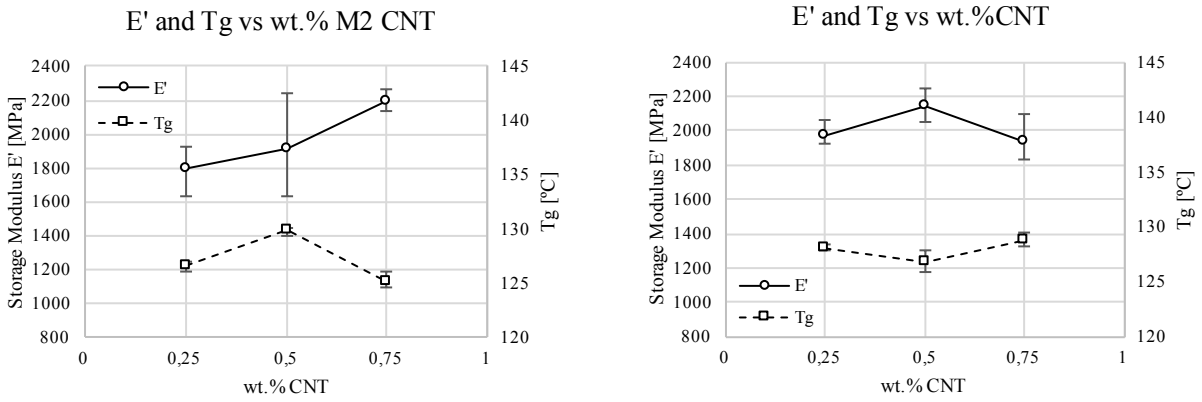

(a) (b)

Figure 3.19: Glass-transition temperature (T_g) for the various contents of (a) carboxylic M2 and (b) thermally oxidized M3 carbon nanotubes.

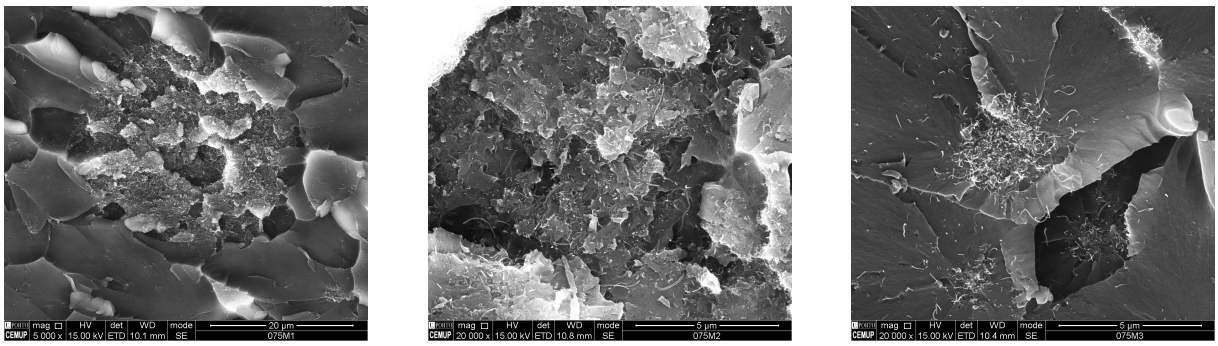

(a) (b) (c)

Figure 3.20: SEM images of 0.75% of: (a) pristine nantubes at 5000× magnification, (b) of 0.75% carboxylic nantoubes 20000× and (c) thermally oxidized at 20000×

Figure 3.20 contains scanning electron microscopy (SEM) images for 0.75wt.% of each functionalization. For untreated nanotubes (fig.3.20a), agglomerations are very noticeable and

with well defined boundaries, which is in agreement with the expected higher tendency to form agglomerates. On the other hand, thermally oxidized exhibit smaller agglomerates (fig.3.20c) and some surrounding disentangled nanotubes that suggest a better dispersion and less tendency to agglomerate. Figure 3.20b exhibits the carboxylic functionalized nanotubes and shows an apparent good dispersion, with nanotubes spread and no well defined agglomerates. It is noteworthy to refer that SEM imaging not always is representative of the dispersion.

3.1.3.1 Dispersion Agents

The effect of two dispersion agents on the dispersion of pristine (M1) carbon nanotubes, as an alternative to the chemical functionalization of their surface, was ascertained. First, the effect on the properties of the epoxy resin was determined, revealing a small effect on the glass-transition temperature (T_g) and on the loss coefficient tan δ value (fig.3.22). Analyzing the effect on the storage modulus of the resin, it is possible to see a moderate increase associated to the R's addition and a substantial increase with the addition of the B (fig.3.21).

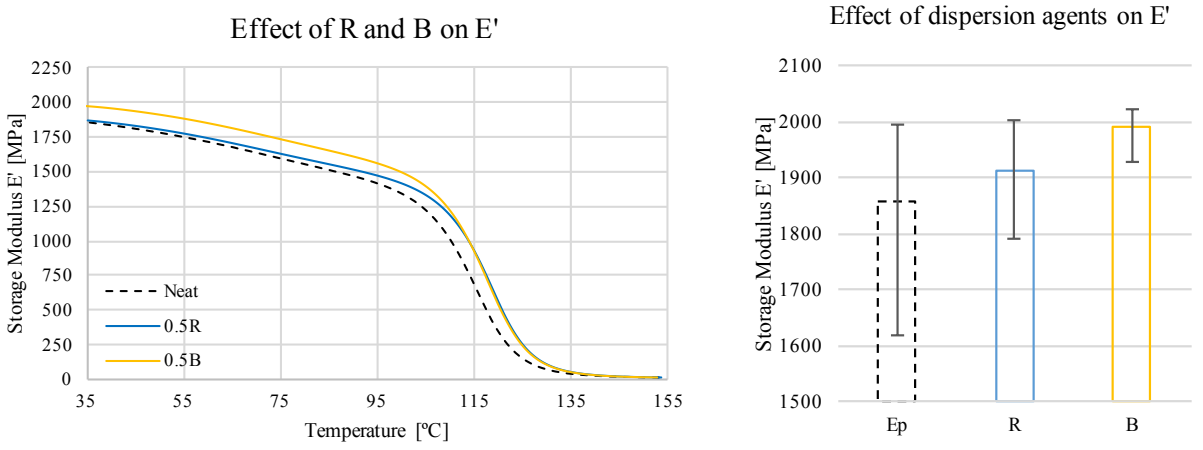

(a) (b)

Figure 3.21: (a) Storage modulus E' against temperature and (b) storage modulus at 35^{o}C, for the neat epoxy resin and the epoxy with 0.5% of each dispersion agent.

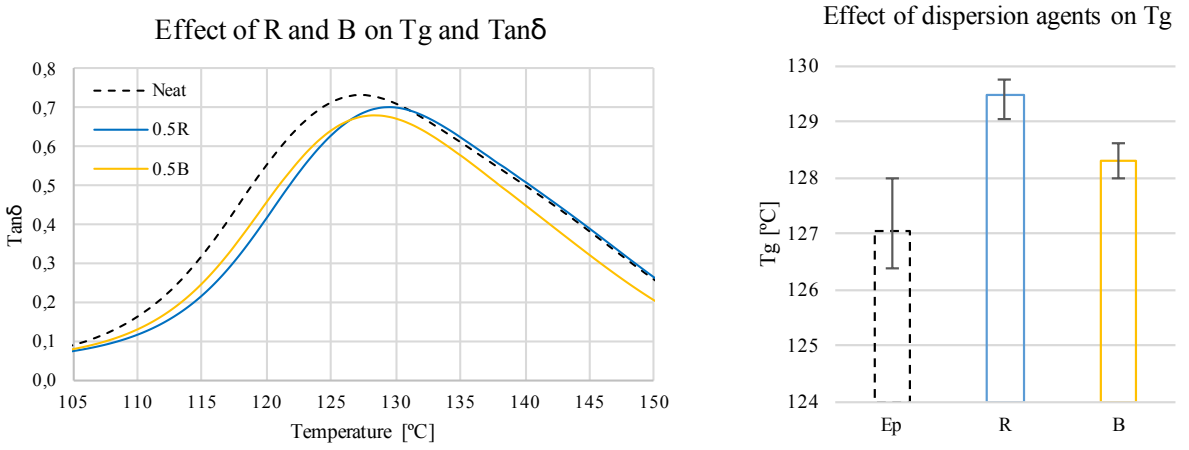

(a) (b)

Figure 3.22: (a) Loss coefficient tan δ against temperature and (b) glass-transition temperature, for the neat epoxy resin and the epoxy with 0.5% of each dispersion agent.

Figure 3.23 and 3.24 exhibit the effect of the dispersion agents to an epoxy/0.5wt.% of pristine carbon nanotube composite, and reveal a considerable decrease of 13 and 15% in the modulus for the R and B addition, respectively. R also lowers the T_g value by more than 2 degrees Celsius, while the effect of B is negligible. This could be caused by local breakage of epoxy crosslinks.

Although enhancements have been reported for some dispersion agents for the Young's modulus in previous reports [37], the implemented dispersion agents did not efficiently worked, at least for pristine carbon nanotubes, deteriorating the modulus of the system, which might be induce by a decrease in the bonding strength between nanotubes and matrix. Since this dispersion agents were made to create a nanostructure within the epoxy, instead of reinforcing, they could be giving additional mobility the matrix polymer chain, which might enhance other properties, such as impact strength for example.

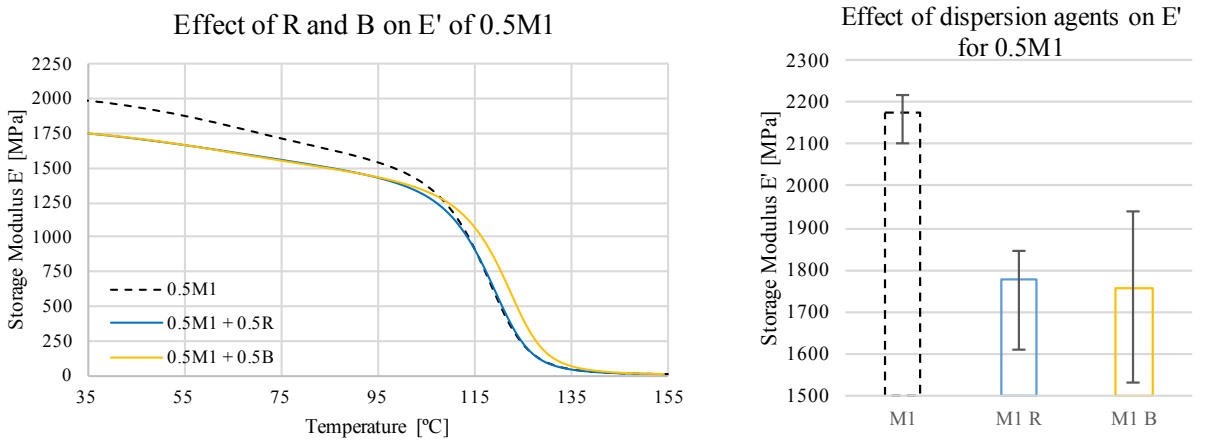

(a) (b)

Figure 3.23: (a) Modulus E' against temperature and (b) storage modulus at 35^{o}C, for the epoxy with 0.5% pristine carbon nanotubes (M1) and the same nanoreinforced resin with 0.5% of each dispersion agent.

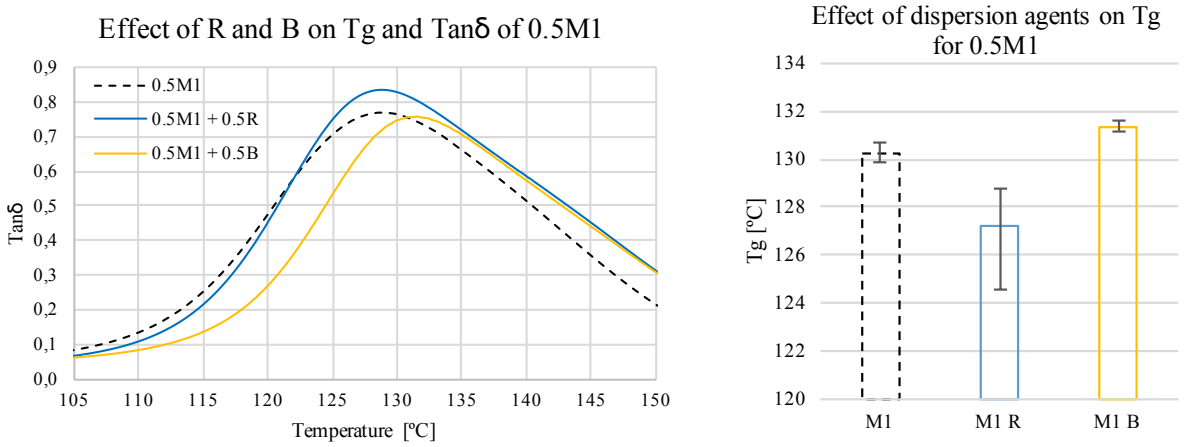

(a) (b)

Figure 3.24: (a) Loss coefficient tan δ against temperature and (b) T_g, for the epoxy with 0.5% pristine carbon nanotubes (M1) and the same nanoreinforced resin with 0.5% of each dispersion agent.

3.2 Carbon Fiber/Carbon Nanotube Nanocomposite

3.2.1 Carbon Fiber Prepreg

The carbon fiber reinforced plastic samples were made using Teijin Tenax IMS60 24k Intermediate Modulus carbon fibers (table 3.2) pre impregnated with the epoxy LY556.

Table 3.2: Properties of the carbon fibers used [80]. For more detailed information, see Appendix B

Type of fibers	Number of filaments	Elastic modulus [GPa]	Tensile strength [MPa]	Elongation at break [%]	Density $[g/cm^3]$
IMS60	24000	290	5600	1.9	1.8

The pre-impregnating process was performed with the machine in figure 3.25a and totally conducted in INEGI facilities. The resulting prepreg in shown in figure 3.25b.

(a)

(b)

Figure 3.25: (a) Prepreging machine and (b) example of a IMS60 prepreg sheet used for the samples.

3.2.2 Experimental Procedure

The experimental work of this part consisted in producing several small-sized test specimens, with 0.5wt.% of different sorts of carbon nanotubes (CNTs), with a three layered lay-up, with the objective of evaluating the action of this nanofiller on the mechanical and thermal properties of the carbon fiber/carbon nanotube composite.

- CNT functionalization - untreated (M1), carboxylic (M2) and thermally oxidized (M3);
- Percentage of addition of CNTs to the Epoxy matrix - None and 0.5 weight % content;
- Number of laminae - 3
- Lay-up orientation sequence - $[0^o, 0^o, 0^o]$.

Initial tests were conducted to the $[0^o]$ specimens, however, due to the extremely low thickness, in the order of 0.1mm, the dynamic mechanical analyzer was working on the edge of its measurable stiffness resolution (around 1000 N/m), showing erroneous values. Therefore, all tests made to the single laminae $[0^o]$ had to be discarded. Although they were manufactured, the $[0^o, 0^o]$ and $[0^o, 90^o]$ were not tested to prevent similar problems.

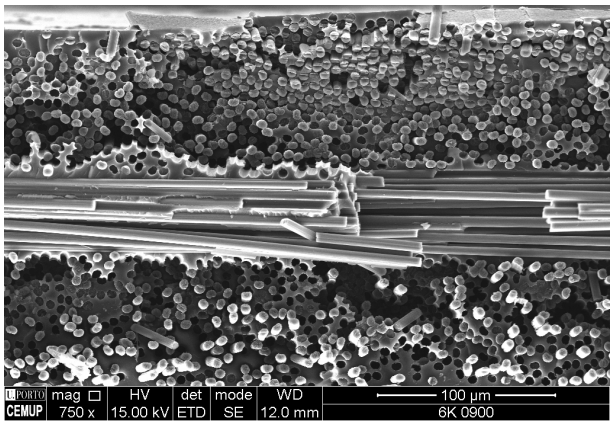

Figure 3.26: SEM image of a three layered $[0^o, 90^o, 0^o]$ lay-up carbon fiber/epoxy composite, not used in this thesis.

Impregnating carbon fibers with epoxy resin with carbon nanotube contents over 0.5wt.%, is rather difficult, due to their high viscosity (see section 2.3.2, figure 2.12a), therefore it's commercial viability is questionable. Thus, and taking into account the higher stiffness enhancement of the epoxy resin achieved in the previous section 3.1.3, the content of nanotube was limited to 0.5wt.%.

3.2.2.1 Sample Preparation

The sample preparation process begun by cutting small 60 by 60 milliliters squares from the previously prepared pre-impregnated carbon fiber sheets. The following images show the sequence of the sample preparation, starting with the cutting of sample 60 by 60 millimeters squares (fig. 3.27a and 3.27b); applying the blue transparent film, which prevents the sample from sticking and retains the excess resin, to the prepreg lay-up (fig. 3.27c); insert the samples,

within Teflon protecting sheets, into the hot plate press to cure at 120^{o}C for 2 hours with an equivalent pressure of 5 bar (fig.3.27d); and the final cured samples (fig. 3.27e and 3.27f)

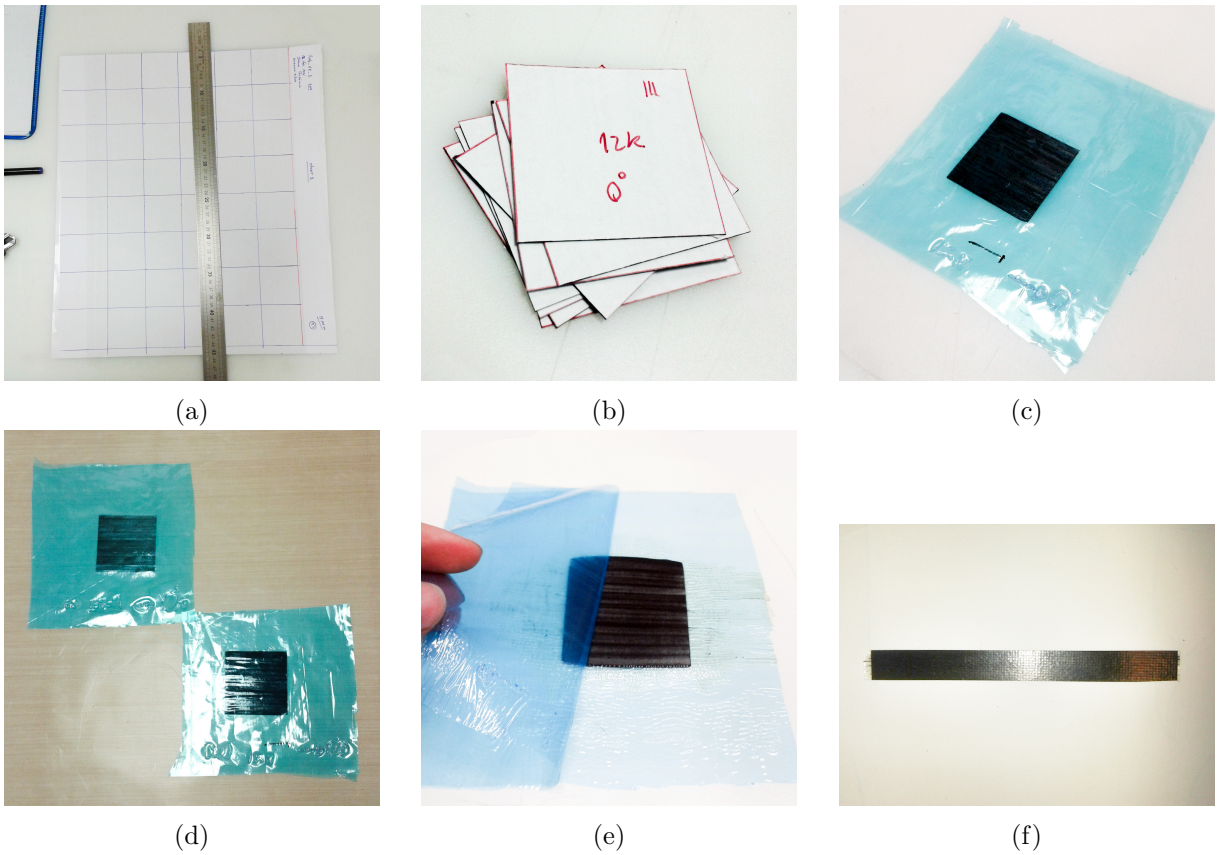

(a) (b) (c)

(d) (e) (f)

Figure 3.27: Preparation sequence of the hybrid composite samples: (a) cutting the squares from the prepreg sheet, (b) 60 by 60 millimeters with the respective reference name, (c) applying the blue transparent film, which prevents the sample from sticking and retains the excess resin, to the prepreg lay-up, (d) insert the samples, within Teflon protecting sheets, into the hot plate press (120^{o}C for 2 hours) and (e) and (f) the final cured samples.

3.2.2.2 Dynamic Mechanical Tests

The single cantilever bending tests were conducted using a Dynamic Mechanical Analysis (DMA) testing machine (DMA Q800 - TA Instruments, see section 2.6). The samples were tested at with constant strain of 1% and single frequency of 1Hz, with a temperature ramp of 4^oC/min and with a temperature range from ambient to 200^oC. The temperature ramp value was chosen taking into account suggested conditions for these materials [69], chapter 10 - *DMA Applications to Real Problems Guidelines*, page 198, with some extrapolation to a lower thickness values. It recommends, for specimens with 1 to 2 millimeters in thickness, a heating ramp of 3 degrees per minute, however, since the the test specimens used were in the order of 0.3 millimeters, the ramp was increased to 4^oC/min, without jeopardizing the even distribution of temperature.

This mode is useful to study the flexural behavior of the material over a wide range of temperatures and to determined the glass-transition temperature T_g, the peak in the tan δ, and the respective loss coefficient tanδ. Since the manufacturing process used was pre-impregnation, it is assumed that the void content is negligible, therefore, there was no need to adjust the results, which has been done in the previous section 3.1.3.

3.2.2.3 Thermogravimetric Analysis

Samples were cut into small pieces ($\approx$ 10 mg), and scanned by a SDT Q600 (TA Instruments, New Castle, US) (fig. 2.26), which is a simultaneous thermogravimetric (TGA) and differential scanning calorimeter (DSC) analyzer.

For the epoxy and the carbon fiber reinforced epoxy samples, during the analysis, the temperature was increased from ambient to 700^{o}C at a rate of 10^{o}C/min. For the carbon fiber samples, the temperature range was from ambient to 1500^{o}C, at the same conditions, only to assess at which temperature carbon fiber start to degrade (table 3.3).

Table 3.3: Parameters used in the thermogravimetric analysis.

Sample	Maximum Temperature [^{o}C]	Heating rate [^{o}C/min]	Purge gas	Purge flow rate [mL/min]
Epoxy	700	10	N_2	100
Carbon fiber	1500	10	N_2	100
Carbon fiber reinforced epoxy	700	10	N_2	100

3.2.2.4 Physical Alignment Method

An additional experiment was conducted to analyze the influence of a physical process in the orientation of the carbon nanotubes during the curing process. To a 60$\times$60 mm^2 pre-impregnated IMS60 carbon fiber, a physical method was applied and maintained during the curing process, in order to lock the carbon nanotubes in an oriented state.

3.2.3 Results and Discussion

3.2.3.1 Thermogravimetric Analysis

With the densities of the resin and carbon fiber and with the experimental values of the residue's mass of the composite and carbon fiber at two temperatures, one bellow the decomposition temperature of the resin (e.g. 24^{o}C), and one between that and the decomposition of the carbon fibers (e.g. 600^{o}C), it is possible to calculate the volume content of carbon fibers of a given sample of composite . Nevertheless, the following assumptions had to be made:

1. The residual weight of the epoxy resin levels off close to the end of the heating program, therefore, at 600^o the residue is considered stable. This is supported by the thermograms of neat resin in figure 3.28.

2. The residue of the carbon fibers is considered stable at 600^{o}C.

3. The carbon fibers do not affect the degradation kinetics of the epoxy resin and thus the measured weight loss is proportional to the weight fraction of the resin.

$$W_{residue} = R_f W_f + R_m W_m \tag{3.2}$$

$$W_{residue} = R_f W_c \%W_f + R_m \left(1 - \%W_f\right) W_c \tag{3.3}$$

and in order to the weight percentage of fiber

$$\%W_f = \frac{W_{residue}/W_c - R_m}{R_f - R_m} \tag{3.4}$$

with W as the weight measured in the TGA, $\%W$ as weight percentage in the composite, R as the residue's weight percentage obtained from the TGA and the subscripts f, m and c referring to the fiber, matrix and composite, respectively [81]. It is necessary to convert the weigh fraction into a volume fraction:

$$\%V_f = \frac{\%W_f}{\%W_f/100 + (\rho_f/\rho_m) - (\rho_f/\rho_m) \times \%W_f/100} \tag{3.5}$$

TGA analysis for three types of carbon fibers, including the IMS60 carbon fiber used, is presented in figure 3.28. It is noteworthy that the initial 1 to 2% mass loss, at around 300-400^{o}C (fig. 3.29), is caused by the degradation of the sizing used in the fibers, values that are consistent with the data sheets in B.

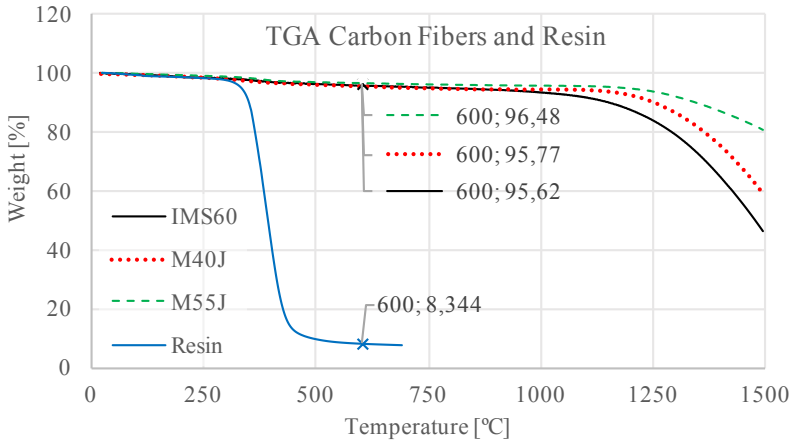

Figure 3.28: Thermogravimetric analysis for three types of carbon fibers, including the IM60 carbon fiber used, and for the LY556 epoxy resin.

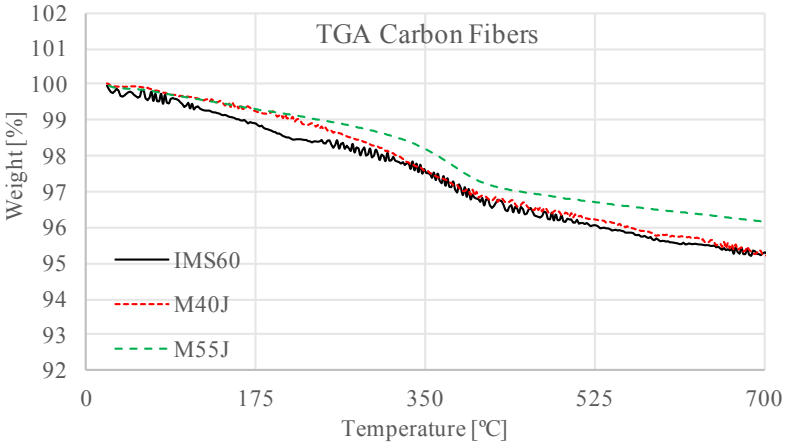

Figure 3.29: Zoomed in TGA of the carbon fibers. The 1 to 2% mass loss is caused by the degradation of the fiber sizing.

3.2.3.2 Dynamic Mechanical Analysis

In figure 3.31 is possible to see the effect of the addition of carbon nanotubes into the matrix on the flexural storage modulus of the composite. The content of fiber of a fibrous composite, since it is the reinforcement component, is crucial in the final mechanical properties, thus, it is mandatory to compare values with the same fiber volume content. Therefore, fiber content was determined, using the Thermogravimetric Analysis (see section 2.5), and all values of storage modulus are computed for a constant 60% fiber volume.

By applying the rule-of-mixtures in order to have an estimation of the modulus, DMA results of the flexural storage modulus revealed to be substantially inferior to the expected. In figure 3.30, it is possible to analyze this disparity for the neat epoxy reinforced with 60% IMS60 carbon fiber content. This might be explained by the misalignment of the carbon fibers, caused by the flow of epoxy induced by the pressure applied, effect that was amplified by the small scale of the samples. Being a laboratory impregnating process, not fully optimized for this sort of carbon fiber and filament count, could also influence the quality of the process. In addition, one should further consider the effect of being in a flexure deformation mode, which may lead to a lower modulus when compared to a deformation in tension [82, 83]. Thus, storage modulus values were analyzed relatively to the neat composite, and not to the expected absolute value.

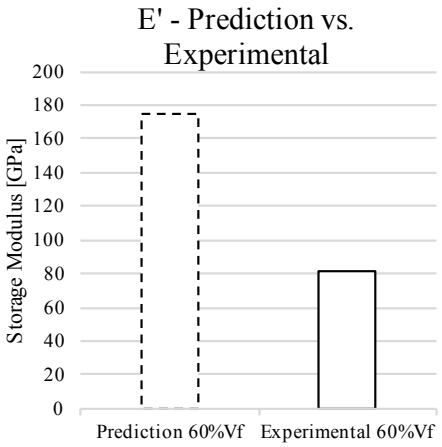

Figure 3.30: Experimental results of neat system compared to rule-of-mixture estimation of the modulus.

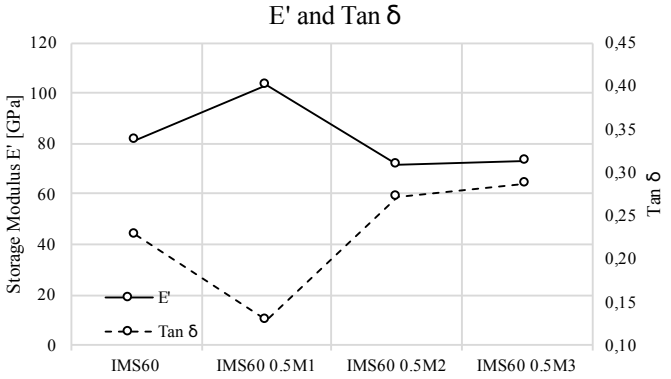

Figure 3.31: Results of tan δ and storage modulus for IMS60 composite specimens. It is noteworthy the consistent inverse relationship between the modulus and the tan δ values.

The storage modulus of the composite is affected by the quality of the bonding between the reinforcements, fibers and nanotubes, and the epoxy matrix. This quality of the interfacial adhesion can be characterized by the value of tan δ [84]. Thus, the system with the highest reinforcement (27%) is the one with pristine carbon nanotubes, as can be seen in figure 3.31. The other two systems, with carboxylic (M2) and thermally oxidized (M3) carbon nanotubes, exhibited a 10 and 12% decrease in the modulus, which suggests a reduction in the crosslinking degree due to the introduction of well dispersed nanotubes.

The tan δ can also be affected by the fiber volume fraction and, therefore, the maximum values of tan δ have to be computed for the same 60% fiber volume fraction [84]. Although the relationship between the tan δ and the fiber content is unknown, the prediction to a 60% volume fiber (black dots) should not result in substantial errors, as can be seen in figure 3.32. The blue interrupted lines are predictions considering the values of the tan δ of the epoxy nanocomposites (without fiber reinforcement) and the yellow interrupted lines are prediction based on the assumption that 100% fibers means a null value of tan δ, which could not be confirmed.

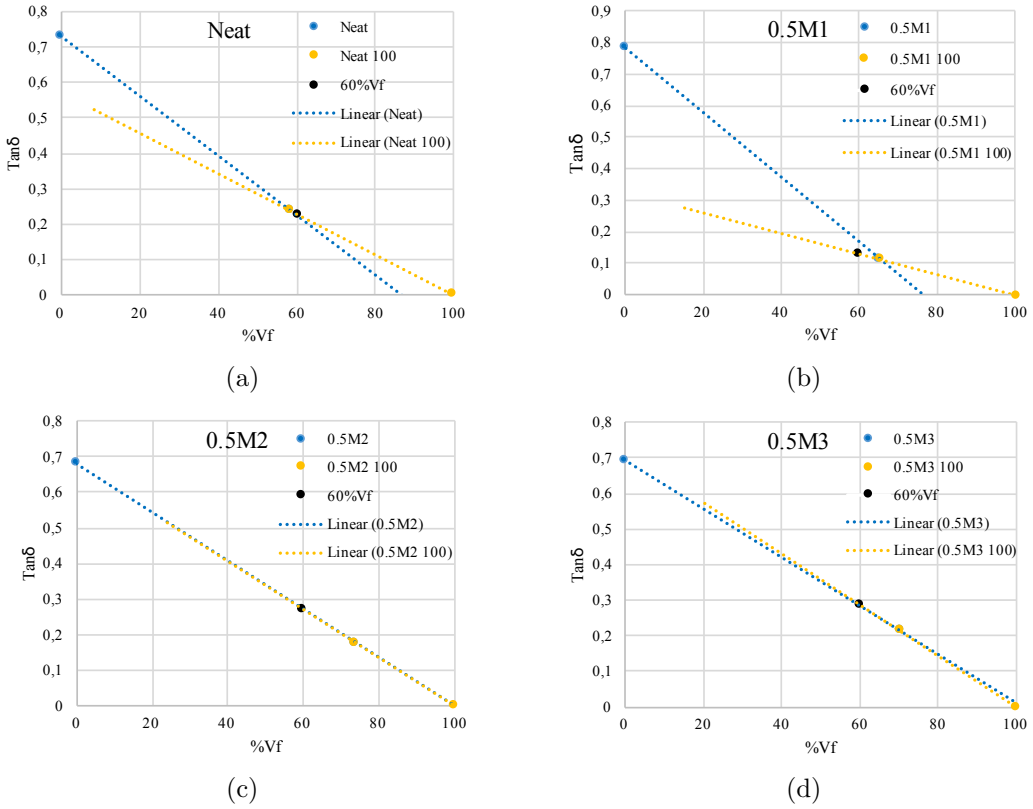

Figure 3.32: Predictions of the tan δ for 60% volume fiber for: (a) Neat systems, systems with (b) 0.5wt.% pristine nanotubes (M1), (c) 0.5wt.% carboxylic nanotubes (M2) and (c) 0.5wt.% thermally oxidized nanotubes (M3).

Although the fiber sizing might affect the tangent value [85], for this analysis, only IMS60 carbon fiber reinforced epoxy samples were considered, maintaining the same sizing conditions in all tests.

In figure 3.33, the glass-transition temperature (T_g) of each sample are compared. It is possible to see that all samples with carbon fiber registered a consistent, yet small, increase of the T_g, due to the presence of the carbon fibers [86]. Such increases are explained by the filler surface area effects, restriction of polymer molecular motion, packing density changes of polymer chains and modification of conformation and orientation of the polymer chains segments as a result of the adhesion between the fiber and the matrix [87, 88].

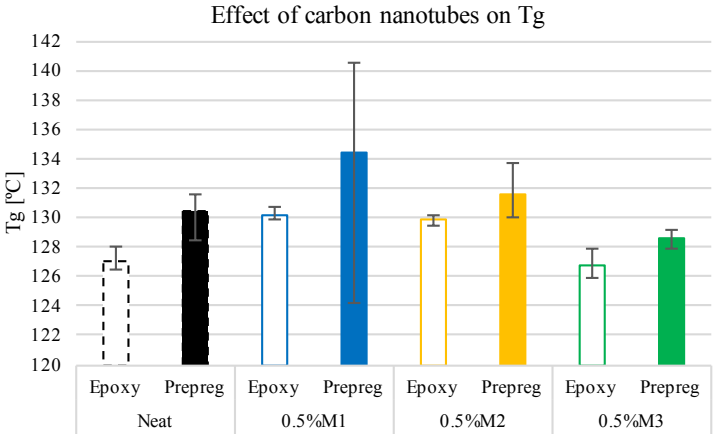

Figure 3.33: The effect of the nanotube functionalization on the glass-transition temperature T_g.

Pristine (M1) and carboxylic functionalized (M2) nanotubes exhibited an increase in the T_g of almost 4^{o}C for the former and around 1^{o}C for the latter. This can be related to a balance between the hindrance in the movement of the polymer chain segments that increase the rigidity of the system, caused by introduction of the nanotubes as a reinforcement element, and the reduction on the crosslinking degree due to the replacement of the crosslinks sites with nanotubes. This phenomena needs to be further exploited and related with both variables. The addition of 0.5 wt.% of thermally oxidized (M3) carbon nanotubes resulted in an almost 2 degree decrease, which suggests a reduction in the crosslinking degree due to the introduction of well dispersed nanotubes. The raise in the glass transition temperature might enhance, even if marginally, the capacity of maintaining the modulus of the composite system with the increase in temperature.

Physical Alignment Method Results

Dynamic mechanical tests performed to a sample of carbon fiber reinforced epoxy with 0.5wt.% pristine carbon nanotubes and the same material with a physical alignment process, exhibited a 14% higher flexural storage modulus, for the same 60 % fiber content. In figure 3.35a, the marks from the bottom to the top are made by the Teflon sheet surface, were the sample was cured, however, it is possible to see several white nanoscale filaments with a clear orientation from the bottom left to the top right. Figure 3.35b and, with further magnification, figure 3.36 revealed a two dimensional perpendicular orientation with a interlocking between nanotubes, somehow similar to a football goal net. The scale difference, with the diameter of the tubes around 30-40 nm, excludes the possibility of these regular marks being made by the Teflon sheet.

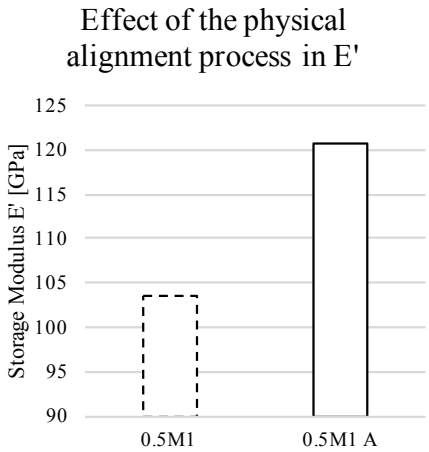

Figure 3.34: Storage modulus comparison between a sample of carbon fiber reinforced epoxy with 0.5wt.% pristine carbon nanotubes and the same material subjected to a physical alignment process.

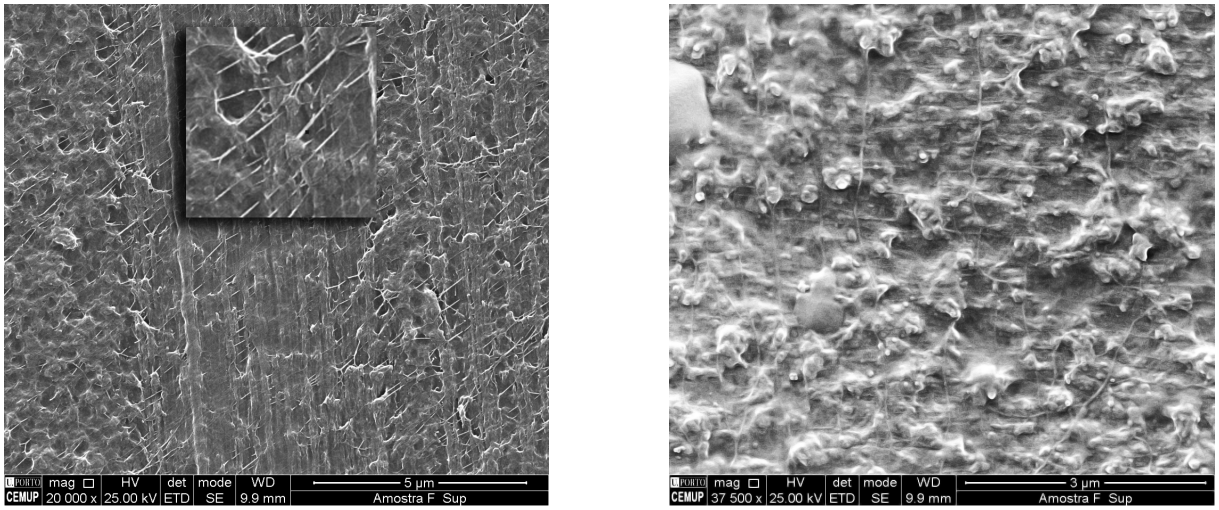

(a) (b)

Figure 3.35: SEM imagens from CEMUP, University of Porto, of the sample, reveal the effect of the method used: (a) 20000x magnification image where several white nanoscale filaments have a clear orientation from the bottom left to the top right, and (b) 37500x revealed a two dimensional perpendicular orientation between nanotubes, similar to a football goal net.

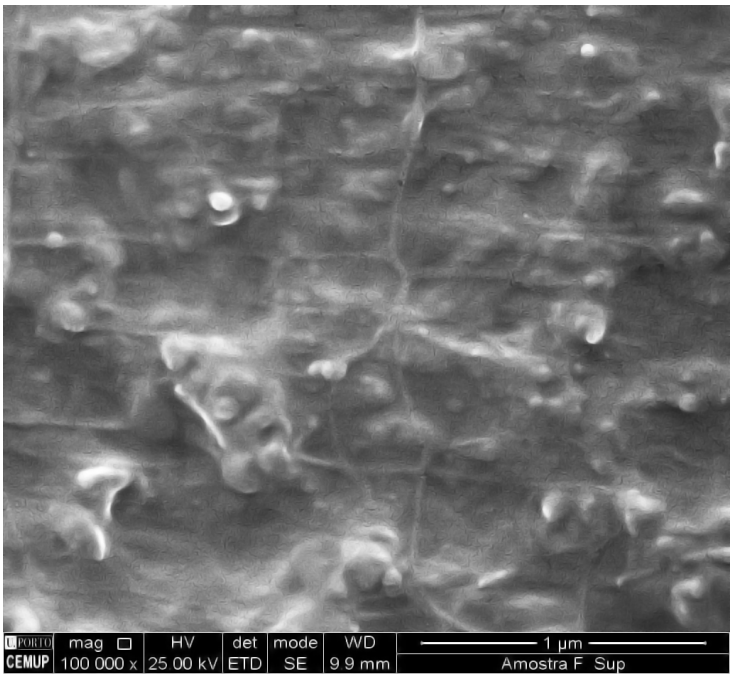

Figure 3.36: Further magnification at 100000x of figure 3.35b, revealing a two dimensional perpendicular orientation between nanotubes, similar to a football goal net.

This process might be the cause of the increase in modulus, since it orients the nanotubes into two perpendicular directions, creating a anisotropic behavior. It is possible to conclude that this process effectively oriented the nanotubes present in the matrix and improved significantly the storage modulus. However, the actual direction of orientation of the nanotubes has to be reconfirmed. Further tests should be performed to assess other relevant properties.

Chapter 4

Prediction of the Mechanical Properties of Nanocomposites

The reinforcement effect of carbon nanotube in a polymeric matrix depends not only on their content within the hosting system according to traditional micro-mechanics of composites but also by the level of dispersion within the final nano-composite. In a CNT/polymer composite, aggregation or networking of CNT may become a defect causing a deterioration of mechanical properties for the final nano-composite material [29].

The prediction of the mechanical properties of nanocomposites require knowing some important factors, such as the properties of the nanofiller and polymer matrix, the processing methods and conditions, the structure and morphology of the nanocomposites and, more important, the nature of the interfacial region.

The prediction methods for nanocomposites properties are available at many different levels of complexity, length and time scales, such as molecular, microscale, mesoscale and macroscale (fig.**??**). They can be divided into two main categories: Analytical and Numerical.

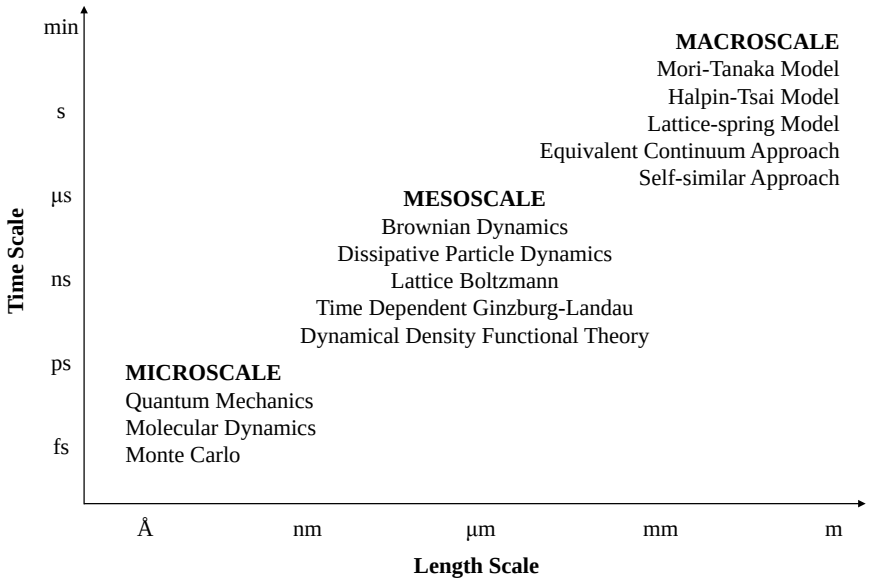

Figure 4.1: Various Modeling and simulation techniques for polymer nanocomposites [7].

Analytical models have on their side the simplicity and minimal computational resources requirement. However, this simplicity may compromise the level of detail that can be considered and the accuracy of the predictions. Thus, analytical models are mainly used for rough preliminary studies, since they are based on an idealized morphology rather than on the real detailed morphology of the system.

On the other hand, **numerical simulations** can provide more accurate predictions, since their models are based on more realistic physics and detailed morphology of the system of interest. With the increasing need for understanding of nanocomposites properties allied with the increasing computational power and efficiency, further sophisticated numerical models will be developed and rapid numerical simulation with enhanced accuracy will be possible, somehow overtaking the preliminar rough analytical models.

4.1 Analytical Models

Analytical, or theoretical, models consist of mathematical models that describe changes in a system with closed-form solutions to equations. There are analytical models that have been developed to general use and others to highly specific applications. Micromechanical models are normally developed to analyze composite materials on the level of individual constituents. With the properties of each constituent, these models can predict the properties of the whole composite material. In order to statistically represent the local continuum properties, an representative volume element (RVE) is created and may be used in a repeating or periodic sequence [89].

Although theoretical models have been extensively explored for predicting the effective properties of complex materials, some inherent limitations restrain their capability [90]:

- Most existing analytical models are based on simplified physics and structures, often with some assumptions to turn the problem ideal. This may make the models simple and easy to use, but simplifications also restrict them to only simple structures. Consequently, none of the existing models is able to manage directly the effects on the material properties of morphological changes in the microstructure;
- Improving accuracy narrows model applicability. Combining models for more complex structures leads to an escalating computational needs;
- Empirical parameters might not have physical understanding, such values have to be determined case by case and might turn the model more difficult to use;
- Phase interaction in multiphase systems, such as liquid-solid wetting, can be a problem to the current models;
- Even for the relatively successful theoretical models, they can only calculate the properties of existing materials, rather than make predictions for new material. Therefore, they are not of much value in optimization or design for new materials.

Micromechanical methods can account for discontinuities, for interfaces between constituents, and for coupled mechanical and nonmechanical properties [89]. This methods have been widely used to estimate the mechanical and transport properties of composite materials and have recently been extended to estimate them for polymer nanocomposites as well. These models are still preferred in the study of nanocomposites due to their reasonable accuracy for simplified structures and their predictive power associated with low computational cost and ease

of use.

The significant scale difference between carbon nanotubes and typical carbon fibers might affect the predictions. Therefore, for modeling the mechanical behavior of nanocomposites, in particular for single-walled carbon nanotube (SWCNT) polymer nanocomposites, two methods have been developed that have the scale difference into account: the Equivalent-Continuum Approach [91] and the Self-Similar Approach [92].

4.1.1 Micromechanical Models

Micromechanical models provide a simple approach to predict overall properties of composites, using geometries and properties of the individual phases that constitute the materials. A wide variety of models, which have been developed to predict the elastic properties of traditional fibrous composites, are based on each constituent's properties and on the geometry of the reinforcement [93]. This approach is generally called "micromechanics" because the models deal with the geometric heterogeneity at the microscopic scale (microstructures).

4.1.1.1 Rule of Mixtures

For continuous fiber-reinforced composites, it is well known that the effective axial Young's modulus follows the rule-of-mixtures [93]. This rule, according to carbon nanotube (CNT) nomenclature, takes the following form:

$$E_c = V_{CNT}E_{CNT} + (1 - V_{CNT})E_m \tag{4.1}$$

where E is the elastic modulus and V stands for the volume fraction, respectively, and subscripts c, CNT and m represent composite, carbon nanotube and matrix, respectively. Nevertheless, carbon fibers and carbon nanotubes are rather different reinforcements. Hence, George et al. [94] included a coefficient of efficiency K, creating a special form of the rule of mixtures, more adjusted to the nature of the nanotubes.

$$E_c = KV_{CNT}E_{CNT} + (1 - V_{CNT})E_m \tag{4.2}$$

where K is the carbon nanotube efficiency parameter, which is computed with the following formula:

$$K = 1 - \frac{\tanh(n.s)}{n.s} \tag{4.3}$$

with s as the aspect ratio (l/d) of the nanotubes and

$$n = \left(\frac{2E_m}{E_{CNT}\,(1 + \upsilon_m)\,ln\left(\frac{1}{V_{CNT}}\right)} \right)^{\frac{1}{2}} \tag{4.4}$$

This modification of the rule of mixtures seeks for a better prediction, taking into account the aspect ratio s of the CNTs, the E_m/E_{CNT} ratio, the matrix's Poisson ratio υ_m and the CNT volume fraction.

Several authors reported the validity of the Rule of Mixtures in predicting the elastic modulus of nanocomposites. Griebel et al. [95] examined the elastic moduli of infinite and

short nanotube embedded in polyethylene through molecular dynamics simulations, compared the elastic moduli with the Rule-of-Mixture predictions and found it suits well for the longer nanotubes, failing for the short-nanotube composites. Li and Chou [96] examined the effect of interfacial load transfer on the stress distribution in carbon nanotube/polymer composites and concluded that the effective Young's modulus of the composite calculated from the simulation was in good agreement with that predicted from the rule-of-mixture. However, these authors only compared the rule of mixtures not with experimental data, but with simulations and considering ideal bonding conditions between the matrix and the nanotube, which is not the case.

The equation 4.2 can be modified to estimate elastic properties of carbon fiber/carbon nanotube reinforced polymers:

$$E_c = K_1 V_1 E_1 + K_2 V_2 E_2 + [1 - (V_1 + V_2)] E_m \tag{4.5}$$

where V are volume fractions, E are the elastic modulus, 1 and 2 represent carbon nanotubes and carbon fibers, respectively, E_m is the elastic modulus of the polymer matrix, K_1 is the CNT efficiency parameter and K_2 is the carbon fiber efficiency parameter, which is equal to 1 for continuous aligned fibers in the direction of alignment [5].

4.1.1.2 Modified Rule-of-Mixtures

A modified form of the rule of mixtures, proposed by Omidi et al. [97], was reported to accurately predict the mechanical properties of multi-walled carbon nanotubes/epoxy composites, for both low and high contents of multi-walled carbon nanotubes. It includes an exponential shape function, a length efficiency parameter, an orientation efficiency factor and a waviness parameter for a better prediction.

$$E_{C/M} = (k_l k_o k_w E_{NT/M} - 1) V_{NT} . e^{\alpha V_{NT}} \tag{4.6}$$

where

$$E_{C/M} = \frac{E_C - E_M}{E_M} \tag{4.7}$$

and

$$E_{NT/M} = \frac{E_{NT}}{E_M} \tag{4.8}$$

in which E_C, E_{NT} and E_M are the longitudinal elastic modulus of the composite, carbon nanotube and the matrix, respectively.

The elastic modulus of composites predicted by Eq.4.6 lies between the bounds given by the following equation:

$$(E_{NT/M} - 1) V_{NT} \leq E_{C/M} \leq \frac{(E_{NT/M} - 1) V_{NT}}{E_{NT/M} + (1 - E_{NT/M}) V_{NT}} \tag{4.9}$$

The nanotube length efficiency parameter k_l ranges from 0 to 1, and approaches 1 for large volume fractions of high aspect ratio CNTs.

$$k_l = 1 - \frac{\tanh \lambda\tau}{\lambda\tau} \tag{4.10}$$

in which

$$\lambda = \frac{2l}{d} \tag{4.11}$$

is the CNT aspect ratio, with l is the length and d is the diameter of CNT and

$$\tau = \sqrt{\frac{-2}{E_{NT/M}(1-\upsilon_M).\ln(V_{NT})}} \tag{4.12}$$

υ_M is the matrix Poisson's ratio, typically around 0.3.

The orientation parameter k_o is equal to $\frac{1}{5}$ for 3D-randomly orientated nanotubes.

The waviness parameter k_w ranges from 0 to 1, with 1 being totally straight nanotubes (fig. 4.2). This parameter is considered a fabrication-related factor. For multi-walled carbon nanotube reinforced epoxy, a value of 0.4 for k_w is considered by the author to be a good match.

$$k_w = 1 - \frac{a}{w} \tag{4.13}$$

in which a and w are the amplitude and half-wavelength of a curved CNT.

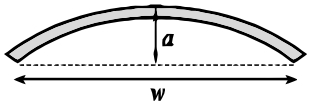

Figure 4.2: Waviness parameter [97]

The relationship between E_C and V_{NT} is typically considered linear. However, considering experimental data reported in the literature [28, 98, 51, 75, 99, 100, 56], this relationship is nonlinear, especially for higher volume fraction of CNTs. Therefore, the exponential term $e^{\alpha V_{NT}}$ is present, to cover a wider range of wt.% of CNTs. The α parameter, present in this exponential factor, is computed with

$$\alpha = \frac{\ln \beta}{\hat{V}_{NT}} \tag{4.14}$$

where

$$\beta = \frac{\hat{E}_{C/M}}{(\hat{k}_l k_o k_w E_{NT/M} - 1)\hat{V}_{NT}} \tag{4.15}$$

and

$$\hat{E}_{C/M} = \frac{\hat{E}_C - E_M}{E_M} \tag{4.16}$$

Parameters with a hat sign should be determined experimentally via tensile test and with curve fitting procedure for a given wt.% of nanotubes. In order to determine the value of the α parameter in equation 4.6 only one dataset of the tensile test may be used for a MWCNT/epoxy composite specimen. The composite's tensile strength theoretically can also be predicted, replacing the various modulus values (E_C, E_{NT} and E_M) with the values of the tensile strengths (S_C, S_{NT} and S_M).

Omidi et al. elaborated a comparison between the present prediction model and a few other micromechanical prediction approaches, namely the Halpin–Tsai model, the Halpin–Kardos model and the modified series model (fig. 4.3). It can be seen that the predictability of the former micromechanical models rapidly fail with an increase of the nanotube content.

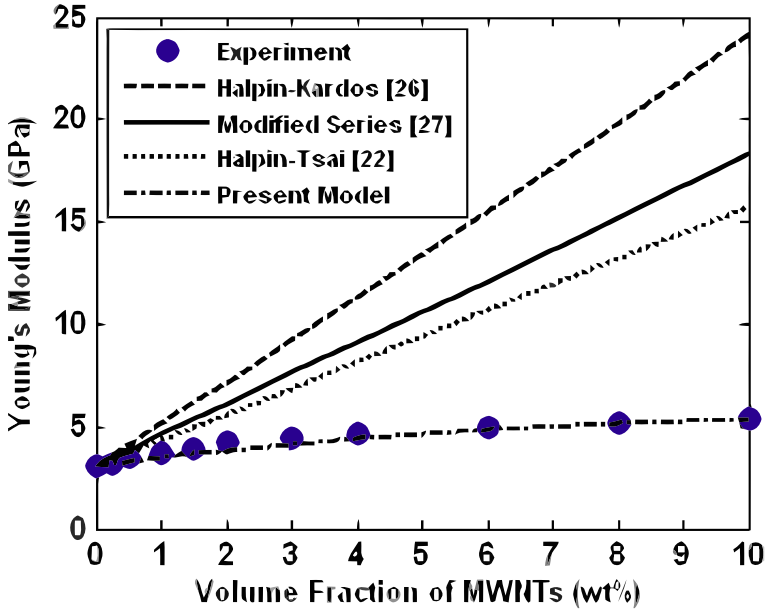

Figure 4.3: Comparison between the presented model and other typically used models [97].

Comparative studies were carried out with other experimental data in the literature to verify the efficiency of the proposed model. Figure 4.4 exhibits an example, correlating the presented model with experimental results from [101]. For a waviness parameter k_w equal to 0.3 for Young's modulus and 0.35 for tensile strength, the proposed model is able to predict the modulus and the tensile strength accurately. The small differences between the waviness parameters were attributed to the interfacial debonding which affects the yield strength of composites.

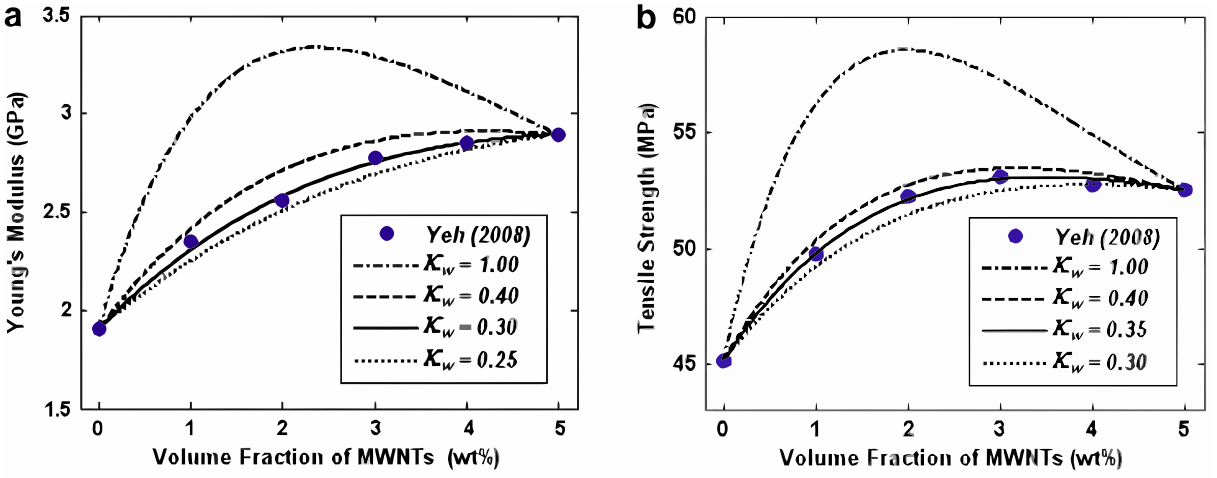

Figure 4.4: (a) Prediction of the Young's modulus of MWCNT/epoxy E120–H100 composites for various values of the waviness parameters and (b) SEM image of fracture surface for 5.0 wt.% nanotube epoxy composite [97, 101].

4.1.1.3 Effective Interface Model

For traditional composites, two-phase micromechanical models assume that in a composite material only matrix and reinforcement phases exist and they are perfectly bonded to each other and, since the reinforcement constituent diameter is in the microns scale, the fiber is treated as

a continuum, with isotropic or anisotropic material properties. Although the models are precise enough for reinforcement size in the order of micrometers or higher (e.g. carbon fibers), they can be inaccurate in predicting properties of the composites with much smaller reinforcements - nanocomposites - since the interfacial zone is much larger comparing to the dimensions of the reinforcement, and so cannot be neglected owing to its dominant role.

Arash et al. [102] proposed the effective interface model, which considers three co-existent phases - matrix, interphase/interfacial region and reinforcement. It can be used to predict the elastic properties of composites with effective reinforcements with an interface of the same shape as the effective fibers and with a finite size surrounding the reinforcement, as illustrated in Figure 4.5. Based on this model, the bulk elastic stiffness of composite (E_c) is predicted as:

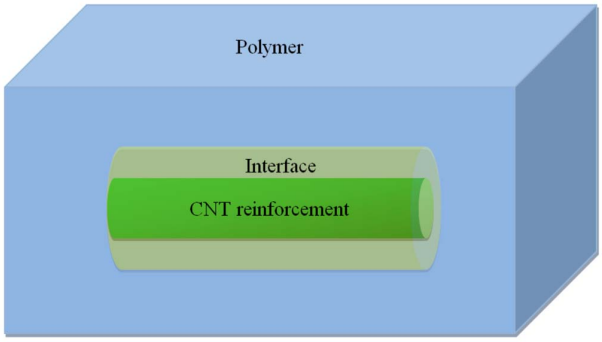

Figure 4.5: Schematic illustration of effective interface micromechanics model [102].

$$E_c = E_m + \frac{(c_f + c_i)(E_i - E_m)T_{fi} + c_f(E_f - E_i)T_f}{c_m + (c_f + c_i)T_{fi}} \tag{4.17}$$

where E_m, E_i and E_f are respectively the Young's moduli of matrix, interfacial region and fiber; and c_m, c_i and c_f are the volume fraction of matrix, interfacial region and fiber. T_f and T_{fi} are the dilute strain concentration tensors given by

$$T_f = 1 - \frac{S_f}{S_f + \dfrac{E_m}{E_f - E_m}} \tag{4.18}$$

where υ is the Poisson's ratio of the matrix, α is the aspect ratio of the fiber (l/d) and

$$T_{fi} = 1 - S_f \left[\frac{c_f}{c_i + c_f} \left(S_f + \frac{E_m}{E_f - E_m} \right)^{-1} + \frac{c_i}{c_i + c_f} \left(S_f + \frac{E_m}{E_i - E_m} \right)^{-1} \right] \tag{4.19}$$

In Eq. (4.18), the Eshelby tensor, S_f, is a function of the fiber aspect ratio α and the matrix elastic constants given by

$$S_f = \frac{1}{2(1-\upsilon)} \left\{ 1 - 2\upsilon + \frac{3\alpha^2 - 1}{\alpha^2 - 1} - \left[1 - 2\upsilon + \frac{3\alpha^2}{\alpha^2 - 1} \right] g \right\} \tag{4.20}$$

with

$$g = \frac{\alpha}{(\alpha^2 - 1)^{\frac{3}{2}}} \left\{ \alpha(\alpha^2 - 1)^{\frac{1}{2}} - \cosh^{-1}\alpha \right\} \tag{4.21}$$

The key result of the Eshelby tensor [103] is to define that, within a fiber, the strain is uniform. Arash et al. [102] reported an "excellent agreement between results obtained from the effective

interface model and molecular simulations". However, no correlation between this model and experimental results was presented.

4.1.1.4 Modified Halpin-Tsai Model

In this approach, the structure of the nanotube is taken into account and the properties of an "effective fiber" are defined and used to determine the elastic properties of the composite, based on a micromechanics approach. The Halpin and Tsai model is implemented to determine the properties of a unidirectional discontinuous fiber composite [75].

For fiber-like materials, load is transferred to the reinforcement through shear stresses at the fiber/matrix interface. However, the relatively weak bonding between the layers of the multiwalled nanotube (MWCNT) (see section 2.1) results in minimal load transfer between them. Consequently, the outer layer of the multiwalled nanotube will carry almost the entire load transferred at the nanotube/matrix interface [104] (fig.4.6).

The effective solid fiber elastic modulus of the MWCNT is determined by transferring the load carrying capability of the outer layer to the entire cross-section of the nanotube, considering the same deformation behavior and diameter. For modeling of the composite elastic properties, it can be considered that, at low strain, the interfacial stresses do not result in debonding at the nanotube/matrix interface[93].

An applied external force on the nanotube and the fiber will result in an iso-strain condition [75]:

$$\epsilon_{NT} = \epsilon_{eff} \tag{4.22}$$

where the subscripts NT and eff refer to the nanotube and the effective fiber, respectively. Using the previous condition and the fact that the applied force is the same in both cases, it is possible to relate the elastic properties of the nanotube to the effective fiber and express the effective modulus in terms of the cross section areas ratio:

$$E_{eff} = \frac{A_{NT}}{A_{eff}} E_{NT} \tag{4.23}$$

The modulus of the effective fiber can then be expressed in terms of the nanotube outer layer thickness (t = 0.34 nm), the nanotube diameter (d) and the elastic modulus of the nanotube, assuming the validity for $(t/d) < 0.25$:

$$E_{eff} = \frac{4t}{d} E_{NT} \tag{4.24}$$

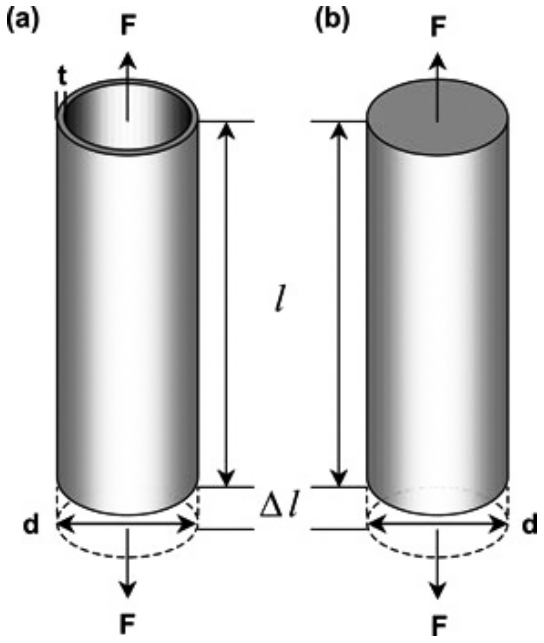

Figure 4.6: Schematic of (a) outer layer of the multiwalled nanotube and (b) effective fibre used to model the elastic properties of a nanotube embedded in a composite [75].

The Halpin–Tsai equations [105]:

$$E_c = E_m \left(\frac{1 + \zeta \eta V_f}{1 - \eta V_f} \right) \tag{4.25}$$

$$\eta = \frac{\frac{E_f}{E_m} - 1}{\frac{E_f}{E_m} - \zeta} \tag{4.26}$$

with E_c as the composite elastic modulus, V_f as the fiber volume fraction and E_f and E_m as the fiber and matrix modulus. In the previous equations, the parameter ζ depends on the geometry and boundary conditions of the reinforcement phase. For an aligned short fiber composite, it can be expressed as [75]:

$$\zeta = \frac{l}{d} + 40 V_f \tag{4.27}$$

Since in carbon nanotube composites the volume fractions are typically small, this expression can be simplified to

$$\zeta = \frac{l}{d} \tag{4.28}$$

Substituting equations 4.22, 4.26 and 4.28 into 4.25, it is possible to express the elastic modulus of the nanocomposite in terms of the properties of the polymer matrix and the nanotube reinforcement:

$$E_{11} = E_m \left(1 + 2 \left(\frac{l}{d} \right) \left(\frac{\frac{E_{NT}}{E_m} - \frac{d}{4t}}{\frac{E_{NT}}{E_m} - \frac{l}{d}} \right) V_{NT} \right) \left(1 + \left(\frac{\frac{E_{NT}}{E_m} - \frac{d}{4t}}{\frac{E_{NT}}{E_m} - \frac{l}{d}} \right) V_{NT} \right)^{-1} \tag{4.29}$$

E_{11} is the elastic modulus in the principal direction, which is coincident to the nanotube's orientation. This equation is valid for $l > d > 4t$. Contrasting with traditional fibrous composites, the reinforcement efficiency of the nanotube is highly sensitive to the diameter, therefore, the diameter must be known. In addition, because the volume of a nanotube is proportional to d^2, the volume fraction of the reinforcement is also influenced by the diameter.

Nanotube Dimensions

Studies have shown that the properties of nanotube-based composites are strongly influenced by the nanotube diameter [75], therefore, modeling the diameter distribution of the nano reinforcement is essential for an accurate modeling of overall nanocomposite elastic properties.

The distribution of nanotube diameters for a specific nanotube sample can be statistically determined by measuring the outside diameter of a statistically large sample of nanotubes and then determine the diameter probability distribution $\xi(d)$, and the volume distribution of nanotubes per unit length $\psi(d)$.

$$\psi(d) = \frac{d^2\xi(d)}{\int_0^\infty (d^2\xi(d))d(d)} \tag{4.30}$$

To obtain a statistically meaningful distribution of diameters, a high amount of measurements of the outside diameter have to be taken. Thostenson et al. [75] took nearly seven hundred measurements of nanotube diameters to create the diameters probability distribution (fig.4.7a). The nanotube diameters exhibited a bimodal distribution with peaks near 18 and 30 nm. In figures 4.8a and 4.8b SEM images with measured nanotube diameters are exhibited, although the amount of measurements might not be statistically meaningful, it is possible to conclude that the diameter distribution is similar.

A non-linear regression was used in the report to fit the data to a double Lorentzian (fig.4.7b) and a double Gaussian distribution and the curves were normalized such that the area under the curve is equal to the unity. Since the Gaussian distribution underestimates the higher diameter, and consequently higher volume, nanotubes, only the Lorentz distribution (equation 4.31) will be addressed.

$$\xi(d) = \frac{a_1}{\left(1 + \frac{d - a_2}{a_3}\right)^2} + \frac{a_4}{\left(1 + \frac{d - a_5}{a_6}\right)^2} \tag{4.31}$$

Table 4.1: Lorentz parameters [75].

	a_1	a_2	a_3	a_4	a_5	a_6
Lorentz parameters	0.8025	18.23	-3.56	0.02149	31.84	2.946

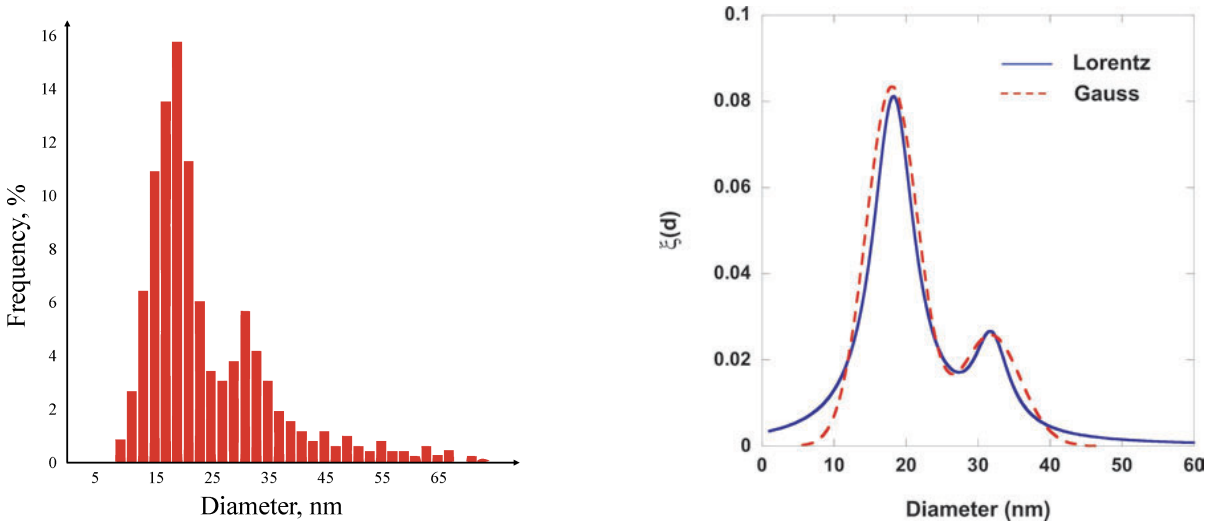

(a) (b)

Figure 4.7: (a) Histogram of the diameter distribution of carbon nanotubes, and (b) the non linear fit to a Lorentz distribution [75].

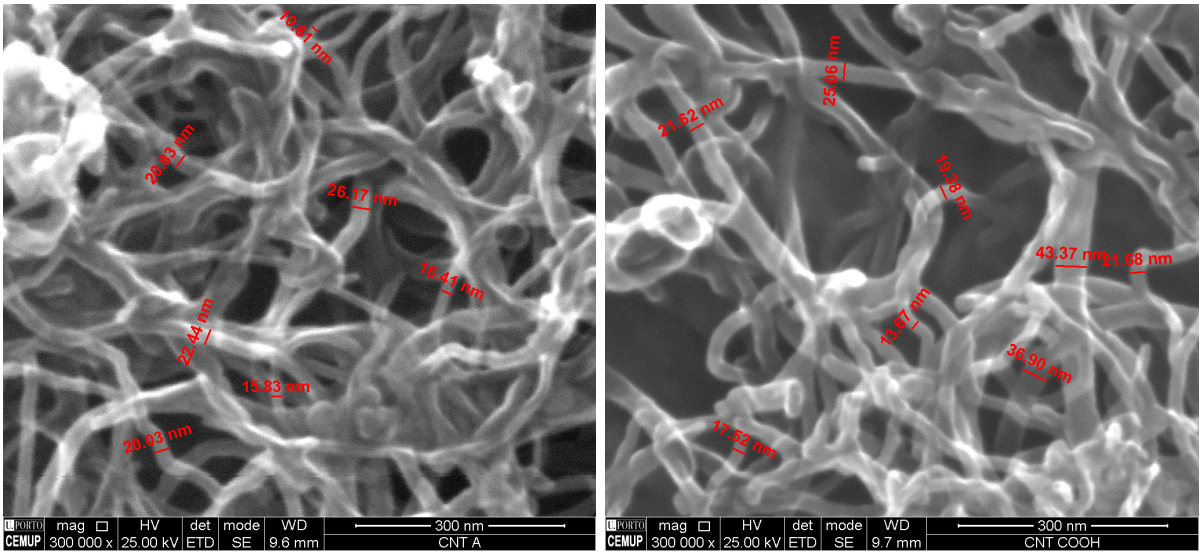

(a) (b)

Figure 4.8: SEM micrograph of multi-walled carbon nanotubes (a) without any functionalization and (b) with COOH functionalization, with measurements of outside diameter indicated.

Since the weight fraction is easily calculated based on the mass of the constituents added during processing, typically, it is used in the experimental data for nanocomposites. However, the weight fraction does not fully describe the content of reinforcement, because it depends on the relative densities of the matrix and the filler. Moreover, the nanotube diameter and wall structure will significantly influence the nanotube's density.

To convert the weight fraction into volume fraction V_f, needed for equation 4.29, it is essential to have the knowledge of the matrix and reinforcement densities.

$$V_f = \frac{W_{NT}}{W_{NT} + (\rho_{NT}/\rho_m) - (\rho_{NT}/\rho_m)W_{NT}} \tag{4.32}$$

where the W_{NT} is the weight fraction of the nanotube, ρ is the density and the subscripts NT and m refer to the nanotube and matrix. From the measurements of inside and outside diameter, which can be made with TEM images (fig.4.9a), and assuming the density of the nanotube layers equal to fully dense graphite ($\rho_g = 2.25 g/cm^3$), the nanotube density per unit of length can be calculated with:

$$\rho_{NT} = \frac{\rho(d^2 - d_i^2)}{d^2} \tag{4.33}$$

where the d is the outer diameter and d_i is the inner diameter. The outside and inside diameters can be measured from TEM micrographs (fig. 4.9a). Experimental measurements indicate a strong linear relationship between the diameter and the wall thickness, with some deviation in small diameter nanotubes. Using the previous equation 4.33, density can be calculated. Figure 4.9b exhibits the wall thickness as a function of the diameter and the figure 4.10a shows the density as a function of the diameter. At larger diameter, the density tends to the theoretical density of graphite (2.25 g/cm^3). Figure 4.10b shows the histogram of the calculated nanotube densities and the mean density is around 1.9 g/cm^3.

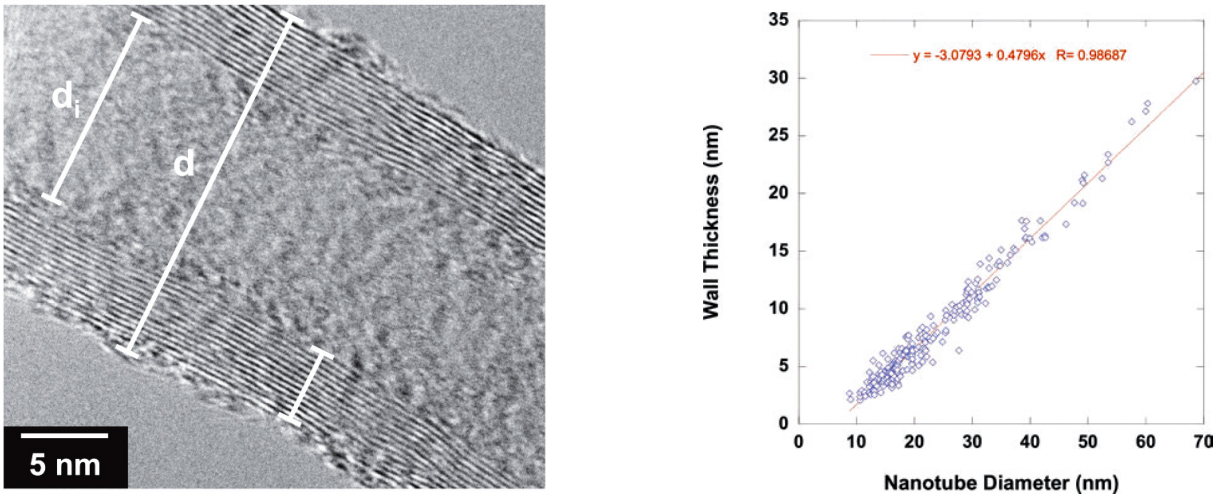

(a) (b)

Figure 4.9: (a) TEM micrograph of a multi-walled carbon nanotube with measurements of outside diameter, inside diameter and wall thickness indicated and (b) linear relationship between wall thickness and nanotube diameter [75].

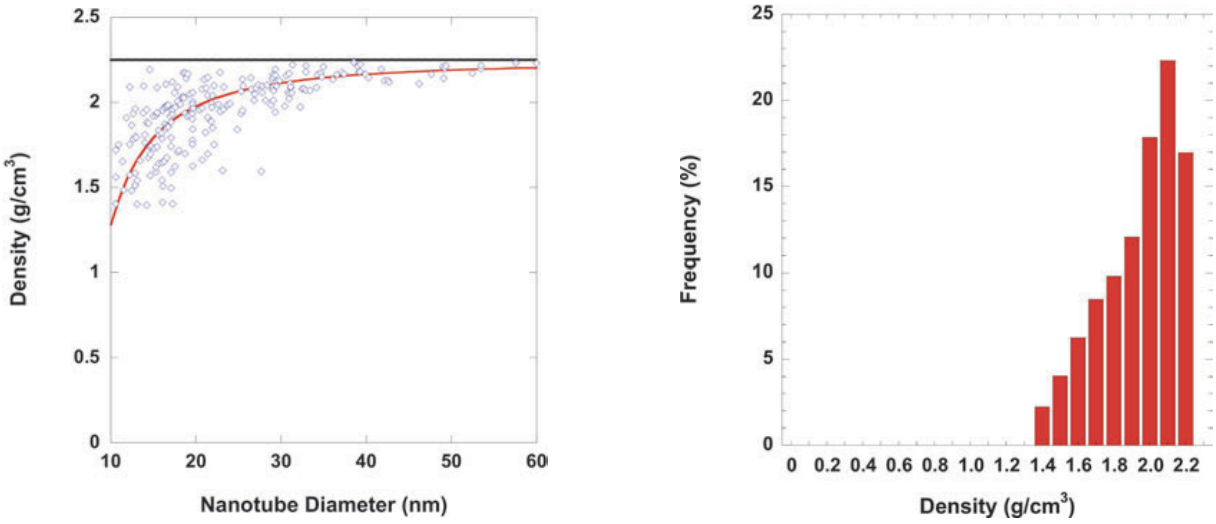

(a) (b)

Figure 4.10: (a) Variation in calculated nanotube density with the outside diameter and (b) Histogram showing the distribution of nanotube density [75].

The nanotube length is, as well, an important parameter. However, measurements are quite difficult to quantify. In TEM, the initial microtome cutting process usually crops the nanotubes, but using measurements from the apparently intact nanotubes, Thostenson et al. [75] concluded that the nanotubes length range between 500 nm and 2 μm, with an average of around 1μm.

Composite Elastic Modulus

Equation 4.29 reveals the diameter-dependence of the carbon nanotube reinforcement on the nanocomposite properties. However, distribution of nanotube diameters cannot be implemented in the equation to directly calculate the nanocomposite elastic modulus. Thus, the contribution from each nanotube diameter to the overall elastic modulus must be taken into account and the volume fraction that nanotubes of a specific diameter occupy within the composite must be computed.

Assuming that the nanotubes are uniformly dispersed and aligned throughout the matrix phase and assuming iso-strain, the contribution of each diameter can be considered to act in parallel. The entire volume of the composite is divided into N individual composites reinforced by a specific diameter nanotubes. Each of the N individual composites will have a specific elastic modulus that depends on the local volume fraction of nanotubes at the respective diameter. Hence, the elastic modulus of the composite can be calculated as the sum of parallel composites over the range of nanotube diameters (fig. 4.11):

$$E_c = \sum_{n=1}^{N} v_n E_n|_{d_n} \tag{4.34}$$

with

$$v_n = \frac{V_n}{V} \tag{4.35}$$

$$\sum_{n=1}^{\infty} v_n = 1 \tag{4.36}$$

where $E_n|_{d_n}$ is the elastic modulus of the composite calculated from the equation 4.29 at the nanotube diameter included in the nth segment and v_n is the partial volume of the same segment.

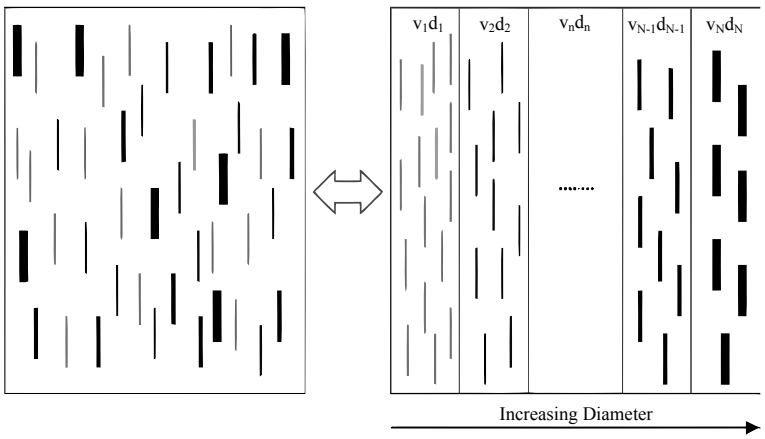

Figure 4.11: Illustration of the equivalence between a dispersed composite and N composites each with a specific nanotube diameter and partial volume acting in parallel [75].

In order to calculate the elastic modulus E_n at a given diameter, the local volume fraction at this nanotube diameter $V_{NT}|_d$ can be computed from the volume distribution of the nanotubes (equation 4.30)

$$V_{NT}|_{d_n} = \frac{\int_{d_n}^{d_n+\Delta d_n} (V_{NT}\psi(d)d(d)}{v_n} \tag{4.37}$$

where V_{NT} is the total volume fraction of nanotubes in the composite calculated from equation 4.32 and the integral limits are the range of diameters included in the nth composite.

4.2 Multiscale Modeling

In the early stage of carbon nanotube–related research, **molecular mechanics** and **molecular dynamics** simulations have been used to estimate the mechanical properties of individual nanotubes and bundles [106, 107, 95]. In this methods, the atomic interactions between the carbon atoms of a carbon nanotube are computed using the force potentials from the bonded and non-bonded interactions, being the latter either due to the van der Waals force or electrostatic interactions. Since they simulate the behavior of each atom, they require a considerable amount of computational power to achieve length and time scales that are representative of real applications.

Continuum modeling which is based on continuum mechanics, has been applied for investigating the overall mechanical deformation of carbon nanotubes. It can use, for example, vibration analysis to study the structural rigidity of carbon nanotubes [108]. However, it considers the nanotube as a continuum medium, not considering the structure and bonding of the carbon nanotube, which might not be valid at the nanometer-scale [75].

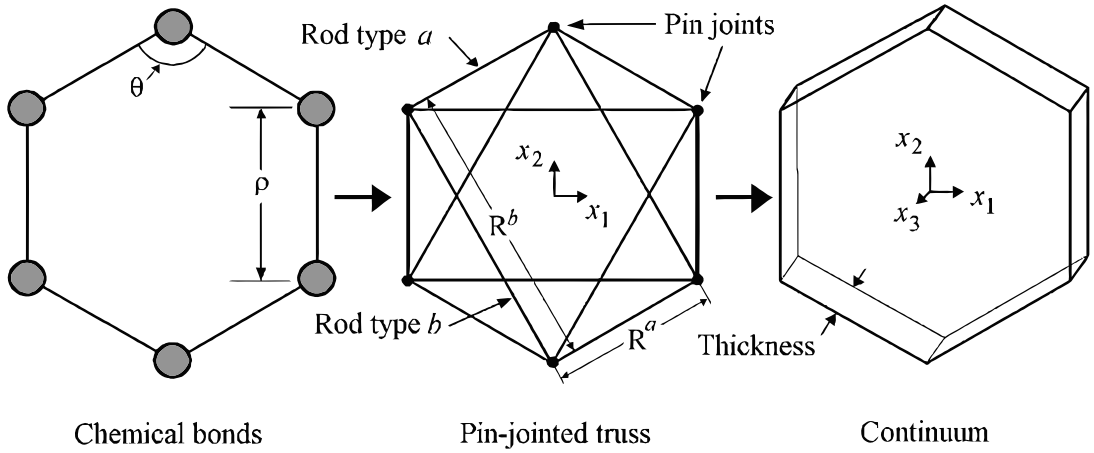

Figure 4.12: Representative volume elements for molecular, structural and continuum models [109].

Thus, to simulate the behavior of nanocomposites at various scales, a **multi-scale** modeling techniques, where both molecular level simulation and continuum modeling are interconnected, should be used. Each level addresses a phenomenon over a specific window of length and time. For example, they are able to incorporate the interfacial characteristics of the nanotube and the surrounding polymer matrix at the molecular level into finite element modeling to predict the mechanical behavior of carbon nanotube/polymer composites, connecting the atomistic models to the continuum models [32].

Two examples of multiscale modeling techniques to study of carbon nanotube/polymer composites, namely **Molecular Structural Mechanics** and **Equivalent-Continuum Mechanics**, are presented in the following sections.

4.2.1 Molecular Structural Mechanics

The visual similarities between a steel frame structure and the nanoscale atom structure of a fullerene (fig. 4.13) lead Li and Chou [110, 111] to the concepts behind the molecular structural mechanics. The fundamental concepts of this model are the notion that the carbon nanostructure can be simulated by a frame-like structure and the primary bond interactions between two neighbor carbon atoms can be considered as load-bearing beam members, where the atoms act as joints (fig.4.14).

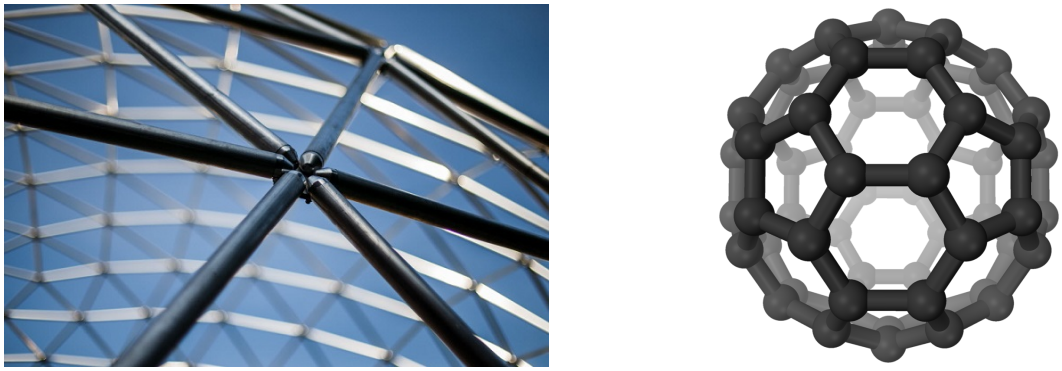

(a) (b)

Figure 4.13: (a) Example of a truss stucture [112] and (b) a reoresentation os a fullerene [13].

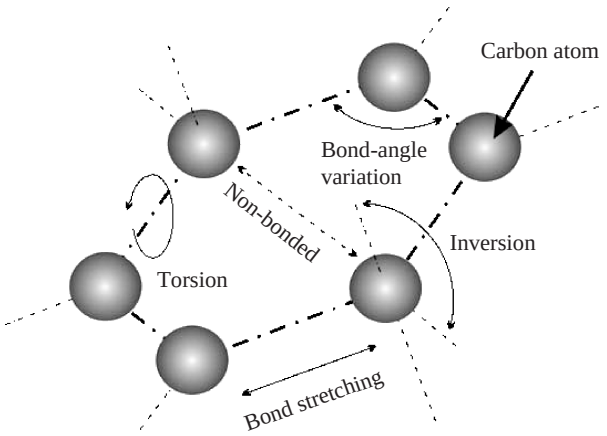

Figure 4.14: Bond structures and corresponding energy terms of a graphene cell [32].

The first step is to consider the atoms as joints and bonds as beams in the equivalent frame-like structure. The total potential energy of the molecular structure is the sum of the energies due to bonded and non-bonded interactions [110, 111]:

$$U = \sum U_r + \sum U_\theta + \sum U_\phi + \sum U_\omega + \sum U_{vdW} \tag{4.38}$$

where U_r is for bond stretch interaction, U_θ is for bond angle bending, U_ϕ and U_ω represent dihedral angle torsion and out-of-plane torsion, respectively, and U_{vdW} is for non-bonded van der Waals interaction.

$$U_r = \frac{1}{2} k_r \left(\Delta r\right)^2 \tag{4.39}$$

with k_r as the bond stretching force constant and Δr the bond stretching increment;

$$U_\theta = \frac{1}{2} k_\theta \left(\Delta \theta\right)^2 \tag{4.40}$$

k_θ bond angle bending force constant and $\Delta\theta$ the bond angle change;

$$U_\tau = U_\phi + U_\omega = \frac{1}{2} k_\tau \left(\Delta \phi\right)^2 \tag{4.41}$$

k_τ is the torsional resistance and $\Delta\phi$ the angle change of bond twisting.

Secondly, it is necessary to determine the sectional parameters from molecular force fields constants. The equivalent beam's section is assumed to be circular, therefore, $I_x = I_y = I$. Thus, only three stiffness parameters have to be determined: the tensile resistance EA, the flexural rigidity EI and the torsional stiffness GJ, where E is the elastic modulus, A is the section's area, G is the shear modulus and J is the polar momentum of inertia. Structural mechanics imply that the deformation of the frame results in strain energy variation. The strain energy for a beam element is given by

$$U = \sum U_A + \sum U_M + \sum U_T \tag{4.42}$$

where U_A, U_M, and U_T are the strain energies for axial tension, bending, and torsion, respectively.

$$U_A = \frac{EA}{2L} \left(\Delta L\right)^2 \tag{4.43}$$

$$U_M = \frac{EI}{2L} \left(2\alpha\right)^2 \tag{4.44}$$

$$U_T = \frac{GJ}{2L} \left(\Delta \beta\right)^2 \tag{4.45}$$

where L is the length of the equivalent beam, ΔL is the axial deformation, α is the bending angle of rotational at the ends of the beam and $\Delta\beta$ is the relative axial rotation between the ends of the beam.

By assuming the energy equivalence between Eq.4.38 and Eq.4.42, it is established a direct analogy between the structural and molecular mechanics and a direct relationship between the molecular force constants and the structural mechanics parameters:

$$\frac{EA}{L} = k_r \qquad (4.46) \qquad \frac{EI}{L} = k_\theta \qquad (4.47) \qquad \frac{GJ}{L} = k_\tau \qquad (4.48)$$

The last steps are creating the stiffness matrices and the elemental load vectors, assemble the global stiffness matrix and the global load vector and finally solve the displacement of atoms and calculate the elastic properties of the carbon nanotubes.

The van der Waals interaction is simulated by a truss rod that connects the two interacting atoms with rotatable end joints, thus it only transmits tensile or compressive forces. This force is a non-bonded interaction and has a inherent non-linearity and it can be an attraction or a repulsion force. The attraction occurs when the two atoms approach each other within a certain distance and the repulsion occurs when the distance between the interacting atoms becomes less than the sum of their contact radii. This interaction is often modeled using the general Lennard–Jones "6–12" potential, which is not explored in this work. In figure 4.15a it is possible to analyze the van der Waals force variation against the distance between atoms.

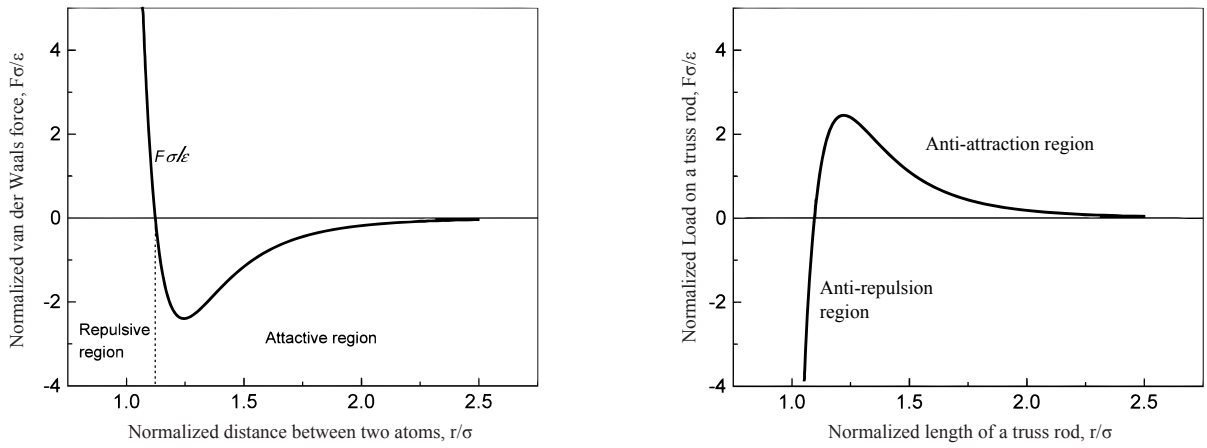

(a) (b)

Figure 4.15: (a) Normalized van der Waals force versus normalized atomic distance [104], and (b) load-displacement curve of the non-linear truss rod.

The truss rod connecting the atoms is a non-linear element with its load–displacement relation characterized by the van der Waals force but with the opposite sign, in other words, Fig. 4.15b gives the load-displacement relation when a load is applied to the truss rod to overcome the van der Waals force. At the nanotube/polymer interface, the activation of the van der Waals truss rod is determined by the distance between the carbon atom in the nanotube and a node in the polymer. If this distance is inferior to 2.5 times the $0.34nm$ distance, the truss rod is "activated". The center of the atoms of the nanotube is located in the midsection of the tube thickness, which is assumed to be 0.34nm. With this technique it is possible to create an equivalent truss model.

By combining this approach to model the nanotube and finite element method (FEM) to model the polymer matrix, Li and Chou further examined the effect of interfacial load transfer on the stress distribution in carbon nanotube/polymer composites. They found the existence of stress concentrations in the nanotube and the polymer matrix, which may cause the premature failure of the nanotube and polymer matrix. They also concluded that the effective Young's modulus of the nanotube/polymer composite calculated from the simulation was in good agreement with that predicted from the rule-of-mixtures.

4.2.2 Equivalent-Continuum Approach

For a polymer composite system reinforced with single-walled carbon nanotubes (SWCNT), the Equivalent-Continuum Approach, proposed by Odegard et al. [51] provides the steps to model the nanotube, the local polymer near the nanotube, and the nanotube/polymer interface into an effective continuum fiber, using an equivalent-continuum model. The effective fiber retains the local molecular structure and bonding characteristics, defined by molecular dynamics, linking the equivalent-continuum and micromechanics models.

This model consists of three major steps. Firstly, a suitable representative volume element (RVE) of the polymer nanocomposite system is chosen. The typical RVE is a nanotube surrounded by a cylindrical volume of polymer (fig. 4.16). Since it is on the nanometer length scale, the material of the RVE is not continuous and it is considered an assembly of many atoms. Interaction between these atoms and the polymer ones is described with Molecular Dynamics.

Then, an equivalent truss model of the RVE is developed using molecular mechanics (section 4.2.1) to do the connection between the molecular model and equivalent-continuum model. In the equivalent truss model, each atom in the molecular model is represented by a pin-joint and each truss element represents the interactions (atomic bonded and non-bonded). Using molecular mechanics it is possible to determine the elastic modulus of the truss elements.

Finally, an equivalent-continuum model of the RVE is constructed by equating the total strain energies under identical loading conditions. For example, the equivalent-truss model is replaced with an equivalent-continuous plate with a finite thickness, which is also called effective thickness. Odegard and co-workers [51, 113] established constitutive equations for both functionalized and non-functionalized nanotube polyethylene composites by using equivalent-continuum modeling technique. The RVE they developed is a continuum solid cylinder shown in figure 4.16.

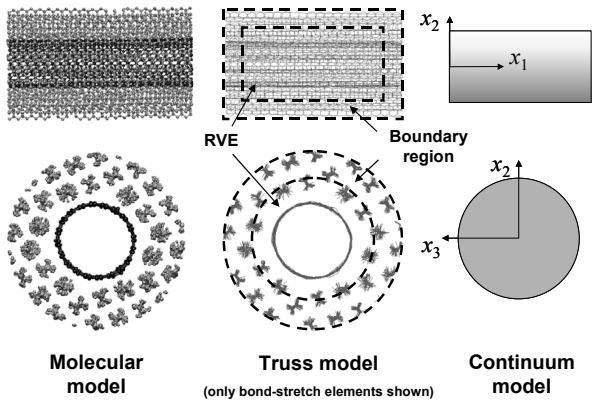

Figure 4.16: Equivalent-continuum modeling of non-functionalized

The moduli of both nonfunctionalized and functionalized nanotube/ polyethylene composite systems were examined for various nanotube lengths, volume fractions, and orientations. For a fixed nanotube volume fraction of 1% and various nanotube lengths 4.17a, the Young's modulus and the shear modulus of the randomly-orientated-filler composite, and the longitudinal Young's modulus of the aligned composite actually revealed a decrease up to 10% when the nanotube is functionalized.

For a fixed nanotube length of 400 nm and various nanotube volume fractions, the longitudinal Young's modulus of the random and aligned composite, and the shear modulus of the random composite have also shown to decrease up to 12% when the nanotubes are functionalized (fig.4.17b). These results indicated that the functionalization has degraded the elastic stiffness of carbon nanotube/polyethylene composite.

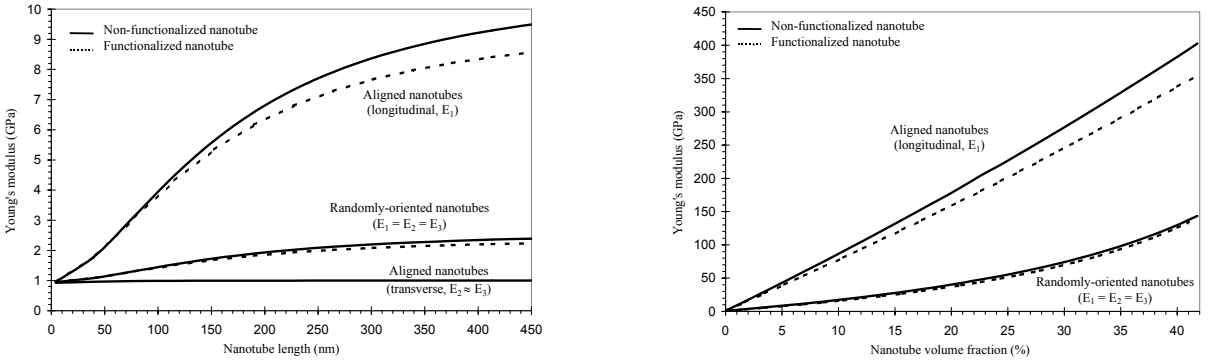

(a) (b)

Figure 4.17: Young's moduli of both composite systems against nanotube length for a constant 1% nanotube volume fraction, and (b) Longitudinal Young's moduli of both composite systems against nanotube volume fraction for a constant nanotube length of 400 nm [113].

4.3 Model Correlation

The results scatter are easily noticeable when analyzing experimental data for the three types of carbon nanotube/epoxy composites 4.18. Although this scatter might deteriorates the quality of predictions, some of the models presented in the previous sections were computed with the objective of finding the best prediction model for carbon nanotube/epoxy composites.

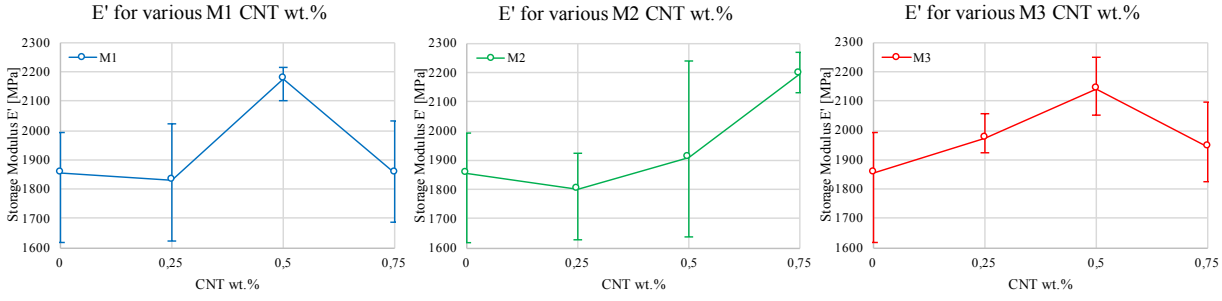

(a) (b) (c)

Figure 4.18: Storage modulus E', with the respective scatter, for the various contents and functionalizations: (a) Untreated (M1), (b) carboxylic (M2) and (c) thermally oxidized (M3) carbon nanotubes.

All following models were applied considering the following assumptions:

- $\rho_m = 1.2$ and $\rho_{NT} = 1.9$ for the matrix and nanotube densities, respectively.
- $E_m = 1856$ MPa and $E_{NT} = 1$ TPa for the matrix and nanotube modulus, respectively.
- The average nanotube diameter was defined as 25nm.
- Models were only applied to the pristine carbon nanotube experimental results, since it is the one that has more experimental data available.

In figure 4.19 two predictions based on the **rule of-mixtures** are exhibited: the simple version of the rule-of-mixtures (equation 4.1) and a special form of the latter that includes a nanotube efficiency parameter (equation 4.2). It is easily concluded that the predictions are not accurate and substantially over predict the modulus of the system.

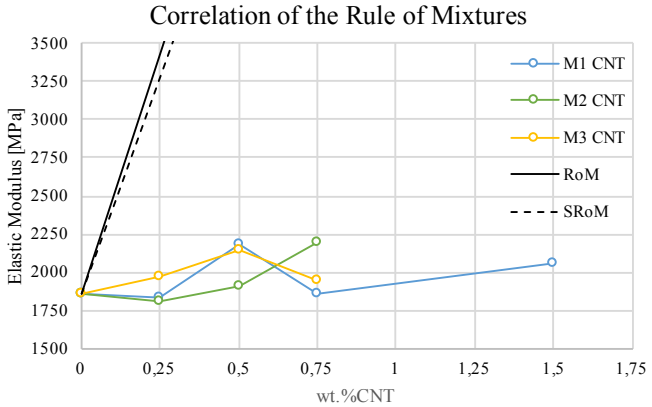

Figure 4.19: Correlation of two sorts of the rule-of-mixtures with experimental data, presented in section 4.1.1.1.

The **modified rule-of mixtures**, presented in section 4.1.1.2, was applied to the experimental data and prediction results are shown in figure 4.20. In order to determine the value of the α parameter in equation 4.6, section 4.1.1.2, and as recommended by the author, only one experimental result was used. The experimental result chosen was the 1.5wt.% because it revealed the best fitting curves.

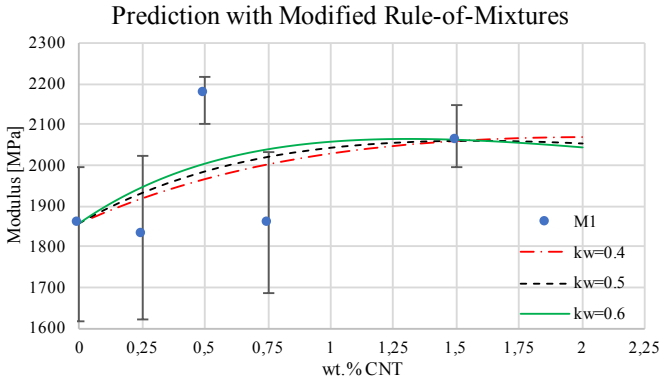

Figure 4.20: Correlation of the modified rule-of-mixtures developed by Omidi et al. [97], presented in section 4.1.1.2, with experimental data from the pristine carbon nanotubes.

The best fitting was found for the $k_W = 0.5$, which gives the smallest maximum error of 8.9%, although it gives a marginally higher average error of 4.7%, relatively to lower values of k_W. With lower k_W values, the curve gets closer to the lower modulus points 0.25 and 0.75% points, decreasing the average error (4.5% for $k_W = 0.4$), but, on the other hand, increasing the maximum error to around 10%. In addition, 0.25 and 0.75% points have high scatter associated.

From SEM images (fig. 4.21), various measurements were taken to assess the a and w values needed to compute the k_W waviness parameter, which was estimated at around 0.6, revealing a satisfactory agreement with the 0.5 value that gives the best fit to the experimental points in figure 4.20.

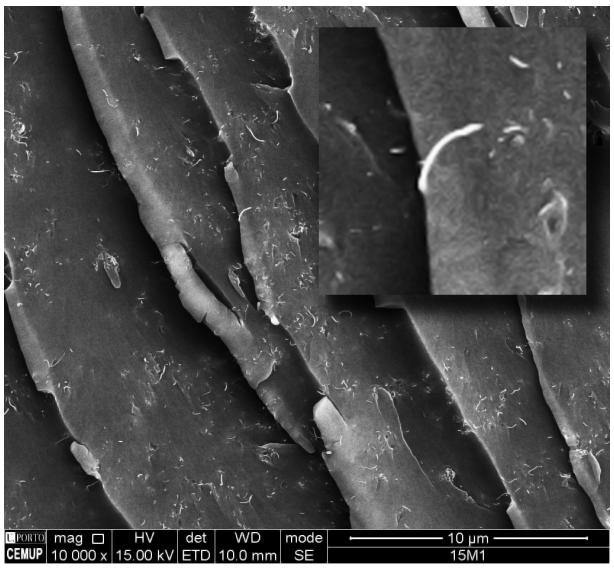

Figure 4.21: SEM image from the 1.5wt.% pristine carbon nanotubes.

The **Modified Halpin-Tsai** model, present in section 4.1.1.4, equation 4.29, was implemented for the untreated (M1) carbon nanotubes, considering an average nanotube diameter of 25 nm and a average lengths of 2, 5 and 10μm.

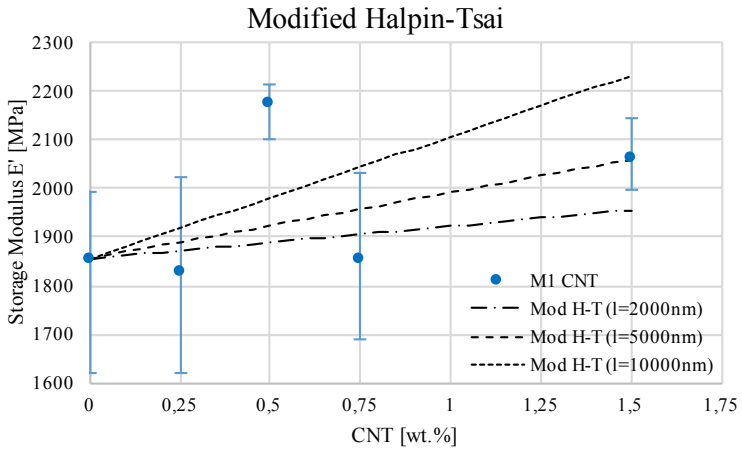

Figure 4.22: Correlation of the Modified Halpin-Tsai model, presented in section 4.1.1.4, with experimental data, for various legth values.

Figure 4.22 reveals good agreement between this model, for the 5 μ m length nanotubes, and experimental data, with an average error around 5%. However, the assessment of the actual length values is hindered by the entangled nature of the carbon nanotubes.

The intention of this section was to find which one of the analytical models previously presented gives the best modulus prediction to the experimental data acquired for the epoxy nanocomposites. Then, that prediction could be used as matrix input data for carbon fiber/carbon nanotube reinforced composites property predictions. However, experimental data revealed to have a rather large scatter of values without of a solid tendency, which seriously hindered the models application. Another relevant issue is the fact that none of the previously presented models predicts an initial decrease in modulus for small percentages of carbon nanotubes, which happened for the 0.25wt.% addition of pristine and carboxylic carbon nanotubes. Nevertheless, both **Modified Rule-of-Mixtureas** and **Modified Halpin-Tsai** revealed satisfactory agreement with experimental data.

In order to apply the Effective Interface Model, presented in section 4.1.1.3, it is necessary to determine interphase properties, which was done by the authors using computacional molecular simulations. Hence, this models could not be applied. None of the more complex multi-scale models were applied due to the programming nature of the models, which is outside the scope of this work.

Chapter 5

Conclusions

Although it has been reported that the storage modulus of a resin increases with increase in carbon nanotube loading, regardless of the dispersion, explaining it with the fact that "nanotubes form a percolated structure due to their high aspect ratio of about 1000 and high surface area", this behavior could not be assessed in our nanocomposite system.

It is possible to conclude that 0.25wt.% of the pristine (M1) and carboxylic (M2) functionalized nanotubes, do not bring any stiffness enhancement, which induces the fact that, at this low content reinforcement, the nanotubes actually act as defect sites and do not play a reinforcement role. On the other hand, the thermally oxidized carbon nanotubes (M3) stand out with an increase in the modulus of more than 6%, which might reveal better bonding between the nanotubes and the matrix permitted by the functionalization that allows a more efficient load transfer and better dispersion.

For 0.5%, M1 and M3 nanotubes stand out, acting as reinforcement and increasing considerably the modulus of the system by more than 17% and 15%, respectively. This can be explained by load transfer to the nanotubes, even if they are in bundles, increasing the modulus of the system. Carboxylic (M2) functionalized nanotubes only reveal a substantial increase (of 18%) for 0.75wt.% addition, while M1 and M3 reduce their influence at this content. This behavior suggests that M1 and M3 functionalizations have their maximum effect on the storage modulus somewhere between 0.25 and 0.75%, and with contents above the latter, nanotubes tend to agglomerate and the amount of the nanotubes contacting each other increases, triggering an attenuation of the reinforcing efficiency. This can be explained by the reduction of the load transfer efficiency between the nanotubes and the surrounding matrix and a decrease of the effective aspect ratio of the nanotubes [35]. Another factor that could influence is the extremely high viscosity of the resins with M1 and M3, which might hamper the process of dispersion.

In some cases the scatter associated to an average value is too large to be possible to assess conclusions with total assurance. On the other hand, the scatter can also induce that the dispersion was not even and some samples had higher nanotubes concentration than others.

The higher viscosity systems such as M3 are considered the ones with better dispersion, which is indicative of stronger interfacial interactions [76]. In addition, the M3 modified nanotubes reveal higher enhancement in modulus compared to the pristine. Although carboxylic carbon nanotubes are functionalized, they reveal lower viscosity and consequently lower modulus. High viscosity at the low shear rates, can be attributed to the formation of a percolated structure by the carbon nanotubes [76]. This structure breaks down as the shear rate increases, resulting in similar viscosity at higher shear rates for all the systems.

In what concerns to the dispersion agents, although enhancements have been reported for some dispersion agents for the Young's modulus in previous reports [37], the implemented dispersion agents do not efficiently worked, at least for pristine carbon nanotubes, deteriorating the modulus of the system, which might be induced by a decrease in the bonding strength between nanotubes and matrix. Since this dispersion agents were made to create a nanostructure within the epoxy, instead of reinforcing, they could be giving additional mobility to the matrix polymer chain, which might enhance other properties such as impact strength. Therefore, in a future work, additional tests should be done to assess other mechanical properties such as fracture toughness and tensile strength.

The storage modulus of a carbon fiber/carbon nanotube composite is affected by the quality of the bonding between the reinforcements, fibers and nanotubes, and the epoxy matrix. This quality of the interfacial adhesion can be characterized by the value of tan δ [84]. Thus, the system with the highest reinforcement (27%) is the one with pristine carbon nanotubes. The other two systems, with carboxylic (M2) and thermally oxidized (M3) carbon nanotubes, exhibited a 10 and 12% decrease in the modulus, which suggests a reduction in the crosslinking degree due to the introduction of well dispersed nanotubes.

Pristine (M1) and carboxylic functionalized (M2) nanotubes exhibited a T_g increase of almost 4^oC for the former and around 1^oC for the latter. This can be related with a balance between the hindrance in the movement of the polymer chain segments that increase the rigidity of the system, caused by introduction of the nanotubes as a reinforcement element, and the reduction on the crosslinking degree due to the replacement of the crosslinks sites with nanotubes. This phenomena needs to be further exploited and related with both variables. The addition of 0.5 wt.% of thermally oxidized (M3) carbon nanotubes resulted in an almost 2 degree decrease, which suggests a reduction in the crosslinking degree due to the introduction of well dispersed nanotubes. This raise in the glass transition temperature enhances, even if marginally, the capacity of maintaining the modulus of the composite system with the increase in temperature.

Dynamic mechanical tests performed to a sample of carbon fiber reinforced epoxy with 0.5wt.% pristine carbon nanotubes and the same material with a physical alignment process, exhibited a 17% higher flexural storage modulus, for the same 60 % fiber content. From the SEM images, it was possible to see several white nanoscale filaments with a clear orientation and revealed a two dimensional perpendicular orientation with a interlocking between the filaments. The scale difference, with the diameter of the tubes around 30-40 nm, excluded the possibility of the regular marks being made by the Teflon sheet. Therefore, it is possible to conclude that this alignment process effectively oriented the nanotubes present in the matrix and improved the storage modulus significantly.

The intention of the section 4.3 (Model Correlation) was to find which one of the analytical models presented gave the best modulus prediction for the experimental data acquired. However, experimental data revealed to have a rather large scatter of values without of a solid tendency, which hindered the model application. Another relevant issue is the fact that none of the previously presented models predicts an initial decrease in modulus for small percentages of carbon nanotubes, which happened for the 0.25wt.% addition of pristine and carboxylic carbon nanotubes. Nevertheless, both Modified Rule-of-Mixtureas and Modified Halpin-Tsai revealed satisfactory agreement with experimental data.

Efficient dispersion and the alignment of carbon nanotubes within a matrix is still a challenge and it could play the main role driving the diffusion of nanotubes as nano-reinforcement on industrial scale. In order to achieve optimal enhancement in the properties of nanotube/polymer composites, two key issues should be addressed:

- Homogeneous dispersion of the nanofiller in the polymer resin, which might be achieved with nanotube functionalization, employment of physical treatment techniques or incorporation of dispersion agents, or even a combination of more than one technique;
- Strong interfacial bonding between the nanotubess and the polymer matrix, which might be possible with appropriate selection of the matrix material and the functionalization.

5.1 Future Work

In future scope, some points should be addressed to further understand the behavior of the nanocomposites studied:

- Carboxylic functionalized carbon nanotubes might have an even higher enhancement of modulus for contents over 0.75%, which might be explained by the lower viscosity, comparing to the other functionalization at the same loading, that could help the dispersion;
- Regarding the process of physical alignment process, further analysis should be performed to assess the actual orientation of the carbon nanotubes;
- Further tests should be performed to assess other relevant properties that might have been improved with the carbon nanotube addition, not only mechanical, such as tensile strength, fracture toughness and interlaminar shear strength, but also thermal and electrical properties as well.

Bibliography

[1] Daniel L. Schodek Michel F. Ashby, Paulo J. Farreira. Nanomaterials,Nanotechnologies and Design. 2009.

[2] Kin-Tak Lau and David Hui. Effectiveness of using carbon nanotubes as nano-reinforcements for advanced composite structures. Carbon, 40(9):1605–1606, 2002.

[3] S. Bal and S. Samal. Carbon nanotube reinforced polymer composites—A state of the art. Bulletin of Materials Science, 30(4):379–386, 2007.

[4] F. H. Gojny, M. H G Wichmann, U. Köpke, B. Fiedler, and K. Schulte. Carbon nanotube-reinforced epoxy-composites: Enhanced stiffness and fracture toughness at low nanotube content. Composites Science and Technology, 64:2363–2371, 2004.

[5] Amal M K Esawi and Mahmoud M. Farag. Carbon nanotube reinforced composites: Potential and current challenges. Materials and Design, 28:2394–2401, 2007.

[6] Veena Choudhary and Anju Gupta. Polymer/carbon nanotube nanocomposites. Carbon Nanotubes - Polymer Nanocomposites, pages 65–90, 2011.

[7] Peng Cheng Ma, Naveed a. Siddiqui, Gad Marom, and Jang Kyo Kim. Dispersion and functionalization of carbon nanotubes for polymer-based nanocomposites: A review. Composites Part A: Applied Science and Manufacturing, 41(10):1345–1367, 2010.

[8] Lv Radushkevich. O strukture ugleroda, obrazujucegosja pri termiceskom razlozenii okisi ugleroda na zeleznom kontakte, 1952.

[9] Sumio Iijima. Helical microtubules of graphitic carbon. Nature, 354(November):56–58, 1991.

[10] Marc Monthioux and Vladimir L. Kuznetsov. Who should be given the credit for the discovery of carbon nanotubes? Carbon, 44:1621–1623, 2006.

[11] Http://tradingcomputersnow.com/wp content/uploads/2013/10/carbon-nanotube 2040-300x300.jpg. No Title.

[12] Http://jdr.sagepub.com/content/early/2013/05/15/0022034513490957/F1.large.jpg. MWCNT.

[13] Https://clemente.io/seminar-macroscopicity/assets/images/buckyball.png. fullereneC60.

[14] Http://www.chm.bris.ac.uk/webprojects2001/andrews/balls2tubes.jpg. cap.

[15] M. Yu. Strength and Breaking Mechanism of Multiwalled Carbon Nanotubes Under Tensile Load. Science, 287(January):637–640, 2000.

[16] Mf Yu, Bs Files, S Arepalli, and Rs Ruoff. Tensile loading of ropes of single wall carbon nanotubes and their mechanical properties. Physical review letters, 84:5552–5, 2000.

[17] Ch Laurent, E. Flahaut, and a. Peigney. The weight and density of carbon nanotubes versus the number of walls and diameter. Carbon, 48(10):2994–2996, 2010.

[18] http://carbonlab.roma2.infn.it/.

[19] T. Belin and F. Epron. Characterization methods of carbon nanotubes: A review. Materials Science and Engineering B: Solid-State Materials for Advanced Technology, 119:105–118, 2005.

[20] Kalpana Awasthi, Anchal Srivastava, and O N Srivastava. Synthesis of carbon nanotubes. Journal of nanoscience and nanotechnology, 5:1616–1636, 2005.

[21] Jay P Gore and Anup Sane. Flame Synthesis of Carbon Nanotubes. 2000.

[22] Mukul Kumar and Yoshinori Ando. Chemical vapor deposition of carbon nanotubes: a review on growth mechanism and mass production. Journal of nanoscience and nanotechnology, 10(6):3739–3758, 2010.

[23] a Bandyopadhyay and G M Odegard. Molecular Modeling of Epoxy Polymers. 128(Mm):660–666, 2013.

[24] Epotek. T g - Glass Transition Temperature for Epoxies.

[25] B. D. Sanditov, S. Sh. Sangadiev, and D. S. Sanditov. Relation between elastic modulus and glass softening temperature in the delocalized atom model. Journal of Experimental and Theoretical Physics, 115(3):445–454, 2012.

[26] I.M.Ward and D.W.Hadley. An Introduction to the Mechanical Properties of Solid Polymers. 1993.

[27] TA Instruments. TA Instruments Dynamic Mechanical Analyzer.

[28] Lijie Ci and JinBo Bai. The reinforcement role of carbon nanotubes in epoxy composites with different matrix stiffness. Composites Science and Technology, 66:599–603, 2006.

[29] a. Martone, C. Formicola, M. Giordano, and M. Zarrelli. Reinforcement efficiency of multi-walled carbon nanotube/epoxy nano composites. Composites Science and Technology, 70(7):1154–1160, 2010.

[30] G. Pircheraghi, R. Foudazi, and I. Manas-Zloczower. Characterization of carbon nanotube dispersion and filler network formation in melted polyol for nanocomposite materials. Powder Technology, 276:222–231, 2015.

[31] J. K W Sandler, J. E. Kirk, I. a. Kinloch, M. S P Shaffer, and a. H. Windle. Ultra-low electrical percolation threshold in carbon-nanotube-epoxy composites. Polymer, 44(19):5893–5899, 2003.

[32] Jihua Gou and Kin-tak Lau. Modeling and Simulation of Carbon Nanotube / Polymer Composites. 2005.

[33] Erik T Thostenson, Zhifeng Ren, and Tsu-Wei Chou. Advances in the science and technology of carbon nanotubes and their composites: a review. Composites Science and Technology, 61:1899–1912, 2001.

[34] Jonathan N. Coleman, Umar Khan, and Yurii K. Gun'ko. Mechanical reinforcement of polymers using carbon nanotubes. Advanced Materials, 18:689–706, 2006.

[35] J. B. Bai and A. Allaoui. Effect of the length and the aggregate size of MWNTs on the improvement efficiency of the mechanical and electrical properties of nanocomposites - Experimental investigation. Composites Part A: Applied Science and Manufacturing, 34:689–694, 2003.

[36] Andreas Hirsch and Otto Vostrowsky. Functionalization of carbon nanotubes. Topics in Current Chemistry, 245:193–237, 2005.

[37] Qianqian Li, Michael Zaiser, and Vasileios Koutsos. Carbon nanotube/epoxy resin composites using a block copolymer as a dispersing agent. Physica Status Solidi (A) Applied Research, 201(13):89–91, 2004.

[38] M. S. Dresselhaus M. Endo, H.Muramatsu, T.Hayashi, Y. A.Kim, M. Terrones. 'Buckypaper' from coaxial nanotubes. Nature, 433(February):476, 2005.

[39] C. Schmid and D. Klingenberg. Mechanical Flocculation in Flowing Fiber Suspensions. Physical Review Letters, 84(2):290–293, 2000.

[40] J Sandler, M S P Shaffer, T Prasse, W Bauhofer, K Schulte, and A H Windle. Development of a dispersion process for carbon nanotubes in an epoxy matrix and the resulting electrical properties. 40:5967–5971, 1999.

[41] Shiuh Chuan Her and Chun Yu Lai. Dynamic behavior of nanocomposites reinforced with multi-walled carbon nanotubes (MWCNTs). Materials, 6(6):2274–2284, 2013.

[42] S. Osswald, E. Flahaut, H. Ye, and Y. Gogotsi. Elimination of D-band in Raman spectra of double-wall carbon nanotubes by oxidation. Chemical Physics Letters, 402(4-6):422–427, 2005.

[43] J. G. Wiltshire, a. N. Khlobystov, L. J. Li, S. G. Lyapin, G. a D Briggs, and R. J. Nicholas. Comparative studies on acid and thermal based selective purification of HiPCO produced single-walled carbon nanotubes. Chemical Physics Letters, 386(4-6):239–243, 2004.

[44] K. Behler, S. Osswald, H. Ye, S. Dimovski, and Y. Gogotsi. Effect of thermal treatment on the structure of multi-walled carbon nanotubes. Journal of Nanoparticle Research, 8(5):615–625, 2006.

[45] B. McCarthy, J. N. Coleman, R. Czerw, a. B. Dalton, M. in het Panhuis, a. Maiti, a. Drury, P. Bernier, J. B. Nagy, B. Lahr, H. J. Byrne, D. L. Carroll, and W. J. Blau. A Microscopic and Spectroscopic Study of Interactions between Carbon Nanotubes and a Conjugated Polymer. The Journal of Physical Chemistry B, 106(9):2210–2216, 2002.

[46] Darron E. Hill, Yi Lin, Apparao M. Rao, Lawrence F. Allard, and Ya Ping Sun. Functionalization of carbon nanotubes with polystyrene. Macromolecules, 35(25):9466–9471, 2002.

[47] Andreas Hirsch. Functionalization of single-walled carbon nanotubes. Angewandte Chemie - International Edition, 41(Cvd):1853–1859, 2002.

[48] Jang-Kyo Kim, Yiu-Wing Mai, and Kevin Kendall. Engineered Interfaces in Fiber Reinforced Composites. Elsevier, 1998.

[49] Jonathan N. Coleman, Umar Khan, Werner J. Blau, and Yurii K. Gun'ko. Small but strong: A review of the mechanical properties of carbon nanotube-polymer composites. Carbon, 44(9):1624–1652, 2006.

[50] Young Seok Song and Jae Ryoun Youn. Influence of dispersion states of carbon nanotubes on physical properties of epoxy nanocomposites. Carbon, 43(7):1378–1385, 2005.

[51] G. M. Odegard, T. S. Gates, K. E. Wise, C. Park, and E. J. Siochi. Constitutive modeling of nanotube-reinforced polymer composites. Composites Science and Technology, 63:1671–1687, 2003.

[52] W. D. Callister and D. G. Rethwisch. Materials Science and Engineering: An Introduction. page 992, 2010.

[53] C. L. Kane and E. J. Mele. Size, Shape, and Low Energy Electronic Structure of Carbon Nanotubes. Physical Review Letters, 78(c):1932–1935, 1997.

[54] Wenjie Wang and Ns Murthy. Characterization of Nanotube-Reinforced Polymer Composites. Carbon Nanotubes - Polymer Nanocomposites, pages 155–172, 2011.

[55] C. Bower, R. Rosen, L. Jin, J. Han, and O. Zhou. Deformation of carbon nanotubes in nanotube–polymer composites. Applied Physics Letters, 74(22):3317, 1999.

[56] L. H. Shao, R. Y. Luo, S. L. Bai, and J. Wang. Prediction of effective moduli of carbon nanotube-reinforced composites with waviness and debonding. Composite Structures, 87(3):274–281, 2009.

[57] M Senthil Kumar, S H Lee, T Y Kim, T H Kim, S M Song, J W Yang, K S Nahm, and E Suh. DC electric field assisted alignment of carbon nanotubes on metal electrodes. 47:2075–2080, 2003.

[58] S U Khan, J R Pothnis, and J.-K. Kim. Effects of carbon nanotube alignment on electrical and mechanical properties of epoxy nanocomposites. Composites Part A: Applied Science and Manufacturing, 49:26–34, 2013.

[59] Tohru Kimura, Hiroki Ago, Masayuki Tobita, Satoshi Ohshima, Mutsumasa Kyotani, and Motoo Yumura. Polymer Composites of Carbon Nanotubes. (19):1380–1383, 2002.

[60] Peter Morgan. In-plane-aligned membranes of carbon nanotubes, volume 338. 2005.

[61] E. S. Choi, J. S. Brooks, D. L. Eaton, M. S. Al-Haik, M. Y. Hussaini, H. Garmestani, D. Li, and K. Dahmen. Enhancement of thermal and electrical properties of carbon nanotube polymer composites by magnetic field processing. Journal of Applied Physics, 94(9):6034–6039, 2003.

[62] Ehsan Moaseri, Majid Karimi, Majid Baniadam, and Morteza Maghrebi. Improvements in mechanical properties of multi-walled carbon nanotube-reinforced epoxy composites through novel magnetic-assisted method for alignment of carbon nanotubes. Composites Part A: Applied Science and Manufacturing, 64:228–233, 2014.

[63] Asad Hameed, Mohammad Islam, Iftikhar Ahmad, Nasir Mahmood, Shaukat Saeed, and Hassan Javed. Thermal and mechanical properties of carbon nanotube/epoxy nanocomposites reinforced with pristine and functionalized multiwalled carbon nanotubes. Polymer Composites, pages n/a–n/a, 2014.

[64] C J G, F Noville, C Bossuot, and J Pirard. Qualitative assessment of the purity of multi-walled carbon nanotube samples using krypton adsorption. pages 265–271, 2007.

[65] Deborah D L Chung. Carbon fiber composites, volume 9. 1978.

[66] Peter Morgan. Carbon FIber and their Composites. Taylor & Francis Group, 2005.

[67] E. T. Thostenson, W. Z. Li, D. Z. Wang, Z. F. Ren, and T. W. Chou. Carbon nanotube/carbon fiber hybrid multiscale composites. Journal of Applied Physics, 91(9):6034–6037, 2002.

[68] International Standard. International Standard ISO-6721. 2011, 2011.

[69] K P Menard. Dynamic Mechanical Analysis: A Practical Introduction, Second Edition. CRC Press, 2008.

[70] Na Siddiqui, Cy Li, Youshan Yu, Pc Ma, and Jk Kim. Prepregging And Mechanical Properties Of Cnt-cfrp Hybrid Composites. 17th International Conference on Composite Materials, 2009.

[71] a. Allaoui, S. Bai, H. M. Cheng, and J. B. Bai. Mechanical and electrical properties of a MWNT/epoxy composite. Composites Science and Technology, 62(15):1993–1998, 2002.

[72] J. a. Choren, S. M. Heinrich, and M. B. Silver-Thorn. Young's modulus and volume porosity relationships for additive manufacturing applications. Journal of Materials Science, 48(15):5103–5112, 2013.

[73] Timothy L Weadon, Thomas H Evans, and Edward M Sabolsky. An Analytical Model for Porous Polymer-Ceramic Capacitive Pressure Sensors. 14(12):4411–4422, 2014.

[74] M Dehghan and I Sbarski. Thermo-Mechanical Characterization of MWCNTs-Modified Epoxy Resin. International Journal of Chemical, Nuclear, Metallurgical and Materials Engineering, 8(2):119–124, 2014.

[75] Erik T Thostenson and Tsu-Wei Chou. On the elastic properties of carbon nanotube-based composites: modelling and characterization. Journal of Physics D: Applied Physics, 36(5):573–582, 2003.

[76] Mohamed Abdalla, Derrick Dean, David Adibempe, Elijah Nyairo, Pamela Robinson, and Gregory Thompson. The effect of interfacial chemistry on molecular mobility and morphology of multiwalled carbon nanotubes epoxy nanocomposite. Polymer, 48(19):5662–5670, 2007.

[77] Babak Kaffashi, Amir Kaveh, O. Moini Jazani, and M. R. Saeb. Improving rheological properties of covalently MWCNT/epoxy nanocomposites via surface re-modification. Polymer Bulletin, 68(8):2187–2197, 2012.

[78] Jin Ah Kim, Dong Gi Seong, Tae Jin Kang, and Jae Ryoun Youn. Effects of surface modification on rheological and mechanical properties of CNT/epoxy composites. Carbon, 44(10):1898–1905, 2006.

[79] Jean Louis Halary. Structure – property relationships in epoxy-amine networks of well-controlled architecture †. 12(May 1999):141–153, 1999.

[80] Toho Tenax Europe GmbH. IMS60 E13 24K 830tex Carbon Fiber, 2008.

[81] R. Y. Yee and T. S. Stephens. A TGA technique for determining graphite fiber content in epoxy composites. Thermochimica Acta, 272(1-2):191–199, 1996.

[82] Göran Tolf and Per Clarin. Comparison between flexural and tensile modulus of fibre composites. Fibre Science and Technology, 21(4):319–326, 1984.

[83] Eric Finot, Ali Passian, and Thomas Thundat. Measurement of mechanical properties of cantilever shaped materials. Sensors, 8(5):3497–3541, 2008.

[84] Ping Chua and Seng. Dynamic Mechanical Analysis Studies of the lnterphase. 8(5), 1987.

[85] Richard L Clark and Thomas C Ward. Influence of the Interphase on the Mechanical Properties of Nylon 66 PhD thesis, 1996.

[86] Rickey J Seyler. Assignment of the Glass Transition. 1994.

[87] Edith A Turi. Front Matter. Social Service Review, 35(1):1981, 1961.

[88] R F Landel and L E Nielsen. Mechanical Properties of Polymers and Composites, Second Edition. Mechanical Engineering. Taylor & Francis, 1993.

[89] Vikas Mittal. Optimization of Polymer Nanocomposite Properties. 2010.

[90] Peter Morgan. Predictions of effective physical properties of complex multiphase materials, volume 63. 2005.

[91] Charles L Tucker and Erwin Liang. Stiffness predictions for unidirectional short- fiber composites : Review and evaluation. Composites Science and Technology, 59:655–671, 1999.

[92] G. M. Odegard, R. B. Pipes, and P. Hubert. Comparison of two models of SWCN polymer composites. Composites Science and Technology, 64:1011–1020, 2004.

[93] Tsu-Wei Chou. Microstructural design of fiber composites. 1992.

[94] R. George, K. T. Kashyap, R. Rahul, and S. Yamdagni. Strengthening in carbon nanotube/aluminium (CNT/Al) composites. Scripta Materialia, 53(10):1159–1163, 2005.

[95] Michael Griebel and Jan Hamaekers. Molecular dynamics simulations of the elastic moduli of polymer-carbon nanotube composites. Computer Methods in Applied Mechanics and Engineering, 193(17-20):1773–1788, 2004.

[96] Chunyu Li and Tsu-Wei Chou. Multiscale modeling of carbon nanotube reinforced polymer composites. Journal of nanoscience and nanotechnology, 3(5):423–430, 2003.

[97] Meisam Omidi, Hossein Rokni D.T., Abbas S. Milani, Rudolf J. Seethaler, and R. Arasteh. Prediction of the mechanical characteristics of multi-walled carbon nanotube/epoxy composites using a new form of the rule of mixtures, 2010.

[98] P. K. Valavala and G. M. Odegard. Modeling techniques for determination of mechanical properties of polymer nanocomposites. Reviews on Advanced Materials Science, 9(1):34–44, 2005.

[99] Gary D. Seidel and Dimitris C. Lagoudas. Micromechanical analysis of the effective elastic properties of carbon nanotube reinforced composites. Mechanics of Materials, 38(8-10):884–907, 2006.

[100] Vijay Anumandla and Ronald F. Gibson. A comprehensive closed form micromechanics model for estimating the elastic modulus of nanotube-reinforced composites. Composites Part A: Applied Science and Manufacturing, 37(12):2178–2185, 2006.

[101] Meng K. Yeh, Tsung H. Hsieh, and Nyan H. Tai. Fabrication and mechanical properties of multi-walled carbon nanotubes/epoxy nanocomposites. Materials Science and Engineering A, 483-484(1-2 C):289–292, 2008.

[102] B Arash, Q Wang, and V K Varadan. Mechanical properties of carbon nanotube/polymer composites. Nature, pages 1–8, 2014.

[103] Gp P Tandon and Gj J Weng. The effect of aspect ratio of inclusions on the elastic properties of unidirectionally aligned composites. Polymer composites, 5(4):327–333, 1984.

[104] C Li. Elastic moduli of multi-walled carbon nanotubes and the effect of van der Waals forces. Composites Science and Technology, 63:1517–1524, 2003.

[105] J.C. Halpin. Effects of Environmental Factors on Composite Materials. (June), 1969.

[106] Tienchong Chang and Huajian Gao. Size-dependent elastic properties of a single-walled carbon nanotube via a molecular mechanics model. Journal of the Mechanics and Physics of Solids, 51(6):1059–1074, 2003.

[107] Nan Yao, Vincenzo Lordi, and I Introduction. Young's modulus of single-walled carbon nanotubes. 84(4):1939–1943, 1998.

[108] Karl Sohlberg, Bobby G Sumpter, Robert E Tuzun, and Donald W Noid. Continuum methods of mechanics as a simplified approach to structural engineering of nanostructures. Nanotechnology, 9(1):30–36, 1999.

[109] Gregory M. Odegard, Thomas S. Gates, Lee M. Nicholson, and Kristopher E. Wise. Equivalent-continuum modeling of nano-structured materials. Composites Science and Technology, 62:1869–1880, 2002.

[110] Chunyu Li and Tsu Wei Chou. A structural mechanics approach for the analysis of carbon nanotubes. International Journal of Solids and Structures, 40:2487–2499, 2003.

[111] Chunyu Li and Tsu Wei Chou. Vibrational behaviors of multiwalled-carbon-nanotube-based nanomechanical resonators. Applied Physics Letters, 84:121–123, 2004.

[112] http://teoriadetudo.blogfolha.uol.com.br/files/2014/09/Cupula.jpg.

[113] G M Odegard, S J V Frankland, and T S Gates. AIAA 2003-1701 THE EFFECT OF CHEMICAL FUNCTIONALIZATION ON MECHANICAL PROPERTIES OF NANOTUBE / POLYMER COMPOSITES American Institute of Aeronautics and Astronautics American Institute of Aeronautics and Astronautics. (April):1–14, 2003.

Appendix A

Other Relevant Curves

Effect of carbon nanotube content for the three types of nanotubes in the epoxy nanocomposites (section 3.1). For the pristine carbon nanotubes (M1):

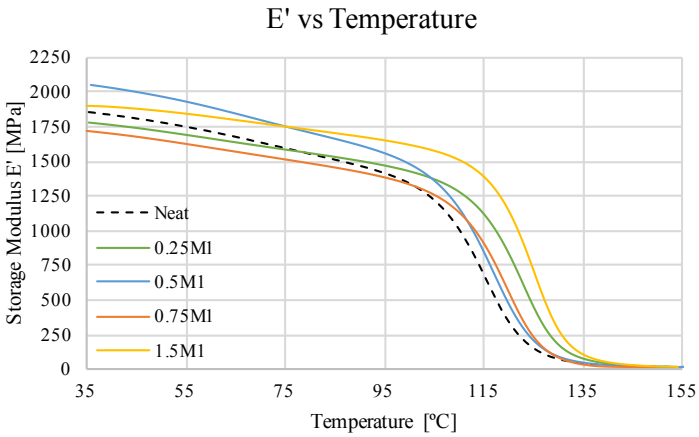

Figure A.1: Storage modulus against temperature, for various contents of Pristine carbon nanotubes.

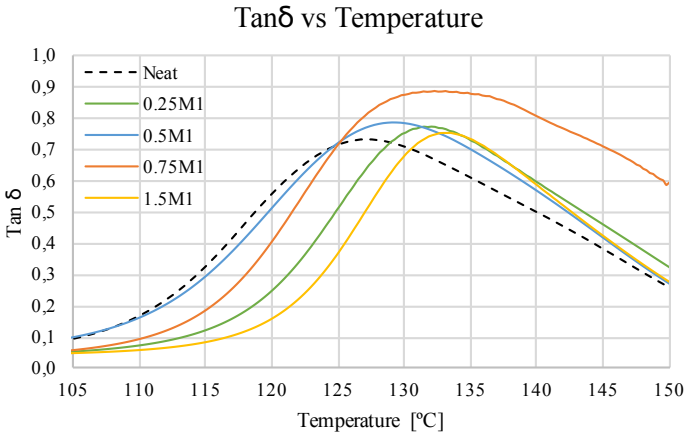

Figure A.2: Tan δ against temperature, for various contents of Pristine carbon nanotubes.

For the carboxylic functionalized carbon nanotubes (M2):

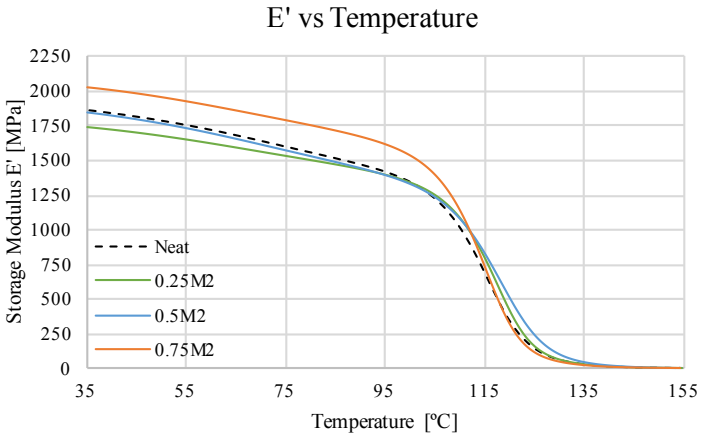

Figure A.3: Storage modulus against temperature, for various contents of carboxylic functionalized carbon nanotubes.

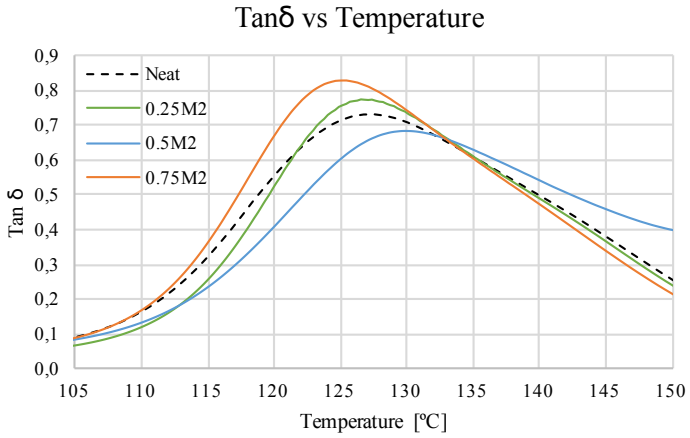

Figure A.4: Tan δ against temperature, for various contents of carboxylic functionalized nanotubes.

For the thermally oxidized functionalized carbon nanotubes (M3):

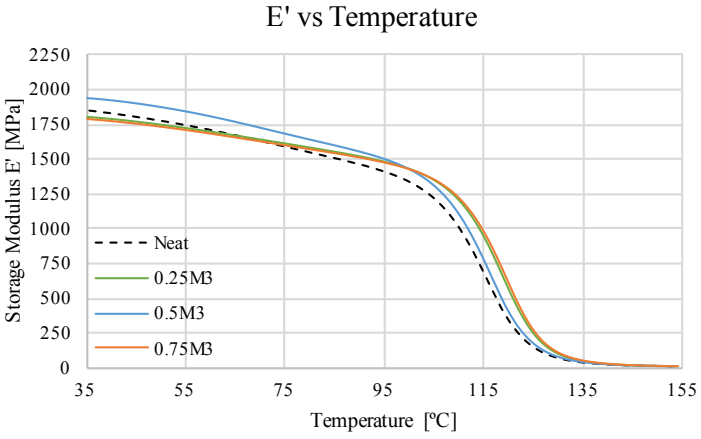

Figure A.5: Storage modulus against temperature, for various contents of thermally oxidized functionalized carbon nanotubes.

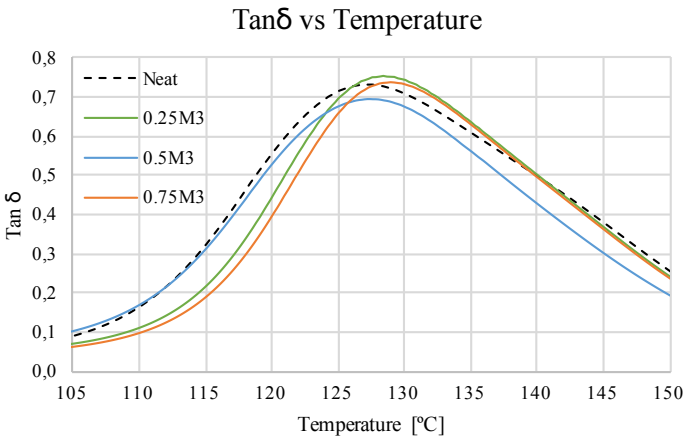

Figure A.6: Tan δ against temperature, for various contents of thermally oxidized functionalized carbon nanotubes.

Appendix B

Technical Sheets

HUNTSMAN
Enriching lives through innovation

Advanced Materials

Araldite® LY 556* / Aradur® 5021* / Hardener XB 3403* / Hardener XB3471*

PREPREG SYSTEM FOR LOW TEMPERATURE CURE

Araldite® LY 556 (epoxy resin)
Aradur® 5021 (hardener paste)
Hardener XB 3403 (hardener based on polyamine)
Hardener XB 3471 (hardener based on polyamine)

APPLICATIONS	Industrial composites		
PROPERTIES	Prepreg system with a long shelf life and curable from 80°C on		
PROCESSING	Prepreging		
KEY DATA	**Araldite® LY 556**		
	Aspect (visual)	clear, pale yellow liquid	
	Viscosity at 25 °C (ISO 9371B)	10000 - 12000	[mPa s]
	Density at 25 °C (ISO 1675)	1.15 - 1.20	[g/cm^3]
	Storage temperature	2 - 40	[°C]
	Aradur® 5021		
	Aspect (visual)	White viscous paste	
	Viscosity at 25 °C	70000 - 90000	[mPa s]
	Density at 25 °C (ISO 1675)	1.0	[g/cm^3]
	Storage temperature	< 8	[°C]
	Hardener XB 3403		
	Aspect (visual)	clear liquid	
	Viscosity at 25 °C	5 - 20	[mPa s]
	Density at 25 °C (ISO 1675)	1.0	[g/cm^3]
	Storage temperature (see expiry date on original container)	2 - 40	[°C]
	Hardener XB 3471		
	Aspect (visual)	transparent liquid	
	Density at 25 °C (ISO 1675)	1.0	[g/cm^3]
	Flash point (ISO 2719)	≥ 100	[°C]
	Storage temperature (see expiry date on original container)	2 - 40	[°C]
STORAGE	Provided that the products described above are stored in a dry place in their original, properly closed containers at the above mentioned storage temperatures they will have the shelf lives indicated on the labels. Partly emptied containers should be closed immediately after use.		

* *In addition to the brand name product denomination may show different appendices , which allows us to differentiate between our production sites: e.g , BD = Germany, US = United States, IN = India,CI = China, etc.. These appendices are in use on packaging, transport and invoicing documents. Generally the same specifications apply for all versions. Please address any additional need for clarification to the appropriate Huntsman contact.*

HUNTSMAN

Enriching lives through innovation

PROCESSING DATA

MIX RATIO

Components, parts by weight	System 1	System 2
Araldite® LY 556	100	100
Aradur® 5021	25	25
Hardener XB 3403	12	
Hardener XB 3471		14

Mix the epoxy Resin LY 556 with the hardener Aradur® 5021 and add the hardener XB 3403 **or** XB 3471 just before the prepregging process. The premix of the resin LY 556 / hardener Aradur® 5021 has a long shelf life at RT (> 1 week)

The prepreg tackiness can be adjusted by the amount of the hardener XB 3403 or XB 3471

We recommend that the components are weighed with an accurate balance to prevent mixing inaccuracies which can affect the properties of the matrix system. The components should be mixed thoroughly to ensure homogeneity. It is important that the side and the bottom of the vessel are incorporated into the mixing process.

When processing large quantities of mixture the pot life will decrease due to exothermic reaction. It is advisable to divide large mixes into several smaller containers.

INITIAL MIX VISCOSITY

		System 1	System 2
at 25°C	*[mPas]*	3900 - 4400	3800 - 4300

POT LIFE

(TECAM, 100 ML, 65 % RH)

all the 3 components		System 1	System 2
	[min]	410 - 460	380 - 430

GEL TIME

(HOT PLATE)

		System 1	System 2
at 80°C	*[min]*	210 - 240	200 - 230
at 90°C	*[min]*		60 - 80
at 100°C	*[min]*	40 - 60	
at 110°C	*[min]*	17 - 25	15 - 23
at 120°C	*[min]*	6 - 10	6 - 10
at 130°C	*[min]*	2- 5	2 - 5

The values shown are for small amounts of pure resin/hardener mix. In composite structures the gel time can differ significantly from the given values depending on the fibre content and the laminate thickness.

PREPREG PRODUCTION

Impregnation bath temperature	25 - 30 °C

B-STAGING

(PRE REACTION)

System 1	System 2
24-48h at 23-25°C	2-3 min at 80-90°C + 6-12h at 23°C

PREPREG SHELF LIFE

	System 1	System 2
at 23 °C	> 6 weeks	> 3 weeks

PROPERTIES OF THE CURED, NEAT FORMULATION

GLASS TRANSITION TEMPERATURE (T_G) (IEC 1006, DSC, 10 K/MIN)	*Cure: after B-Stage*	system 1 *T_G [°C]*	system 2 *T_G [°C]*
	10 h 70 °C	45 - 53	66 - 72
	10 h 70 °C + 4 h 80 °C	82 - 88	
	10 h 70 °C + 8 h 80 °C	87 - 93	98 - 104
	10 h 70 °C + 4 h 90 °C	90 - 96	
	8 h 80 °C	69 - 75	90 - 96
	16 h 80°C	89 - 95	98 - 104
	24 h 80 °C	90 - 96	100 - 106
	10 h 70 °C + 8 h 90 °C	101 - 107	
	4 h 90 °C	84 - 90	98 - 104
	6 h 90 °C	99 - 105	100 - 106
	8 h 90 °C	102 - 108	104 - 110
	10 h 90°C	105 - 111	105 - 111
	4 h 100 °C		110 - 116
	6 h 100 °C	113 - 119	116 - 122
	2 h 120 °C	117 - 123	122 - 128

FLEXURAL TEST (ISO 178) CURE CYCLE			Tested at	system 1	system 2
10H 70°C + 10H 80°C	Flexural strength Ultimate elongation Flexural modulus	[MPa] [%] [MPa]	23 °C	140 - 150 4.0 - 4.6 3600 - 3850	140 - 152 4.5 - 5.7 3350 – 3600
16H 80°C	Flexural strength Ultimate elongation Flexural modulus	[MPa] [%] [MPa]	23 °C	145 - 155 4.8 - 5.5 3600 - 3800	
24H 80°C	Flexural strength Ultimate elongation Flexural modulus	[MPa] [%] [MPa]	23 °C	140 - 150 4.5 - 5.5 3400 - 3650	
10H 90°C	Flexural strength Ultimate elongation Flexural modulus	[MPa] [%] [MPa]	23 °C	146 - 156 6.0 - 7.0 3150 - 3400	150 - 160 6.0 - 8.0 3260 – 3500
10H 90°C	Flexural strength Ultimate elongation Flexural modulus	[MPa] [%] [MPa]	70 °C	100 - 110 5.0 - 5.6 2500 - 2800	
10H 90°C	Flexural strength Ultimate elongation Flexural modulus	[MPa] [%] [MPa]	80 °C	94 - 104 4.6 - 5.2 2500 - 2800	
10H 90°C	Flexural strength Ultimate elongation Flexural modulus	[MPa] [%] [MPa]	90 °C	80 - 90 4.4 - 5.2 2200 - 2450	
6H 100°C	Flexural strength Ultimate elongation Flexural modulus	[MPa] [%] [MPa]	23 °C	120 – 135 4.5 - 5.5 2950 -3150	130 – 150 4.4 - 6.6 3050 - 3250
2H 120°C	Flexural strength	[MPa]	23°C		

	Ultimate elongation	[%]		135-145	130 – 145
	Flexural modulus	[MPa]		7.6 - 9.4	6.0 - 9.2
				2900 - 3100	2850 - 3050
FRACTURE PROPERTIES BEND NOTCH TEST					
(PM 258-0/90)					
CURE 10H 90°C	Fracture toughness K_{1C}	[MPa√m]	23 °C	0.70 - 0.85	0.70 - 0.80
	Fracture energy G_{1C}	[J/m^2]		125 - 175	130 - 160
CURE 6H 100°C	Fracture toughness K_{1C}	[MPa√m]	23 °C	0.65 - 0.75	0.75 - 0.85
	Fracture energy G_{1C}	[J/m^2]		120 – 150	155 - 180
CURE 2H 120°C	Fracture toughness K_{1C}	[MPa√m]	23 °C	0.75 - 0.85	0.75 - 0.85
	Fracture energy G_{1C}	[J/m^2]		170 - 200	170 - 205

PROPERTIES OF THE CURED, REINFORCED FORMULATION

INTERLAMINAR SHEAR TEST

Samples: 12 layers of unidirectional E-glass fabric (425 g/m^2)
Laminate thickness: 3.1 - 3.3 mm

(ASTM D 2344)

CURE CYCLE			Tested at	System 1	System 2
10H 70 °C					
10H 70°C + 8H 80 °C					
24H 80 °C	Shear strength	[MPa]	23°C	12 - 16	
10H 90 °C	Shear strength	[MPa]	23°C	60 - 64	53 - 57
10H 90 °C	Shear strength	[MPa]	23°C	60 - 64	
10H 90 °C	Shear strength	[MPa]	23°C	62 - 66	60 - 64
	Shear strength	[MPa]	70°C	47 - 51	
	Shear strength	[MPa]	70°C	37 - 41	

HANDLING PRECAUTIONS

Personal hygiene

Safety precautions at workplace

protective clothing	yes
gloves	essential
arm protectors	recommended when skin contact likely
goggles/safety glasses	yes

Skin protection	
before starting work	Apply barrier cream to exposed skin
after washing	Apply barrier or nourishing cream
Cleansing of contaminated skin	
	Dab off with absorbent paper, wash with warm water and alkali-free soap, then dry with disposable towels. Do not use solvents
Disposal of spillage	
	Soak up with sawdust or cotton waste and deposit in plastic-lined bin
Ventilation	
of workshop	Renew air 3 to 5 times an hour
of workplaces	Exhaust fans. Operatives should avoid inhaling vapours

FIRST AID

Contamination of the *eyes* by resin, hardener or mix should be treated immediately by flushing with clean, running water for 10 to 15 minutes. A doctor should then be consulted.

Material smeared or splashed on the *skin* should be dabbed off, and the contaminated area then washed and treated with a cleansing cream (see above). A doctor should be consulted in the event of severe irritation or burns. Contaminated clothing should be changed immediately.

Anyone taken ill after *inhaling* vapours should be moved out of doors immediately.

In all cases of doubt call for medical assistance.

Except where explicitly agreed otherwise, the sale of products referred to in this publication is subject to the general terms and conditions of sale of Huntsman Advanced Materials LLC or of its affiliated companies including without limitation, Huntsman Advanced Materials (Europe) BVBA, Huntsman Advanced Materials Americas Inc., and Huntsman Advanced Materials (Hong Kong) Ltd.
Huntsman Advanced Materials is an international business unit of Huntsman Corporation. Huntsman Advanced Materials trades through Huntsman affiliated companies in different countries including but not limited to Huntsman Advanced Materials LLC in the USA and Huntsman Advanced Materials (Europe) BVBA in Europe.

Aradur and Araldite are registered trademarks of Huntsman Corporation or an affiliate thereof.

Main Office :
Huntsman Advanced Materials (Switzerland) GmbH
Klybeckstrasse 200
4057 BASEL
Switzerland
+41 61 299 1111

Toho Tenax

TEIJIN

Delivery programme and characteristics for Tenax® IMS filament yarn

Brand name		**Tenax®**
Production site		**J**
Product designation		**IMS60 E13 24K 830tex**
Sizing properties		E13
Number of filaments		24.000
Nominal linear density [1)]	[tex]	830
Twist	[t/m]	0
Running length per kg	[m/kg]	1200
Package weight, net	[kg]	2 / 4

1) without sizing

Characteristics (typical values)

Filament diameter	[µm]	5
Density	[g/cm^3]	1,80
Tensile strength	[MPa]	5600
Tensile modulus	[GPa]	290
Elongation at break	[%]	1,9
Specific electrical resistance	[Ω cm]	1,45 x 10^{-3}

Sizing properties for fiber family IMS

IMS (Intermediate Modulus) is tailored to suit applications where strength and stiffness are of ultimate priority.

E13 = Type with ca. 1,3 % sizing based on epoxy resin

Please contact our sales team any time for choosing the right type. The stated numbers are typical values. For design purposes please request fiber specification.

Please note the application (aerospace or industry & sports) on your order.

The export or transfer of carbon fibers can be subject to authorization, depending on end-use and final destination.

Toho Tenax Europe GmbH Kasinostraße 19-21 42103 Wuppertal, Germany Tel.: +49 202 32 - 2339 Fax: +49 202 32 - 2360 www.tohotenax-eu.com sales@tohotenax-eu.com

(04/2008)